Ein relativistisches Punktkopplungsmodell: **Formale Untersuchungen und Anwendung auf überschwere Kerne**

Dissertation
zur Erlangung des Doktorgrades
der Naturwissenschaften

vorgelegt beim Fachbereich Physik
der Johann Wolfgang Goethe–Universität
in Frankfurt am Main

von
Anto Sulaksono
aus Jakarta

Frankfurt am Main, 2001
(D F 1)

vom Fachbereich Physik der Johann Wolfgang Goethe–Universit"at als Dissertation angenommen.

Dekan: Prof. Dr. Dr. h.c. mult. W. Greiner
Gutachter: Prof. Dr. J.A. Maruhn
Gutachter: Prof. Dr. Dr. h.c. mult. W. Greiner
Datum der Disputation:

Contents

1 Introduction **11**

2 The Linear Walecka Model **15**

2.1 Approximation 16

2.1.1 Low Momentum Expansion of Meson Propagator 18

2.1.2 Second-Order Derivative Approximation with Additional Parameters 19

2.1.3 Linearisation of the Equation of Motion 22

2.1.4 The Approximate Densities $C_{i\alpha}$ and $B_{i\alpha\mu}$ 25

2.2 Exchange Effect 27

2.3 Long-range Effect 33

2.4 Summary of Approximations Made 36

2.5 Determination of Parameters 37

2.6 Results and Discussions 37

3 Nonlinear Point-Coupling(PC) Model **61**

3.1 PC Model in the Hartree Level 61

3.2 Results 62

3.3 Exchange Effect in the Nonlinear Terms (Qualitative Discussion) 71

4 Nonrelativistic Reduction **73**

4.1 Schrödinger Equation 74

4.2 Dirac Equation 76

4.2.1 Summary of the Approximations in this Section 81

4.3 Comparisons of the Models 81

4.4 Discussion 85

4.4.1 LZ and LDZ2 (Linear Parameter Sets) 85

4.4.2 Linear (LDZ2 or LZ) vs Nonlinear (LDZ2a and NHM) Parameter Sets 86

4.4.3 PC vs Skyrme Hartree-Fock (SHF) model 86

4.4.4 Possible Enhancement in Nonlinear Terms and Isospin Effect 87

5 Superheavy Nuclei **89**

5.1 Results and Discussion 90

5.1.1 Nonlinear Effects in the Heavy and Superheavy Regions 91

5.1.2 Shell Closures Predictions in Superheavy Nuclei 94

5.1.3 Nonrelativistic Limit of the PC vs Skyrme Model (Essential Points) 98

5.1.4 Skyrme Force Inspired by the PC Model 99

6 Conclusion and Outlook **101**

6.1 Conclusion 101

6.2 Outlook 102

A Fierz Transformation (FT) **105**

B Exchange Part from the Derivative Lagrangian Density **107**

C Energy Functional for Spherical Symmetry **113**

Bibliography **117**

Acknowledgments **121**

Zusammenfassung und Ausblick **123**

Zusammenfassung 123

Ausblick 126

Lebenslauf **128**

List of Figures

2.1 Density expansion in the σ field of Oxygen 20

2.2 Comparison of the potential energy density from the exchange of the derivative terms with the potential energy density of the direct terms in Lead. . . 31

2.3 Comparison of the potential energy density from the exchange of the derivative terms with the potential energy density of the direct terms in Oxygen. 32

2.4 Long-range effects in the scalar potential energy of Oxygen 34

2.5 Long-range effect in the scalar potential energy of Lead and Zirconium . . 35

2.6 Comparison of binding energies per mass number and charge radii (r_c) with LDA calculation [27] 40

2.7 Every contribution in the scalar and the vector potential per nucleon mass as a function of radius (fm) in ^{208}Pb 41

2.8 Same figure as figure 2.7 but with a different scale. 42

2.9 Same figure as figure 2.7, but for ^{16}O. 43

2.10 Same figure as figure 2.9 but with a different scale. 44

2.11 Error in the binding energies for the Ca, Ni, Sn and Pb isotopes. 45

2.12 Error in the binding energies for the N=82 and N=126 isotones 46

2.13 Two-neutron separation energies (S_{2n}) for the Sn and Pb isotopes. 47

2.14 Two-proton separation energies (S_{2p}) for the N=82 and N=126 isotones. . 48

2.15 Errors in the diffraction radii for some spherical nuclei. 50

2.16 Error in the surface thicknessess for some spherical nuclei. 51

2.17 Radial charge density for ^{208}Pb and for ^{16}O. 52

2.18 Single-particle spectra for ^{208}Pb, for neutron and proton cases. 54

2.19 Single-particle spectra for ^{16}O, for neutron and protron cases. 55

2.20 Single-particle spectra for ^{132}Sn, for neutron and protron cases. 56

2.21 Error in the spin-orbit splitting for some spherical nuclei, for neutron and proton cases. 57

2.22 Binding energies per mass number of the infinite symetric nuclear matter versus a Fermi wave number 59

3.1 Error in the binding energies for the Ca, Ni, Sn, and Pb isotopes, and the N=82 and N=126 isotones with the parameter sets LDZ2a and NLZ. . . . 64

3.2 Two-neutron separation energies ($\mathrm{S_{2n}}$) for the Sn and Pb isotopes with the parameter sets LDZ2a and NLZ. 65

3.3 Two-proton separation energies ($\mathrm{S_{2p}}$) for the N=82 and N=126 isotones with the parameter sets LDZ2a and NLZ 66

3.4 Error in the diffraction radii and surface thicknessess for some spherical nuclei with the LDZ2a and NLZ parameter sets. 67

3.5 Charge density as a function of the radius for ^{208}Pb with the LDZ2a and NLZ parameter sets. 68

3.6 Single-particle spectra for ^{208}Pb neutron and protron with the LDZ2a and NLZ parameter sets. 69

3.7 Error in the spin-orbit splitting for some spherical nuclei, neutron and proton case with the LDZ2a and NLZ parameter sets. 70

5.1 Error in the binding energies for Cf and Fm isotopic chains. 91

5.2 Two-neutron separation energies (S_{2n}) for Cf and Fm isotopic chain. . . . 92

5.3 The charge density as a function of radius for Z=114, N=184 and Z=126, N=172. 93

5.4 Single-particle spectra for Z=114 for neutrons and protrons. 95

5.5 Single-particle spectra for Z=120 for neutrons and protrons. 96

5.6 Second differences of binding energy with respect to proton (δ_{2p}) and neutron number (δ_{2n}) in the superheavy region for the parameter set LDZ2a 97

List of Tables

2.1 The meson contents of equation. (2.1) 18

2.2 χ^2 results from various approximations. 38

2.3 Values of the six free parameters after they are fitted. 39

2.4 Properties of nuclear matter from various approximations. 53

3.1 Values for the LDZ2a parameter set. 62

3.2 Values for the NLZ parameter set. 62

3.3 χ^2 results from LDZ2a and NLZ 62

6.1 Value of the Test-NLa and LDZ2a parameter sets. 102

6.2 Parameter value of the Test-NLb 103

6.3 χ^2 results from the Test-NLa, the Test-NLb, LDZ2a, and NLZ 103

–I–

INTRODUCTION

The nuclear phenomena range from the structure of finite nuclei to a very hot and dense system which may occur in high-energy heavy-ion collisions or in neutron stars. The existing experimental initiatives and newly completed facilities (GSI, CEBAF, ..) will force us to use relativistic equations to compare the calculations with data of the future [1] and it can be said that for finite nuclei, the spin-orbit part of the relativistic model is superior to that of the nonrelativistic one [2]. Then it is natural to use the relativistic model. There exist, however, new features of the relativistic theories which have no analog in the nonrelativistic calculation, namely the existence of the negative energy sea (Dirac sea) of filled fermion levels. The presence of the Dirac sea is usually ignored, not because its effects are negligible, but because the infinite body problems are difficult to handle [3]. The relativistic mean-field model (RMF) is a such model in which the effects of the Dirac sea are not calculated explicitly, but due to the "magic of the fitting procedure", its effects are absorbed effectively in the coupling constants of the models (no sea-approximation) [4]. What I refer to as "magic of the fitting procedure" describes the fact that for such effective theories many details or ignored corrections can be hidden in the fitted parameters - making it, of course, more difficult to judge the physical correctness or relevance of each term in the models. In this work, however, I will treat only such effective theories and therefore in each case they are compared only after refitting the parameters.

A consistent relativistic mean field model to describe finite nuclei with a quality similar to that of the nonrelativistic model not only in the treatment of the Hartree terms but also in the exchange terms and the pairing correlation is also demanded in nuclear physics. This demand appears not only from aesthetic reasons but also from the physical reason that at the dripline, for example, the Fermi level is close to the continuum and the coupling between bound and continuum states should be taken into account explicitly. Therefore in these regions the pairing correlation becomes very important [5], so that a consistent

Hartree-Fock Bogoliubov calculation is needed in this case. This demand is not yet fullfilled completely. In Ref. [5], for example, an attempt is made to go into this direction: The authors calculate the Hartree parts fully like RMF, but neglect the Fock terms arguing that this effect is already absorbed in the Hartree part; in addition they use the infinite mass (zero-range) approximation of the meson propagators in the pairing sector.

Relativistic mean-fields model, which describe the nucleus as a system of Dirac nucleons that interact with each other by exchanging mean meson fields, have been successful in describing nuclear matter and ground state properties of finite nuclei [6, 7, 2, 8, 9, 10, 11, 12]. Other applications are the calculation of deformed nuclei [12, 14, 15, 16], odd nuclei [12], nuclei at the dripline [17], the potential energy surfaces of heavy nuclei [12], and the prediction of superheavies [13, 12, 18, 34]. From the success of the RMF model, we suppose that the exchange effect is already absorbed effectively in the coupling constants of the model, due to the fitting procedure, but some calculations which take into account the exchange explicitly by using the linear model have shown that this does not seem to be the case [26, 27]. Understanding this situation seems necessary and interesting. Unfortunately, due to the finite range of the mesons and the mesonic nonlinearity of these models, it is difficult to expand these models in the above direction. On the other hand, the finite range of the mesons has the advantage of giving the correct short-range (high momentum) behaviour and the meson dependence of the nonlinear terms is needed to simulate the many-body effects [27] and vacuum contribution [4].

Another possibility is the point-coupling (PC) model [21, 19, 20]. The difference of this model to the Walecka model is the replacement of the mesonic potential from the Walecka model with the density-dependent potential. In Ref. [20], Nikolaus, Hoch, and Madland (this paper will be frequently cited so that I used the abbreviation NHM) used the Hartree form of this model to calculate some observables of finite nuclei and nuclear matter. They obtained similar predictive power as the RMF models, but used different weights and observables from Ref. [6] to obtain their parameter set. The combination of the two facts is remarkable, because it seems that the role of the finite-range of the mesons is not too obviously reflected in the observables of finite nuclei. This fact, if further substantiated, will give a chance to fullfil the previous demand by using this model. Because predictions of finite nuclei still depend on fitting procedure or strategy, therefore our objective in this work is first to study the finite range once again and then exchange effects, where we treat both with the same fitting procedure. We will analyse these effects by observing the predictive power of both models for binding energies of some isotopes and isotones, in the separation energies, in the diffraction radii and surface thicknesses and also in the spin-orbit splitting, the single particle spectra, and in the nuclear matter properties. This investigation is necessary before we expand this model any further.

The second topic of this work are superheavy elements. The history of the superheavy element was enlightened by the works of the Frankfurt group [60, 61, 62, 63, 64, 65], since then, it is known that the study of the possible existence of the shell-stabilized superheavy elements (SHE) becomes very important. In Ref. [13] it was found that different types of self-consistent models did not give unique shell closure prediction in the superheavy region. Why this happens is of considerable importance, therefore the third object of this work is to study the difference in superheavy predictions of relativistic and nonrelativistic self-consistent models by using the point of view of the nonrelativistic limit of the PC model.

In chapter two, we discuss the connection between the linear RMF (Walecka) model and the linear PC model. Here we fit two parameters sets of the linear PC models to experimental data, one taking into account the exchange effect and one without the exchange effects. We use the same fitting procedure as for the NLZ or LZ parameters sets. We calculate some finite nuclear observables as mentioned previously. Note, that what I mean by the long-range effect in chapter two, actually the long range in momentum, is nothing else but a short-range distance effect. In chapter three, we also fit the nonlinear PC parameters to the experimental data with the same fitting procedure as for the NLZ parameter set. This nonlinear model does not take into account the exchange and nonlinear vector densities. In chapter four, we derive the effective Hamiltonian of the nonlinear PC model in the nonrelativistic limit and the relation to the Skyrme Hartree-Fock (SHF) model is shown. In this context we also discuss qualitatively the role of isospin and the nonlinear exchange terms. In chapter five, we use the results of chapter four and three to study the discrepancy in the superheavy predictions between the relativistic and nonrelativistic models.

–II–

The Linear Walecka Model

In this work we will study a simple approximation of the linear Walecka model which takes into account exchange contributions. This approximation can be easily fitted as a Hartree approximation to the experimental data. Then we use it to study the long-range and exchange effects of the linear Walecka model in finite nuclei.

Our motivation to study the exchange effects is based on the following facts: for a long time one has already known that the exchange terms give contributions of the same order as the Hartree terms [22, 23, 24, 25, 26, 27]. They cannot be treated as a small correction to the Hartree terms [22, 23, 24, 25, 26, 27]. But until now only a limited number of relativistic Hartree-Fock (RHF) calculations for finite nuclei have been done [23, 28, 26, 29, 27]. The reason is that RHF calculations are numerically more difficult than the relativistic Hartree(RH) calculation. As far as our knowledge goes, there is only one RHF calculation where the parameters have been fitted directly to the experimental observables of the nuclear ground states [26]. Zhang et al. [26] use a linear model with six fitted parameters and two fixed parameters (pion coupling constant and mass), but the computational time of their RHF code is about ten times longer than a Hartree calculation, and since in the process of searching for the minimum the HF codes need to be called frequently, they selected only five nuclei in order to obtain their parameter sets. They also did not include pairing correlations in their calculations. They obtain $\chi^2/nucleus \sim$ 20 - 46. We compare the result of Ref. [26] with a Hartree calculation in Ref. [6] with $\chi^2/nucleus \sim 250$. It is clear that the exchange effect cannot be absorbed into the linear Hartree model by a suitable choice of parameter sets. A more detailed discussion about it can be found in Ref. [26]. The same conclusion is also obtained in Ref. [27] by using the Local Density Approximation (LDA) to calculate the exchange contributions. On the other hand, recently a new relativistic mean field model by Furnstahl et al. using effective field theories

[30, 31, 32, 33] was proposed, the claim being that effects beyond a Hartree approach are included through the linear and the nonlinear coupling constants.

Our motivation to study the long-range effect is based on the following fact : Recently another relativistic model appeared, namely the Relativistic Point Coupling Model (RPC) [20, 21, 19]. The difference of this model to the Walecka model is to replace the mesonic potential from the nonlinear Walecka model with a densities-dependent potential [21, 20]. Ref. [20] (NHM) used the Hartree form of this model to calculate some observables of finite nuclei and nuclear matter. Similar predictive power in finite nuclei and nuclear matter was obtained as in Ref . [6], but they used weights and observables different from Ref. [6] to obtain their parameter set. This fact is remarkable, because now the role of the long-range effect in the meson theory for finite nuclei can be questioned.

We organize this chapter as follows : in section 1 we briefly review the RHF formalism and the approximation to extract the local parts of the Fock terms. In section 2 we discuss the exchange terms in the above approximation. In section 3 we discuss the long-range effect. In section 4 we give a summary of the approximations made and in section 5 we fit parameter sets in two approximations, i.e., a point-coupling like approximation with and without exchange corrections, with the same procedure as Ref. [7]. Then we use the standard parameter sets LZ (linear Hartree model) and NLZ (nonlinear Hartree model) from Ref. [7] as a guidance to study the long-range and exchange effects from the linear Walecka model in finite nuclei. Finally, in section 6 we present our results and discussion.

2.1 Approximation

Our starting point to study the long-range and exchange effects in finite nuclei is to write down a Lagrangian density operator from the linear Walecka model as [22]:

$$\begin{aligned} \hat{\mathcal{L}}_L &= \hat{\bar{\Psi}}(i\gamma_\mu\partial^\mu - m_B)\hat{\Psi} \\ &+ \sum_{i=S,V,R,A\ldots} s_i[\frac{1}{2}(\partial_\nu\hat{\phi}_i^\mu\partial^\nu\hat{\phi}_{i\mu} - m_i^2\hat{\phi}_i^\mu\hat{\phi}_{i\mu}) - g_i\hat{\bar{\Psi}}\Gamma_i^\mu\hat{\phi}_{i\mu}\hat{\Psi}], \end{aligned} \qquad (2.1)$$

where the meson contents can be seen in table. 2.1. The $\phi_{i\mu}$ satisfy the gauge condition $\partial^\mu\phi_{i\mu} = 0$. For the $\phi_{i\mu}$, the fields used are $\hat{\varphi}(x)$, $\hat{V}_\mu(x)$, $\hat{\vec{R}}_\mu(x)$ and $\hat{A}_\mu(x)$, denoting a scalar-isoscalar, a vector-isoscalar, a vector-isovector and the electromagnetic field operators, respectively. g_i and m_i are coupling constants and masses of each field operator $\hat{\phi}_{i\mu}$. Here we use the standard definition for the field operators as [22]

$$\hat{\phi}_{i\mu}(x) = \hat{\phi}_{i\mu}^0(x) + g_i\int d^4y D(x-y, m_i)\hat{\bar{\Psi}}\Gamma_{i\mu}\hat{\Psi}$$

$$\begin{aligned}\hat{\phi}^0_{j\mu}(x) &= \sum_\alpha (f_{\alpha j\mu}(x)\hat{a}_{\alpha j} + f^\dagger_{\alpha j\mu}(x)\hat{a}^\dagger_{\alpha j}) \\ \hat{\Psi}(x) &= \sum_\alpha (\Psi_\alpha(x)\hat{b}_\alpha + \tilde{\Psi}_\alpha(x)\hat{d}^\dagger_\alpha),\end{aligned} \tag{2.2}$$

where $\Psi_\alpha(x)$, $\tilde{\Psi}_\alpha$ and $f_{\alpha i\mu}$ denote a nucleon, an antinucleon, and a meson wavefunction with α enumerating the states. The operators $\hat{a}_{\alpha j}$, $\hat{b}_\alpha$ and $\hat{d}_\alpha$ annihilate a free meson, a nucleon and an antinucleon with a momentum k_α, similarly the conjugate operators create a free meson, a nucleon and an antinucleon with a momentum k_α. $D(x, y, m_i)$ is a meson propagator which is defined as a solution of

$$(\Box + m_i^2)D(x - y, m_i) = \delta^4(x - y). \tag{2.3}$$

If we choose a Slater determinant

$$|\phi_0 >= \prod_{\alpha=1}^{A} b^\dagger_\alpha |0 > \tag{2.4}$$

as the ground state of A occupied single nucleon levels, by using the standard procedure we have

$$\begin{aligned}< \phi_0| : \hat{\mathcal{L}}_L : |\phi_0 > &= \sum_{\alpha=A} \bar{\Psi}_\alpha (i\gamma_\mu \partial^\mu - m_B)\Psi_\alpha \\ + \sum_{i=S,V,R,A...} & s_i \quad [\frac{1}{2}(\partial_\nu \phi^\mu_{Hi} \partial^\nu \phi_{Hi\mu} - m_i^2 \phi^\mu_{Hi}\phi_{Hi\mu}) - g_i \bar{\Psi}_\alpha \Gamma^\mu_i \phi_{Hi\mu}\Psi_\alpha] \\ - \sum_{i=S,V,R,A...} \sum_{\alpha\beta} & s_i \quad [\frac{1}{2}(\partial_\nu \phi^\mu_{F\alpha\beta i} \partial^\nu \phi_{F\alpha\beta i\mu} - m_i^2 \phi^\mu_{F\alpha\beta i}\phi_{F\alpha\beta i\mu}) - g_i \bar{\Psi}_\alpha \Gamma^\mu_i \phi_{F\beta\alpha i\mu}\Psi_\beta].\end{aligned} \tag{2.5}$$

The index H (F) in the meson fields denotes Hartree (Fock) contributions, where the meson fields satisfy the Klein Gordon equations as :

$$\begin{aligned}(\Box + m_i^2)\phi^\mu_{Hi}(x) &= -g_i \sum_\alpha J^\mu_{\alpha\alpha i}(x) \\ (\Box + m_i^2)\phi^\mu_{Fi\alpha\beta}(x) &= -g_i J^\mu_{\alpha\beta i}(x),\end{aligned} \tag{2.6}$$

with :

$$J^\mu_{\alpha\beta i}(x) = \bar{\Psi}_\alpha \Gamma^\mu_i \Psi_\beta. \tag{2.7}$$

Meson	$\hat{\phi}_{i\mu}$ (Field)	g_i (Coupling Const)	m_i (Mass)	Γ_i^μ (Coupling terms)	s_i
σ	$\hat{\varphi}(x)$	g_S	m_S	1	1
ω	$\hat{V}_\mu(x)$	g_V	m_V	γ_μ	-1
ρ	$\hat{\vec{R}}_\mu(x)$	$\frac{g_R}{2}$	m_R	$\gamma_\mu\vec{\tau}$	-1
photon	$\hat{A}_\mu(x)$	e	0	$\frac{1}{2}\gamma_\mu(1+\tau_3)$	-1

Table 2.1: The meson contents of equation. (2.1).

From Eq. (2.5), we can easily obtain a relativistic Hartree-Fock equation as :

$$\sum_{\alpha\beta}[(i\gamma_\mu\partial^\mu - m_B)\delta_{\alpha\beta} - \sum_{i=S,V,R,A...} s_i g_i \Gamma_i^\mu(\phi_{Hi\mu}(x)\delta_{\alpha\beta} - \phi_{Fi\mu\beta\alpha}(x))]\Psi_\beta(x) = 0 \tag{2.8}$$

These are a set of coupled differential equations involving a nonlocal Hartree-Fock potential. One simple way to localize Eq. (2.5). is to remove the exchange (Fock) terms in the third line of Eq. (2.5). Then Eq. (2.5) reduces to a relativistic Hartree approximation. This is the same result as if we consider the meson fields as classical fields.

2.1.1 Low Momentum Expansion of Meson Propagator

To see another kind of approximation which can be done, we return to Eq. (2.6). and write the meson fields in Eq. (2.8). as

$$\begin{aligned}\phi^\mu_{Hi}(x) &= g_i \int d^4y D(x-y, m_i) \sum_\alpha J^\mu_{\alpha\alpha i}(y) \\ \phi^\mu_{F\alpha\beta i}(x) &= g_i \int d^4y D(x-y, m_i) J^\mu_{\alpha\beta i}(y),\end{aligned} \tag{2.9}$$

In momentum space, D can be written as

$$\begin{aligned}D(x,y) &= -\int \frac{d^4p}{(2\pi)^4}\frac{e^{-ip.(x-y)}}{p^2 - m_i^2 + i\epsilon} \\ &= \frac{1}{m_i^2}\int \frac{d^4p}{(2\pi)^4} e^{-ip.(x-y)}[1 - \frac{p^2+i\epsilon}{m_i^2}]^{-1}.\end{aligned} \tag{2.10}$$

Suppose that $\epsilon \to 0$ and $\frac{p^2}{m_i^2} < 1$ Then we can expand D as

$$\begin{aligned}D(x,y) &= \frac{1}{m_i^2}\int \frac{d^4p}{(2\pi)^4} e^{-ip.(x-y)}[1 + \frac{p^2}{m_i^2} + \frac{p^4}{m_i^4} + \frac{p^6}{m_i^6} + ...] \\ &= \frac{1}{m_i^2}\delta^4(x-y) - \frac{1}{m_i^4}\Box\delta^4(x-y) + \frac{1}{m_i^6}\Box^2\delta^4(x-y) - ....\end{aligned} \tag{2.11}$$

If we insert this expression into Eq. (2.9), then we will obtain

$$\begin{aligned}
\phi^{\mu}_{Hi} &= -\frac{g_i}{m_i^2}\sum_{\alpha}\bar{\Psi}_{\alpha}\Gamma^{\mu}_{i}\Psi_{\alpha} + \frac{g_i}{m_i^4}\sum_{\alpha}\Box(\bar{\Psi}_{\alpha}\Gamma^{\mu}_{i}\Psi_{\alpha}) - \frac{g_i}{m_i^6}\sum_{\alpha}\Box^2(\bar{\Psi}_{\alpha}\Gamma^{\mu}_{i}\Psi_{\alpha}) + ... \\
\phi^{\mu}_{F\alpha\beta i} &= -\frac{g_i}{m_i^2}\bar{\Psi}_{\alpha}\Gamma^{\mu}_{i}\Psi_{\beta} + \frac{g_i}{m_i^4}\Box(\bar{\Psi}_{\alpha}\Gamma^{\mu}_{i}\Psi_{\beta}) - \frac{g_i}{m_i^6}\Box^2(\bar{\Psi}_{\alpha}\Gamma^{\mu}_{i}\Psi_{\beta}) + ... \qquad (2.12)
\end{aligned}$$

The convergence of these expressions may be questioned, but at present we are still not able to give a rigorous answer, we can only use figure 2.1 as motivation of this approximation. In figure 2.1, σ denotes the scalar field of the linear Walecka model. The index w/pc in the density denotes if the density is calculated by using a mesonic potential/density dependent potential (like the conventional point-coupling model), the constant c denotes $\frac{g_s^2}{m_s^2}$. e denotes the exact scalar potential, e_1 the contribution in the scalar potential from the first-order expansion of the scalar field in the absolute velocity, e_2 the same in second order, e_4 is the same as e_2 but uses the density dependent potential to obtain the densities, like the point coupling model and E is the same as e_4 but uses a parameter set which is directly fitted to observables. We see that e_2 is closer to e than e_1. This fact shows that the density expansion in the sigma field tends to be convergent. But the selfconsistency condition has a negative effect in the convergence of the density expansion, which can be seen by comparing e_2 with e_4. E is closer to e than e_4, which means that adding a free parameter in front of the derivative term and a fitting procedure can help to suppress the selfconsistency effect in the convergence of the density expansion.

2.1.2 Second-Order Derivative Approximation with Additional Parameters

To avoid any further difficulties which can appear if we take all orders of the expansion in Eq. (2.12) in the numerical calculation and the physical interpretation, we decide as a preliminary step to make the following low-order approximation with additional parameters k_i

$$\begin{aligned}
\phi^{\mu}_{Hi} &\equiv -\frac{g_i}{m_i^2}\sum_{\alpha}\bar{\Psi}_{\alpha}\Gamma^{\mu}_{i}\Psi_{\alpha} + k_i\frac{g_i}{m_i^4}\sum_{\alpha}\Box(\bar{\Psi}_{\alpha}\Gamma^{\mu}_{i}\Psi_{\alpha}) \\
\phi^{\mu}_{F\alpha\beta i} &\equiv -\frac{g_i}{m_i^2}\bar{\Psi}_{\alpha}\Gamma^{\mu}_{i}\Psi_{\beta} + k_i\frac{g_i}{m_i^4}\Box(\bar{\Psi}_{\alpha}\Gamma^{\mu}_{i}\Psi_{\beta}). \qquad (2.13)
\end{aligned}$$

The physical motivation of this ansatz is obvious from figure 2.1. The constants k_i are some parameters, which can be used to see how strong the effects beyond second order approximation come into play. For instance, if k_i equals one, it means that these effects play no role at all. Because the terms taken into account, including the fit parameters,

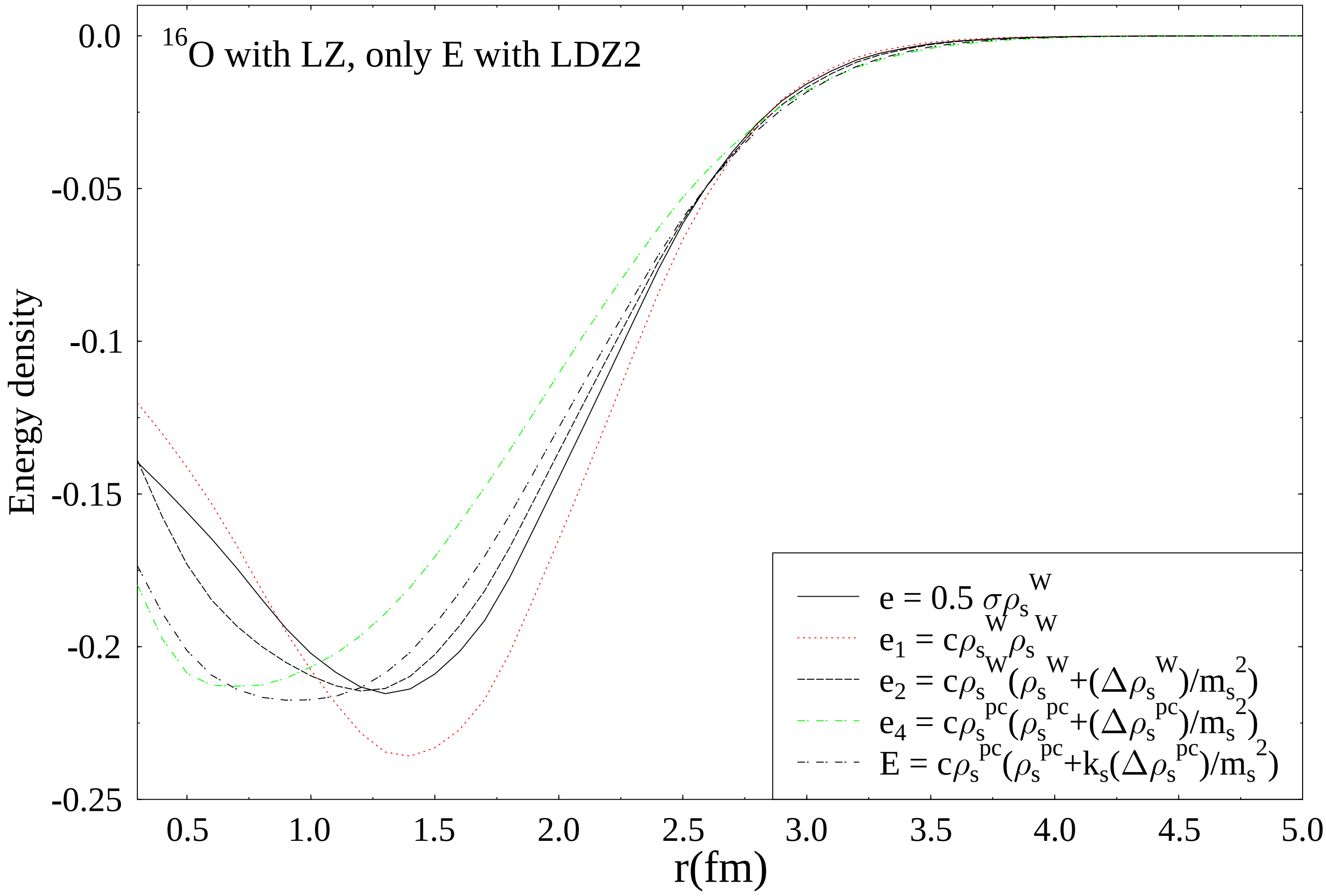

Figure 2.1: Density expansion in the σ field of Oxygen: σ denotes the scalar field of the linear Walecka model. The index w/pc in the density denotes if the density is calculated by using a mesonic potential/density dependent potential (like the conventional point-coupling model), the constant c denotes $\frac{g_s^2}{m_s^2}$. e denotes the exact scalar potential, e_1 the contribution in the scalar potential from the first-order expansion of the scalar field in the absolute velocity, e_2 the same in second order, e_4 is the same as e_2 but uses the density dependent potential to obtain the densities, like the point coupling model and E is the same as e_4 but uses a parameter set which is directly fitted to observables.

correspond to the conventional point-coupling model, from now on, we call the approximation in Eq. (2.13) the "point-coupling approximation". First, we insert Eq. (2.13) into $< \phi_0| : \hat{\mathcal{L}}_L : |\phi_0 >$ and use a Fierz Transformation (FT) to obtain

$$
\begin{aligned}
< \phi_0| : \hat{\mathcal{L}}_L : |\phi_0 > \quad = \quad & \sum_{\alpha=A} \bar{\Psi}_\alpha (i\gamma_\mu \partial^\mu - m_B)\Psi_\alpha \\
+ \sum_{i=S,V,R...} \quad s_i \quad & [\frac{1}{2}\frac{g_i^2}{m_i^2}\sum_{\alpha\beta} \bar{\Psi}_\alpha \Gamma_i^\nu \Psi_\alpha \bar{\Psi}_\beta \Gamma_{\nu i}\Psi_\beta + \frac{1}{2}\frac{g_i^2 k_i}{m_i^4}\sum_{\alpha\beta}\partial_\mu(\bar{\Psi}_\alpha \Gamma_i^\nu \Psi_\alpha)\partial^\mu(\bar{\Psi}_\beta \Gamma_{\nu i}\Psi_\beta)] \\
- \sum_{i,j=S,V,R...} s_i \quad C_{ji} \quad & [\frac{1}{2}\frac{g_i^2}{m_i^2}\sum_{\alpha\beta} \bar{\Psi}_\alpha \Gamma_j^\nu \Psi_\alpha \bar{\Psi}_\beta \Gamma_{\nu j}\Psi_\beta + \frac{1}{2}\frac{g_i^2 k_i}{m_i^4}\sum_{\alpha\beta}(\bar{\Psi}_\alpha \Gamma_j^\nu (\partial_\mu \Psi_\alpha)\bar{\Psi}_\beta \Gamma_{\nu j}(\partial^\mu \Psi_\beta) \\
+ \quad & (\partial_\mu \bar{\Psi}_\alpha)\Gamma_j^\nu \Psi_\alpha (\partial^\mu \bar{\Psi}_\beta)\Gamma_{\nu j}\Psi_\beta + 2\bar{\Psi}_\alpha \Gamma_j^\nu \Psi_\alpha (\partial_\mu \bar{\Psi}_\beta)\Gamma_{\nu j}(\partial^\mu \Psi_\beta))] \\
- \quad & \frac{1}{2}\partial_\nu A^\mu \partial^\nu A_\mu + e\sum_\alpha \bar{\Psi}_\alpha \gamma^\mu A_\mu \frac{1}{2}(1+\tau_3)\Psi_\alpha + \mathcal{L}_{exA}
\end{aligned}
\tag{2.14}
$$

The constants C_{ji} appear due to the Fierz transformation, the explicit form of these constants can be found in Appendix A. $\mathcal{L}_{exA}$ is the electromagnetic exchange contribution. Now we write the above expression as

$$
\begin{aligned}
< \phi_0| : \hat{\mathcal{L}}_L : |\phi_0 > \quad = \quad & \sum_{\alpha=A} \bar{\Psi}_\alpha (i\gamma_\mu \partial^\mu - m_B)\Psi_\alpha \\
+ \quad & \sum_{i=S,V,R...}\sum_{\alpha\beta} s_i[\frac{1}{2}\frac{g_i^2}{m_i^2} J_{i\alpha} J_\beta^i + \frac{1}{2}\frac{g_i^2 k_i}{m_i^4} A_{i\alpha\mu} A_\beta^{i\mu} \\
- \quad & \sum_{j=S,V,R...} C_{ji}[\frac{1}{2}\frac{g_i^2}{m_i^2} J_{j\alpha} J_\beta^j + \frac{g_i^2 k_i}{m_i^4}(\frac{1}{4} A_{j\alpha\mu} A_\beta^{j\mu} - B_{j\alpha\mu} B_\beta^{j\mu} + J_{j\alpha} C_\beta^j)]] \\
- \quad & \frac{1}{2}\partial_\nu A^\mu \partial^\nu A_\mu + e\sum_\alpha \bar{\Psi}_\alpha \gamma^\mu A_\mu \frac{1}{2}(1+\tau_3)\Psi_\alpha + \mathcal{L}_{exA},
\end{aligned}
\tag{2.15}
$$

The definitions of the variables in the expression above are :

$$
\begin{aligned}
A_{\alpha j\mu} &= \partial_\mu(\bar{\Psi}_\alpha \Gamma_j \Psi_\alpha) \\
B_{\alpha j\mu} &= \frac{1}{2i}[\bar{\Psi}_\alpha \Gamma_j (\partial_\mu \Psi_\alpha) - (\partial_\mu \bar{\Psi}_\alpha)\Gamma_j \Psi_\alpha] \\
C_{\alpha j} &= (\partial_\mu \bar{\Psi}_\alpha)\Gamma_j (\partial^\mu \Psi_\alpha) \\
J_{\alpha j} &= \bar{\Psi}_\alpha \Gamma_j \Psi_\alpha.
\end{aligned}
\tag{2.16}
$$

We can see that the non-derivative exchange terms do not give particular problems since they give rise to second-order differential equation like the Hartree case, but the derivative exchange terms force us to introduce new densities $(B_{\alpha j\mu}, C_{\alpha j})$, which qualitatively gives a different effect, since it requires to solve fourth-order differential equation and consequently further boundary conditions need to be specified.

2.1.3 Linearisation of the Equation of Motion

The dominant contributions in Eq. (2.15) are from the terms with $\Gamma_j = 1,\ \gamma_0$. The fine contributions are from the terms with $\Gamma_j = \tau,\ \tau\gamma_0$. It is quite illustrative if we see the order of magnitude of the terms with $\Gamma_j = \gamma_0$ because these terms show a clear order counting and are easy to calculate. They will be represented by :

$$\begin{aligned}
\epsilon_1 &= -\frac{g_v^2}{2m_v^2}\sum_{\alpha\beta}\bar{\Psi}_\alpha\gamma_0\Psi_\alpha\bar{\Psi}_\beta\gamma_0\Psi_\beta \\
\epsilon_2 &= \frac{g_v^2 k_v}{2m_v^4}\sum_{\alpha\beta}\vec{\nabla}(\bar{\Psi}_\alpha\gamma_0\Psi_\alpha).\vec{\nabla}(\bar{\Psi}_\beta\gamma_0\Psi_\beta) \\
\epsilon_{ex1} &= -\frac{c_v g_v^2}{2m_v^2}\sum_{\alpha\beta}\bar{\Psi}_\alpha\gamma_0\Psi_\alpha\bar{\Psi}_\beta\gamma_0\Psi_\beta \\
\epsilon_{ex2}^1 &\approx -\frac{c_v g_v^2 k_v}{4m_v^4}\sum_{\alpha\beta}[\bar{\Psi}_\alpha\gamma_0(\vec{\nabla}\Psi_\alpha) - (\vec{\nabla}\bar{\Psi}_\alpha)\gamma_0\Psi_\alpha].[\bar{\Psi}_\beta\gamma_0(\vec{\nabla}\Psi_\beta) - (\vec{\nabla}\bar{\Psi}_\beta)\gamma_0\Psi_\beta] \\
\epsilon_{ex2}^2 &\approx \frac{c_v g_v^2 k_v}{m_v^4}\sum_{\alpha\beta}\bar{\Psi}_\alpha\gamma_0\Psi_\alpha(\vec{\nabla}\bar{\Psi}_\beta).\gamma_0(\vec{\nabla}\Psi_\beta).
\end{aligned} \tag{2.17}$$

c_v is a constant which appears due to the Fierz transformation. It is a function of the meson coupling constants and masses and fulfills $c_v \leq 1$. In the plane wave approximation the summation is replaced by integration according to

$$\sum_\alpha \bar{\Psi}_\alpha\gamma_0\Psi_\alpha \Longrightarrow \bar{\rho}_0 \equiv \frac{a}{(2\pi)^3}\int d^3k\bar{\Psi}_k\gamma_0\Psi_k, \tag{2.18}$$

with a=(2S+1)(2I+1) a degeneracy factor. S, I denote spin and isospin, respectively. In this framework, Eq. (2.17) yields the following order counting

$$\begin{aligned}
\epsilon_1 &\sim -\frac{g_v^2}{2m_v^2}\bar{\rho}_0^2 \\
\epsilon_2 &\sim 0 \\
\epsilon_{ex1} &\sim -\frac{c_v g_v^2}{2m_v^2}\bar{\rho}_0^2
\end{aligned}$$

$$\begin{aligned}\epsilon^1_{ex2} &\sim -\frac{c_v g_v^2 k_v}{m_v^4}\frac{3.4}{6.02}\bar{\rho}_0^2 p_F^2 \\ \epsilon^2_{ex2} &\sim \frac{c_v g_v^2 k_v}{m_v^4}\frac{3.6}{6.02}\bar{\rho}_0^2 p_F^2 .\end{aligned} \tag{2.19}$$

From eq.(2.19), we obtain that $\mid \epsilon_{ex1/2} \mid > \mid \epsilon_2 \mid$, $\mid \epsilon_{ex1/2} \mid < \mid \epsilon_1 \mid$, $\mid \epsilon_{ex2} \mid < \mid \epsilon_{ex1} \mid$ and $\frac{|\epsilon_{ex2}|}{|\epsilon_1|} \sim c_v \frac{p_F^2}{m_v^2}$. In this approximation, every term in the exchange of the derivative part gives a contribution in order v^2, where v is the absolute velocity of the nucleon and $v < 1$. This appears to lead to a problem, because the contribution from the derivative exchange terms could be similar or a little bit larger than the direct derivative terms, therefore we can not neglect them if we still want to retain the direct derivative terms in the finite nuclei calculations, in view of the fact that the direct derivative terms are important for surface properties of finite nuclei. But it is obvious from the above estimation that these terms are smaller than the nonderivative exchange terms. It is quite reasonable to assume that we will have similar order counting for other contributions.

In any case, it will be instructive to derive the equation of motion from equation (2.15). By using the Euler-Lagrange equation we obtain it as

$$[\gamma_\mu \partial^\mu + i(\tilde{m}^* + \gamma_\alpha \tilde{V}^\alpha + (U_\mu + \gamma^\alpha U_{\alpha\mu})\partial^\mu + (W^1 + \gamma_\alpha W^{2\alpha})\Box)]\Psi_\alpha = 0, \tag{2.20}$$

where

$$\tilde{m}^* = m_B + \alpha_a J_a - (\delta_a + \tilde{\delta}_a)\partial^\mu A_{\mu a} + \frac{2}{3}\tilde{\delta}_a(i\partial^\mu B_{\mu a} + C_a) \tag{2.21}$$

$$\tilde{V}^\alpha = \alpha_b J_b^\alpha - (\delta_b + \tilde{\delta}_b)\partial^\mu A^\alpha_{\mu b} + \frac{2}{3}\tilde{\delta}_b(i\partial^\mu B^\alpha_{\mu b} + C^\alpha_b) \tag{2.22}$$

$$\begin{aligned} U_\mu &= \frac{4}{3} i\tilde{\delta}_a B_{\mu a} \\ U_{\nu\mu} &= \frac{4}{3} i\tilde{\delta}_b B_{\mu\nu b} \\ W_1 &= -\frac{2}{3}\tilde{\delta}_a J_a \\ W_{1\alpha} &= -\frac{2}{3}\tilde{\delta}_b J_{b\alpha} . \end{aligned} \tag{2.23}$$

Here the double index a/b means summations over S,D/V,R. $\tilde{\delta}_{a/b}$ are the contributions from the derivative exchange. The constants in Eq. (2.20) are :

$$\frac{1}{2}\alpha_s = -[\frac{1}{2}\frac{g_s^2}{m_s^2} - (\frac{1}{16}\frac{g_s^2}{m_s^2} - \frac{4}{16}\frac{g_v^2}{m_v^2} - \frac{3}{16}\frac{g_R^2}{m_R^2})] \tag{2.24}$$

$$\begin{aligned}
\frac{1}{2}\alpha_v &= -[-\frac{1}{2}\frac{g_v^2}{m_v^2} - (\frac{1}{16}\frac{g_s^2}{m_s^2} + \frac{2}{16}\frac{g_v^2}{m_v^2} + \frac{3}{32}\frac{g_R^2}{m_R^2})] && (2.25)\\
\frac{1}{2}\alpha_{ts} &= (\frac{1}{16}\frac{g_s^2}{m_s^2} - \frac{4}{16}\frac{g_v^2}{m_v^2} + \frac{1}{16}\frac{g_R^2}{m_R^2}) && (2.26)\\
\frac{1}{2}\alpha_{tv} &= -[-\frac{1}{8}\frac{g_R^2}{m_R^2} - (\frac{1}{16}\frac{g_s^2}{m_s^2} + \frac{2}{16}\frac{g_v^2}{m_v^2} - \frac{1}{32}\frac{g_R^2}{m_R^2})] && (2.27)\\
\frac{1}{2}\delta_s &= -[\frac{1}{2}\frac{g_s^2 k_s}{m_s^4} + (\frac{1}{16}\frac{g_s^2 k_s}{m_s^4} - \frac{4}{16}\frac{g_v^2 k_v}{m_v^4} - \frac{3}{16}\frac{g_R^2 k_r}{m_R^4})] && (2.28)\\
\frac{1}{2}\delta_v &= -[-\frac{1}{2}\frac{g_v^2 k_v}{m_v^4} + (\frac{1}{16}\frac{g_s^2 k_s}{m_s^4} + \frac{2}{16}\frac{g_v^2 k_v}{m_v^4} + \frac{3}{32}\frac{g_R^2 k_r}{m_R^4})] && (2.29)\\
\frac{1}{2}\delta_{ts} &= -[\frac{1}{16}\frac{g_s^2 k_s}{m_s^4} - \frac{4}{16}\frac{g_v^2 k_v}{m_v^4} + \frac{1}{16}\frac{g_R^2 k_r}{m_R^4}] && (2.30)\\
\frac{1}{2}\delta_{tv} &= -[-\frac{1}{8}\frac{g_R^2 k_r}{m_R^4} + (\frac{1}{16}\frac{g_s^2 k_s}{m_s^4} + \frac{2}{16}\frac{g_v^2 k_v}{m_v^4} - \frac{1}{32}\frac{g_R^2 k_r}{m_R^4})] && (2.31)\\
\frac{1}{2}\tilde{\delta}_s &= \frac{3}{2}(\frac{1}{16}\frac{g_s^2 k_s}{m_s^4} - \frac{4}{16}\frac{g_v^2 k_v}{m_v^4} - \frac{3}{16}\frac{g_R^2 k_r}{m_R^4}) && (2.32)\\
\frac{1}{2}\tilde{\delta}_v &= \frac{3}{2}(\frac{1}{16}\frac{g_s^2 k_s}{m_s^4} + \frac{2}{16}\frac{g_v^2 k_v}{m_v^4} + \frac{3}{32}\frac{g_R^2 k_r}{m_R^4}) && (2.33)\\
\frac{1}{2}\tilde{\delta}_{ts} &= \frac{3}{2}[\frac{1}{16}\frac{g_s^2 k_s}{m_s^4} - \frac{4}{16}\frac{g_v^2 k_v}{m_v^4} + \frac{1}{16}\frac{g_R^2 k_r}{m_R^4}] && (2.34)\\
\frac{1}{2}\tilde{\delta}_{tv} &= \frac{3}{2}(\frac{1}{16}\frac{g_s^2 k_s}{m_s^4} + \frac{2}{16}\frac{g_v^2 k_v}{m_v^4} - \frac{1}{32}\frac{g_R^2 k_r}{m_R^4})]. && (2.35)
\end{aligned}$$

Now let us study some densities in nuclear matter and finite nuclei to gain physical feeling in this case. In nuclear matter $\bar{\rho}_i \neq 0$, $\vec{\nabla}\bar{\rho}_i = 0$, $\mid \vec{\bar{B}}_i \mid /(m_B\bar{\rho}_i)$ is of order v and $\mid \bar{C}_i \mid /(m_B^2\bar{\rho}_i)$ is of order v^2, while in finite nuclei $\rho_i \neq 0$ and $\vec{\nabla}\rho_i \neq 0$. Based on figs 2.4 and 2.5, $\mid \vec{\nabla}\rho_i \mid /(m_i\rho_i)$ can be estimated to be of order v or possibly even smaller. Here the index i=V,S. From our experience in nuclear matter, it seems reasonable in finite nuclei to assume that $\mid \vec{B}_i \mid /(m_B\rho_i)$ is of order v and $\mid C_i \mid /(m_B^2\rho_i)$ is of order v^2. The validity of these assumptions can also be checked by using figures 2.3 and 2.2.

With this rough estimate of the order of magnitude in the densities, we will study the form of B_α^σ from the Gordon decomposition [38] by using the exact equation of state in Eq. (2.20). Here we only calculate the scalar case because the vector case is of similar magnitude but more difficult than the scalar case. After a straightforward Dirac matrix algebra calculation we have from the Gordon decomposition that $A_1 + A_2 + A_3 = 0$ with :

$$\begin{aligned}
A_1 &= -\frac{1}{2i}[(\partial^\sigma\bar{\Psi}_\alpha)\Psi_\alpha - \bar{\Psi}_\alpha(\partial^\sigma\Psi_\alpha)] \\
&+ \frac{1}{2}U_\mu[(\partial^\mu\bar{\Psi}_\alpha)\gamma^\sigma\Psi_\alpha - \bar{\Psi}_\alpha\gamma^\sigma(\partial^\mu\Psi_\alpha)] \\
&+ \frac{1}{2}W_1\partial_\mu[(\partial^\mu\bar{\Psi}_\alpha)\gamma^\sigma\Psi_\alpha - \bar{\Psi}_\alpha\gamma^\sigma(\partial^\mu\Psi_\alpha)] \\
&+ \frac{1}{2}U^\sigma_\mu[(\partial^\mu\bar{\Psi}_\alpha)\Psi_\alpha - \bar{\Psi}_\alpha(\partial^\mu\Psi_\alpha)] \\
&+ \frac{1}{2}W^\sigma_2\partial_\mu[(\partial^\mu\bar{\Psi}_\alpha)\Psi_\alpha - \bar{\Psi}_\alpha(\partial^\mu\Psi_\alpha)]
\end{aligned} \tag{2.36}$$

$$A_2 = \frac{1}{2}\partial_\mu(\bar{\Psi}_\alpha\sigma^{\mu\sigma}\Psi_\alpha) - \frac{1}{2}iU_{\alpha\mu}\partial^\mu(\bar{\Psi}_\alpha\sigma^{\alpha\sigma}\Psi_\alpha) - \frac{1}{2}iW_{2\alpha}\Box(\bar{\Psi}_\alpha\sigma^{\alpha\sigma}\Psi_\alpha) \tag{2.37}$$

$$A_3 = \tilde{m}^*\bar{\Psi}_\alpha\gamma^\sigma\Psi_\alpha + \tilde{V}^\sigma\bar{\Psi}_\alpha\Psi_\alpha. \tag{2.38}$$

Let us define $\tilde{m}^* \equiv \bar{m}^* + \Delta m^*$ and $\tilde{V}^\alpha \equiv \bar{V}^\alpha + \Delta V^\alpha$, where Δm^* and ΔV^α are the parts of $\tilde{m}^*$ and $\tilde{V}^\alpha$ with order v^2. Now, if we apply the previous order-of-magnitude estimation to study the magnitude in every term in A_1 through A_3 and we assume that the terms with order $\geq v^2$ are small and can be neglected, then it is obvious that only the first term in A_1 and A_2 will survive and the Δm^* and ΔV^α vanish in A_3. Thus in the limit of small v the B^σ_α can be determined from Dirac equation. We well use this fact as a motivation for the next approximations.

2.1.4 The Approximate Densities $C_{i\alpha}$ and $B_{i\alpha\mu}$

Now we start to make approximations for the terms in the last line of Eq. (2.15) (or approximations for the $C_{i\alpha}$ and the $B_{i\alpha\mu}$ densities). For a moment suppose that we do not know yet the approximate forms of the $C_{i\alpha}$ and $B_{i\alpha\mu}$ densities, but only expect to obtain from the approximate Lagrangian density (the Lagrangian density with the approximate forms of the densities $C_{i\alpha}$ and $B_{i\alpha\mu}$) an approximate equation of motion of the form

$$[\gamma_\mu\partial^\mu + i(m^* + \gamma_\alpha V^\alpha + \sigma_{\alpha\beta}T^{\alpha\beta})]\Psi_\alpha = 0, \tag{2.39}$$

where m^*, V^α and $T^{\alpha\beta}$ are real functions. It implies that there is a connection between the two types of functions: m^*, V^α ,$T^{\alpha\beta}$ and $J_{i\alpha}$, $A_{i\alpha\mu}$, C^j_β, $B_{j\alpha\mu}$. Therefore we will try to

obtain the C^j_β and $B_{j\alpha\mu}$ as functions of the m^*, V^α ,$T^{\alpha\beta}$. Finally we use the approximate form of m^*, V^α ,$T^{\alpha\beta}$ to calculate C^j_β and $B_{j\alpha\mu}$ then from these approximate densities C^j_β and $B_{j\alpha\mu}$ we obtain the approximate Lagrangian density.
The scalar case (Γ =1):
The Gordon decomposition [38] of Eq. (2.39) is

$$\begin{aligned} &\bar{\Psi}_\alpha[\gamma_\mu \overleftarrow{\partial^\mu} - i(m^* + \gamma_\alpha V^\alpha + \sigma_{\alpha\beta}T^{\alpha\beta})] \not{a}\Psi_\alpha \\ -&\bar{\Psi}_\alpha \not{a}[\gamma_\mu \partial^\mu + i(m^* + \gamma_\alpha V^\alpha + \sigma_{\alpha\beta}T^{\alpha\beta})]\Psi_\alpha = 0, \end{aligned} \tag{2.40}$$

$\not{a} = a^\mu \gamma_\mu$ and a^μ is an abritrary vector. A straightforward simplification of this expression gives

$$\begin{aligned} \bar{\Psi}_\alpha(\partial^\nu \Psi_\alpha) - (\partial^\nu \bar{\Psi}_\alpha)\Psi_\alpha &= -i[\partial_\mu(\bar{\Psi}_\alpha \sigma^{\mu\nu}\Psi_\alpha) + 2m^*\bar{\Psi}_\alpha \gamma^\nu \Psi_\alpha \\ &+ 2V^\nu \bar{\Psi}_\alpha \Psi_\alpha + 2\epsilon^{\alpha\beta\nu\theta}T_{\alpha\beta}\bar{\Psi}_\alpha \gamma_\theta \gamma_5 \Psi_\alpha] \end{aligned} \tag{2.41}$$

and from Eq. (2.39). we also have

$$\begin{aligned} (\partial_\mu \bar{\Psi}_\alpha)(\partial^\mu \Psi_\alpha) &= [m^{*2}\bar{\Psi}_\alpha \Psi_\alpha + 2m^* V^\nu \bar{\Psi}_\alpha \gamma_\nu \Psi_\alpha + 1/2\Box(\bar{\Psi}_\alpha \Psi_\alpha) \\ &+ V^\nu V_\nu \bar{\Psi}_\alpha \Psi_\alpha - \partial_\nu(V_\mu \bar{\Psi}_\alpha \sigma^{\mu\nu}\Psi_\alpha) + \bar{\Psi}_\alpha f(T_{\alpha\beta})\Psi_\alpha]. \end{aligned} \tag{2.42}$$

Here $f(T_{\alpha\beta})$ denotes a function of $T_{\alpha\beta}$ which is zero for $T_{\alpha\beta}$=0. We can consider the m^*, V^ν ,$T^{\alpha\beta}$ as

$$\begin{aligned} m^* &= m_B - \frac{\tilde{g}_s^2}{m_s^2}\sum_{\alpha=A}\bar{\Psi}_\alpha \Psi_\alpha + ... \\ V^\nu &= \frac{\tilde{g}_v^2}{m_v^2}\sum_{\alpha=A}\bar{\Psi}_\alpha \gamma^\nu \Psi_\alpha + .. \\ T^{\alpha\beta} &= 0 + ..., \end{aligned} \tag{2.43}$$

where - $\frac{\tilde{g}_s^2}{m_s^2} = \alpha_s$ and $\frac{\tilde{g}_v^2}{m_v^2} = \alpha_v$ are effective coupling constants. They are functions of $\frac{g_s^2}{m_s^2}$, $\frac{g_v^2}{m_v^2}$, $\frac{g_s^2 k_s}{m_s^4}$ and $\frac{g_v^2 k_v}{m_v^4}$, which come from the contribution of the direct and the exchange part in front of the nonderivative and the derivative of the scalar and vector densities respectively. In the above equations ... denote contributions from the derivative, isovector, nonlinear and tensor correction parts. As the next step, we substitute Eq. (2.43) into Eq. (2.40) and Eq. (2.42) and then into a Lagrangian density to obtain :

$$\begin{aligned} \tilde{\mathcal{L}}_S &= \sum_{\alpha\beta} 2[\frac{1}{4}\tilde{A}_{\mu\alpha}\tilde{A}^\mu_\beta - \tilde{B}_{\mu\alpha}\tilde{B}^\mu_\beta + \tilde{J}_\alpha \tilde{C}_\beta] \\ &= \tilde{\mathcal{L}}^{lin}_S + \tilde{\mathcal{L}}^{non-lin}_S, \end{aligned} \tag{2.44}$$

where

$$\tilde{\mathcal{L}}_S^{lin} = -\frac{1}{2}\partial_\mu \rho_s \partial^\mu \rho_s + 2m_B^2 \rho_s^2 - 2m_B^2 J_v^\mu J_{v\mu} - 2m_B J_v^\mu \partial^\nu (J_{T\nu\mu}) - \frac{1}{2}\partial^\nu (J_{T\nu\mu})\partial_\sigma (J_T{}^{\sigma\mu}) \tag{2.45}$$

and

$$\begin{aligned} \tilde{\mathcal{L}}_S^{non-lin} &= -\frac{4m_B \tilde{g}_s^2}{m_s^2}\rho_s^3 + \frac{2\tilde{g}_s^4}{m_s^4}\rho_s^4 + 4m_B \frac{\tilde{g}_s^2}{m_s^2}\rho_s J_v^\mu J_{v\mu} + 2\frac{\tilde{g}_v^2}{m_v^2}\rho_s J_{T\nu\mu}\partial^\nu (J_v^\mu) \\ &+ 2\frac{\tilde{g}_s^2}{m_s^2}\rho_s J_v^\mu \partial^\nu (J_{T\nu\mu}) - \frac{2\tilde{g}_s^4}{m_s^4}\rho_s^2 J_v^\mu J_{v\mu} + \ldots \cdot \end{aligned} \tag{2.46}$$

The last two equations are the scalar case of the approximation to the derivative exchange terms in Eq. (2.15). The other case can be derived similarly. The results are shown in Appendix B.

2.2 Exchange Effect

It seems that the form of $\mathcal{L}^{non-lin}$ is not practically useful in the sense that it has too many terms and every term is a function of constants in a complicated way, which could lead to difficulties if one tries to fit all terms to experimental values of nuclear observables. We find that many terms contain isovector parts, which we know give smaller contributions than those with only isoscalar parts, since one knows that densities of the isovector contribution are smaller than the densities of the isoscalar one [7, 2, 20, 6]. Therefore only the isoscalar contribution from the nonlinear potential will mean a significant difference. We find that the nonlinear terms without isovector parts are not many and their complete form is

$$\mathcal{L}^*_{non-lin} \equiv -\frac{1}{3}\beta_s \rho_s^3 - \frac{1}{4}\gamma_s \rho_s^4 - \frac{1}{4}\gamma_v (J_v^\nu J_{v\nu})^2 - \frac{1}{2}C_3 \rho_s (J_v^\nu J_{v\nu}) - \frac{1}{2}C_5 \rho_s^2 (J_v^\nu J_{v\nu}). \tag{2.47}$$

Then it seems reasonable to take these terms as effective nonlinear terms and the contribution from the other terms can be considered smaller than these leading terms and assumed to be already absorbed effectively in these terms. Because the coupling constants in front of the tensor fields and the tensor field densities themselves are small [31], we expect that $\mathcal{L}_T^{corr}$ also yields small contributions, so that it can be neglected. Now we have the nonlinear Lagrangian density as :

$$< \phi_0 | : \hat{\mathcal{L}}_{NL} : | \phi_0 > = \mathcal{L}_{free} + \mathcal{L}_1 + \mathcal{L}_2 + \mathcal{L}^*_{non-lin} + \mathcal{L}_{dirA} + \mathcal{L}_{exA}, \tag{2.48}$$

with

$$\begin{aligned}
\mathcal{L}_{free} &= \sum_{\alpha=A} \bar{\Psi}_\alpha(i\gamma_\mu\partial^\mu - m_B)\Psi_\alpha \\
\mathcal{L}_1 &= -\frac{1}{2}\alpha_s\rho_s^2 - \frac{1}{2}\alpha_v J_v^\mu J_{v\mu} - \frac{1}{2}\alpha_{tv}\vec{J}_v^\mu \vec{J}_{v\mu} - \frac{1}{2}\delta_s\partial_\mu\rho_s\partial^\mu\rho_s \\
&- \frac{1}{2}\delta_v\partial_\nu J_v^\mu\partial^\nu J_{v\mu} - \frac{1}{2}\delta_{tv}\partial_\nu\vec{J}_{tv}^\mu\partial^\nu\vec{J}_{tv\mu} \\
\mathcal{L}_2 &= -\frac{1}{2}\alpha_{ts}\vec{\rho}_{ts}^2 - \frac{1}{2}\delta_{ts}\partial_\mu\vec{\rho}_{ts}\partial^\mu\vec{\rho}_{ts} - \frac{1}{2}\theta_T J_v^\mu\partial^\nu(J_{T\nu\mu}) - \frac{1}{2}\theta_{TS}\vec{J}_{tv}^\mu\partial^\nu(\vec{J}_{tT\nu\mu}) \\
\mathcal{L}_{dirA} &= -\frac{1}{2}\partial_\nu A^\mu\partial^\nu A_\mu + e\sum_\alpha \bar{\Psi}_\alpha\gamma^\mu A_\mu\frac{1}{2}(1+\tau_3)\Psi_\alpha.
\end{aligned}$$

Later, in section five, we only use the following Lagrangian densities

$$\begin{aligned}
\mathcal{L}_{LDZ2} &= \mathcal{L}_{free} + \mathcal{L}_1 + \mathcal{L}_{dirA} \\
\mathcal{L}_{LDZ1} &= \mathcal{L}_{LDZ2} + \mathcal{L}_2 + \mathcal{L}_{exA}. \qquad (2.49)
\end{aligned}$$

A second step to simplify the problem is to transform the constants (in Appendix B) into simple forms by a redefinition as follows :

$$\frac{1}{2}\alpha_s = -\frac{1}{2}\frac{g_s^2}{m_s^2} \qquad (2.50)$$

$$\frac{1}{2}\alpha_v = \frac{1}{2}\frac{g_v^2}{m_v^2} \qquad (2.51)$$

$$\begin{aligned}
\frac{1}{2}\alpha_{ts} &= \frac{1}{2}[(\frac{1}{15}\frac{g_s^2}{m_s^2} - \frac{2}{3}\frac{g_v^2}{m_v^2} - \frac{1}{4}\frac{g_R^2}{m_R^2}) \\
&+ m_B^2(\frac{676}{1185}\frac{g_s^2k_s}{m_s^4} + \frac{2672}{1185}\frac{g_v^2k_v}{m_v^4} + \frac{941}{1185}\frac{g_R^2k_r}{m_R^4})] \qquad (2.52)
\end{aligned}$$

$$\frac{1}{2}\alpha_{tv} = \frac{1}{8}\frac{g_R^2}{m_R^2} \qquad (2.53)$$

$$\frac{1}{2}\delta_s = -\frac{1}{2}\frac{g_s^2k_s}{m_s^4} \qquad (2.54)$$

$$\frac{1}{2}\delta_v = \frac{1}{2}\frac{g_v^2k_v}{m_v^4} \qquad (2.55)$$

$$\frac{1}{2}\delta_{ts} = -\frac{1}{2}[\frac{13}{237}\frac{g_s^2k_s}{m_s^4} - \frac{58}{237}\frac{g_v^2k_v}{m_v^4} + \frac{7}{158}\frac{g_R^2k_r}{m_R^4}] \qquad (2.56)$$

$$\frac{1}{2}\delta_{tv} = \frac{1}{8}\frac{g_R^2k_r}{m_R^4} \qquad (2.57)$$

$$\frac{1}{2}\theta_T = -\frac{1}{2}m_B[\frac{4}{79}\frac{g_s^2k_s}{m_s^4} + \frac{128}{79}\frac{g_v^2k_v}{m_v^4} + \frac{64}{79}\frac{g_R^2k_r}{m_R^4}] \tag{2.58}$$

$$\frac{1}{2}\theta_{TS} = -\frac{1}{2}m_B[\frac{52}{237}\frac{g_s^2k_s}{m_s^4} - \frac{232}{237}\frac{g_v^2k_v}{m_v^4} + \frac{14}{79}\frac{g_R^2k_r}{m_R^4}]. \tag{2.59}$$

If we define

$$\tilde{C}_S = -[\frac{1}{79}\frac{g_s^2k_s}{m_s^4} + \frac{32}{79}\frac{g_v^2k_v}{m_v^4} + \frac{16}{79}\frac{g_R^2k_r}{m_R^4}], \tag{2.60}$$

and

$$\tilde{C}_V = [\frac{8}{79}\frac{g_s^2k_s}{m_s^4} + \frac{19}{79}\frac{g_v^2k_v}{m_v^4} + \frac{19}{158}\frac{g_R^2k_r}{m_R^4}], \tag{2.61}$$

then we obtain also the nonlinear coupling constants as :

$$\beta_s = -12\tilde{C}_S m_B\frac{g_s^2}{m_s^2} \tag{2.62}$$

$$\gamma_s = 8\tilde{C}_S\frac{g_s^4}{m_s^4} \tag{2.63}$$

$$\gamma_v = -8\tilde{C}_V\frac{g_v^4}{m_v^4} \tag{2.64}$$

$$C_3 = 8m_B(\tilde{C}_S - \tilde{C}_V)\frac{g_s^2}{m_s^2} \tag{2.65}$$

$$C_5 = -4(\tilde{C}_S - \tilde{C}_V)\frac{g_s^4}{m_s^4}. \tag{2.66}$$

Beside the terms with constants $\frac{1}{2}\alpha_i$ and $\frac{1}{2}\delta_i$, with i=S,V,R, the terms in Eq. (2.48) can be interpreted as exchange term corrections. If we take α_i, δ_i, and the remaining parameters as free parameters, this Lagrangian density is nothing else but the point-coupling model of ref. [20, 31, 35, 19]. Therefore this approximation qualitatively corresponds to a point-coupling approximation, even though quantitatively the value of every nonlinear coupling constant is different. The equation of state from this Lagrangian density in the spherically symmetric case can be found in Appendix C.

Before we go any further, let us see the features of our formula in figure 2.2 for a Lead nucleus and figure 2.3 for an Oxygen nucleus, where

$$I_s = \frac{m_s^2}{M_B^2}\rho_s^2$$

$$
\begin{aligned}
dI_s &= \frac{k_s}{M_B^2}\rho_s\Delta\rho_s \\
I_{ts} &= (1/79k_s + \frac{32g_v^2m_s^4}{79g_s^2m_v^4}k_v + \frac{16g_r^2m_s^4}{79g_s^2m_r^4}k_r) \\
&* (\frac{1}{2M_B^2}\rho_s\Delta\rho_s + 2(\rho_s^2-\rho_o^2) - \frac{4g_s^2}{m_s^2M_B}\rho_s(\rho_s^2-\rho_o^2) + \frac{2g_s^4}{m_s^4M_B^2}\rho_s^2(\rho_s^2-\rho_o^2)) \\
I_{tv} &= -(8/79k_s + \frac{19g_v^2m_s^4}{79g_s^2m_v^4}k_v + \frac{19g_r^2m_s^4}{158g_s^2m_r^4}k_r) \\
&* (\frac{1}{2M_B^2}\rho_s\Delta\rho_s + 2\rho_o^2 - \frac{4g_s^2}{m_s^2M_B}\rho_s\rho_o^2 + \frac{2g_s^4}{m_s^4M_B^2}\rho_o^2\rho_s^2 - \frac{2g_v^4}{m_v^4M_B^2}\rho_o^4) \\
I_{tsnl} &= (1/79k_s + \frac{32g_v^2m_s^4}{79g_s^2m_v^4}k_v + \frac{16g_r^2m_s^4}{79g_s^2m_r^4}k_r) \\
&* (-\frac{4g_s^2}{m_s^2M_B}\rho_s(\rho_s^2-\rho_o^2) + \frac{2g_s^4}{m_s^4M_B^2}\rho_s^2(\rho_s^2-\rho_o^2)) \\
I_{tvnl} &= -(8/79k_s + \frac{19g_v^2m_s^4}{79g_s^2m_v^4}k_v + \frac{19g_r^2m_s^4}{158g_s^2m_r^4}k_r) \\
&* (-\frac{4g_s^2}{m_s^2M_B}\rho_s\rho_o^2 + \frac{2g_s^4}{m_s^4M_B^2}\rho_o^2\rho_s^2 - \frac{2g_v^4}{m_v^4M_B^2}\rho_o^4).
\end{aligned}
\tag{2.67}
$$

I_s represents the energy density contribution from the scalar direct nonderivative term. The scalar direct derivative term is represented by dI_s. I_{ts} is the scalar part of the exchange contribution from the derivative terms. I_{tsnl} represents the same quantity as I_{ts} but it takes into account only the nonlinear parts. The $I_{tv/tvnl}$ are similar to $I_{ts/tsnl}$, but come from the contribution of the vector part. From those figures we can see that the contributions of I_{ts} and I_{tv} still have the same order of magnitude as the contribution of the direct derivative term (dI_s), as expected. In the coupling constant redefinition process, the linear parts of the exchange of derivative terms is already absorbed, only the nonlinear parts are left ($I_{tsnl/tvnl}$). The nonlinear term from the scalar part I_{tsnl} still has more or less the same order of magnitude as dI_s, but I_{tvnl} has a larger contribution than dI_s but still smaller than I_s. It is clear now, under the approximation above, that the large value of the nonlinear contribution from the vector part appears because it is needed to compensate the linear part which is already absorbed in the coupling constants redefinition, not because the contribution from the vector part is simply too large. Of course the value of $I_{tsnl/tvnl}$ depends on the parameters we use, but the compensational nature of our approximation does not depend on the parameters.

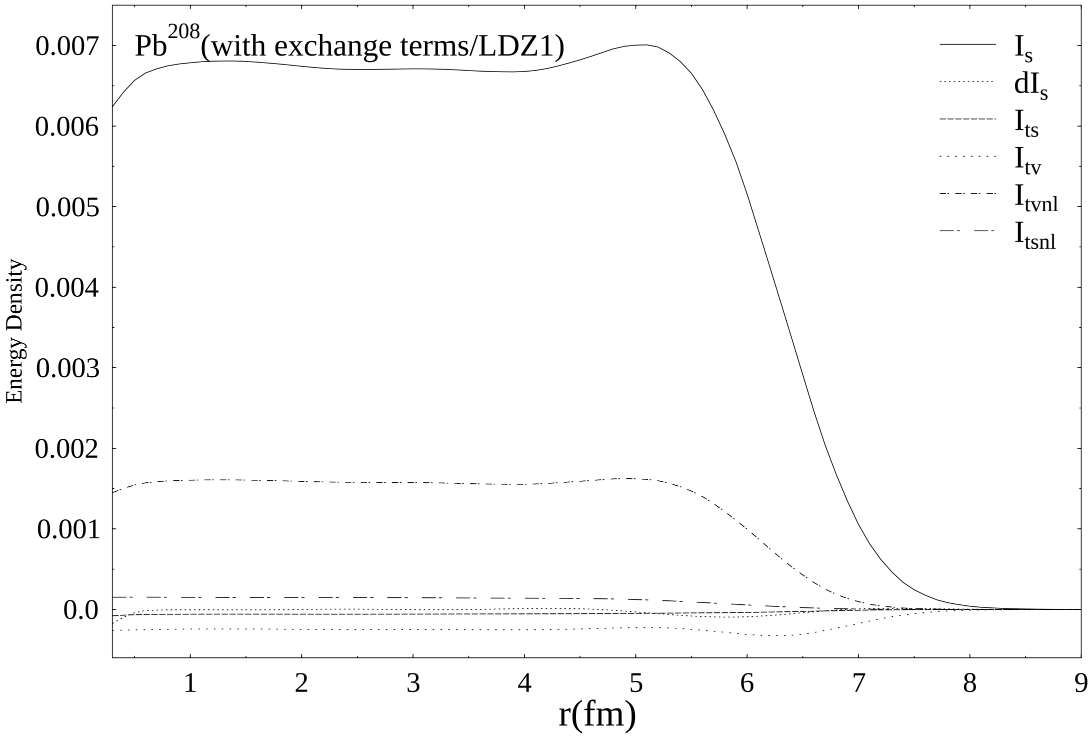

Figure 2.2: Comparison of the potential energy density from the exchange of the derivative terms with the potential energy density of the corresponding direct terms in Lead. The symbols are explained in the text.

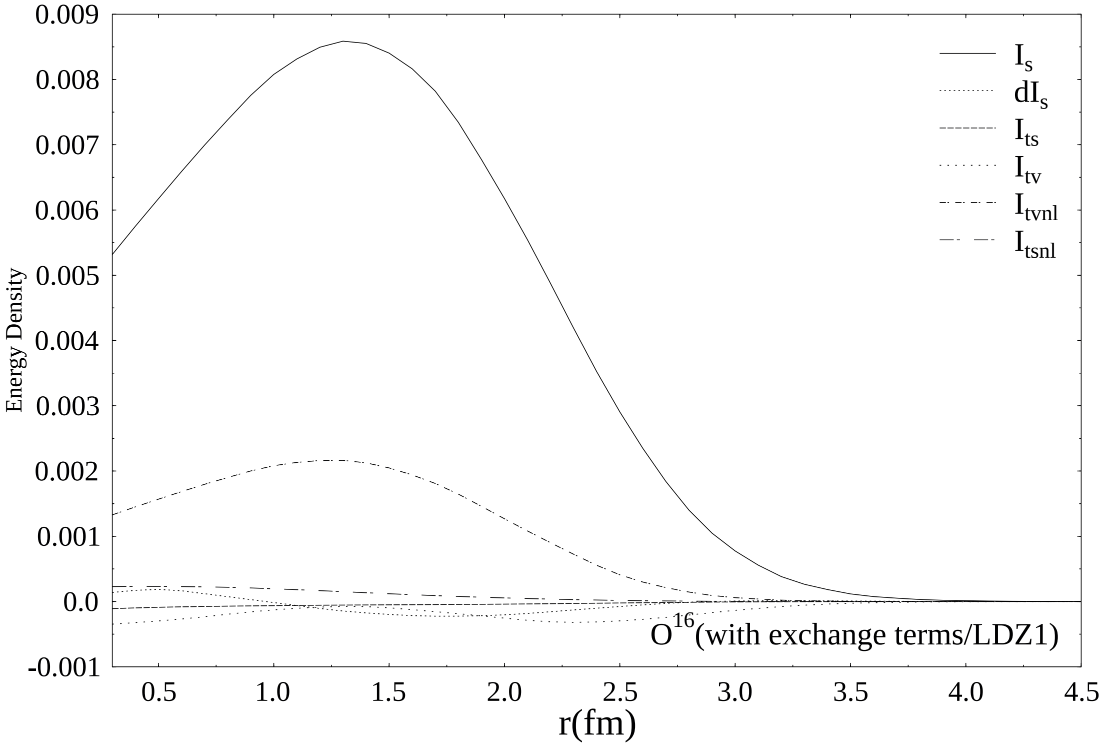

Figure 2.3: Comparison of the potential energy density from the exchange of the derivative terms with the potential energy density of the direct terms in Oxygen.

2.3 Long-range Effect

Figures 2.4 and 2.5 may help to give a clearer understanding of what I mean by the long-range effect. The following additional definitions have been used in figs 2.4 and 2.5: Δe_0 the difference between e and e_1, Δe_1 the difference between e and e_2, Δe_3 the difference between e and e_4, $\Delta e_a/e$ the ratio of e_1 and e, $\Delta e_b/e$ the ratio of ($e_2 - e_1$) and e, and finally $\Delta e_c/e$ shows the deviation of the ratio of e_2 and e from unity.

We see from both figures that for Oxygen, Zirconium and Lead e_2 is closer to e than e_1 or Δe_1 is closer to zero than Δe_0, and one can see also that $\Delta e_a/e$ is close to one and $\Delta e_b/e$ and $\Delta e_c/e$ close to zero and also for large radii $\Delta e_b/e$ is smaller then $\Delta e_c/e$. These facts show that the density expansion in the sigma field tends to be convergent and that for large radii and larger mass numbers this behaviour appears more significant, but the difference between the exact and the approximate form creates a significant effect if we calculate the equation selfconsistently (we have already used the density-dependent potentials in the calculation). The calculation with approximation like the point-coupling model produces a different density than the exact calculation. This fact can be seen comparing Δe_3 with Δe_1 or e_2 with e_4 and the figure of the density versus radii in fig. 2.4. The most significant difference appears in the region of small r. It is clear because in this region the approximation breaks down. Adding a parameter in front of the derivative term and a fitting procedure can help a little bit to reduce the discrepancy, but we can see from the figures that in the region around r equal zero the approximation still shows different behaviour from the exact form. Therefore we can raise the question to what extent this fact has effects in predictions of observables for finite nuclei.

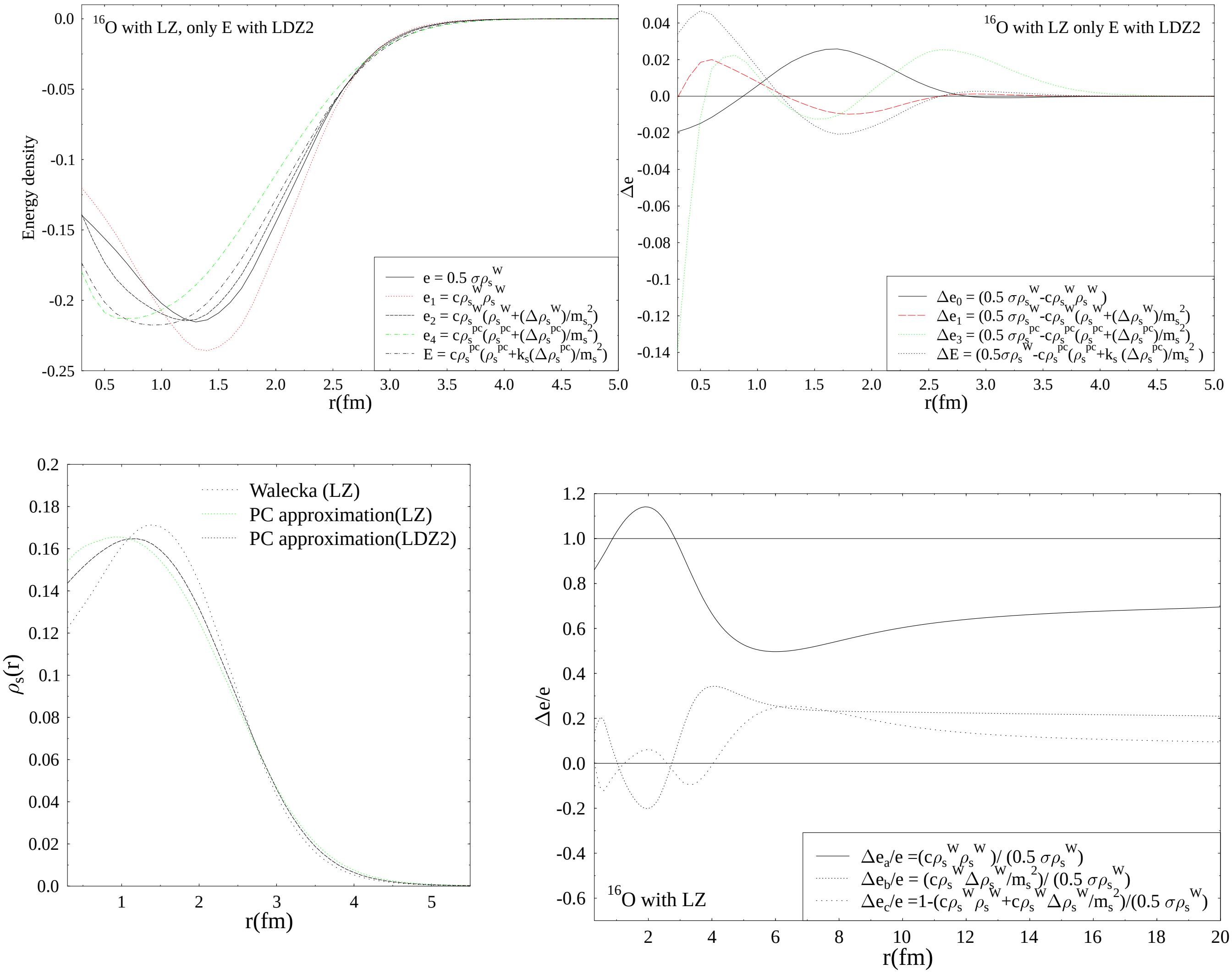

Figure 2.4: Long-range effect in the scalar potential energy of Oxygen.

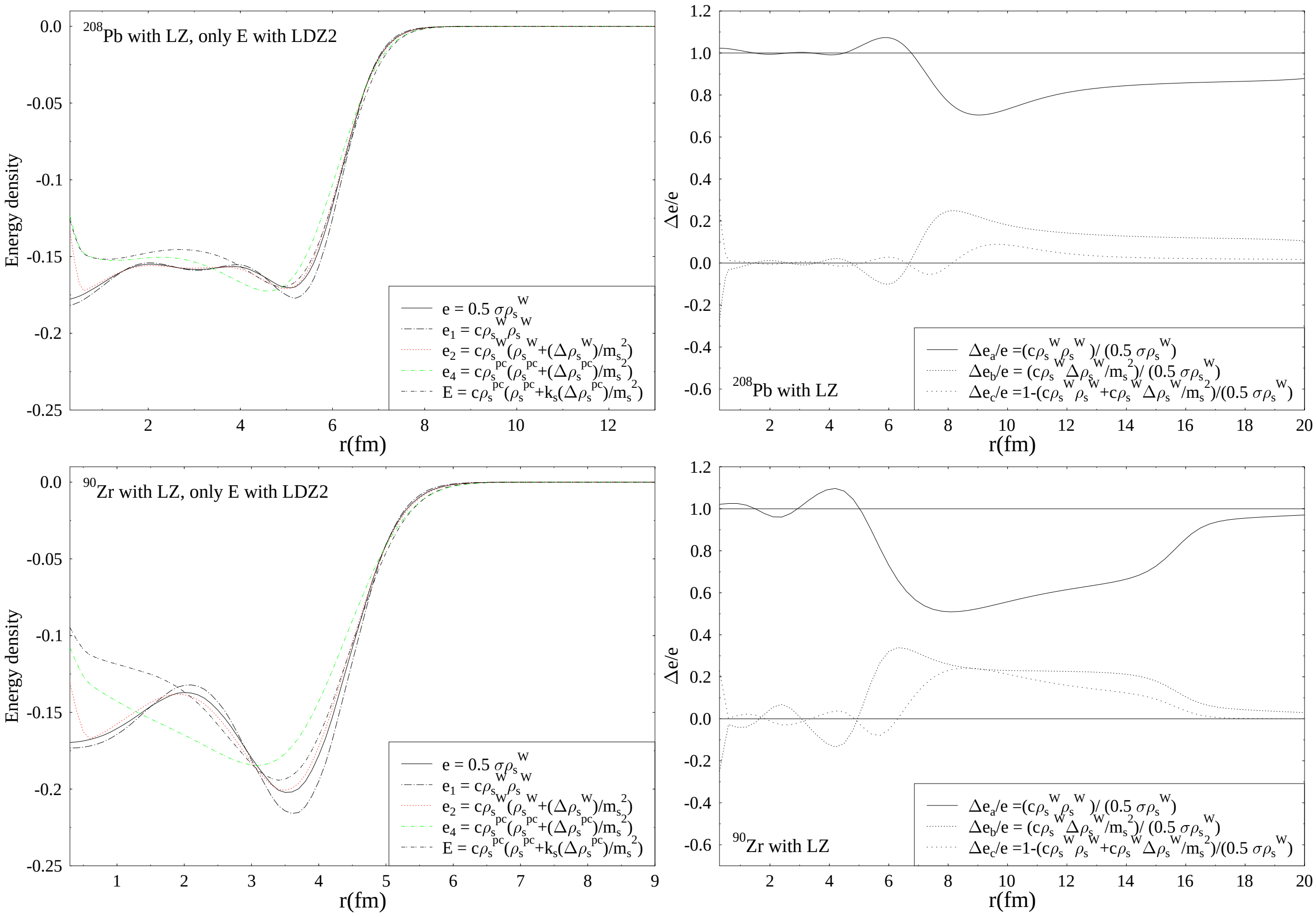

Figure 2.5: Same as the first and fourth figures in figure. 2.4 but for the Lead and Zirconium cases, respectively (top and bottom).

2.4 Summary of Approximations Made

It will be useful for the reader to summarize the approximations made together with the motivation for each.

1. **Low momentum expansion of the meson propagator (2.12)**
   The physical motivation of this approximation is clear: the nucleons in nuclei move slowly. We can use figures 2.4 and 2.5 as motivation of this approximation, but two difficulties still appear if we take all orders of the expansion in this approximation, namely the numerical and the physical interpretation. The first problem is the appearance of fluctuations around r=0 from the terms with the derivative of the densities calculated in higher than second order by using the four point formula. It seems that a more suitable numerical formula is needed in this case. This could be handled with some effort, but the second problem is more difficult: the equation of motion will be an n-th-order differential equation due to the derivative exchange terms, where n-2 is the order of the derivative; what is the meaning of this equation ? It seems that a deeper investigation is needed to understand this situation.

2. **Second-order derivative approximation with additional parameters (2.13)**

   We take the derivative expansion only up to second order. The effects beyond the second-order approximation, partly, are simulated by additional parameters. Due to this approximation, the Lagrangian density of the linear Walecka model now corresponds to the Lagrangian density of the linear Hartree-Fock point-coupling model (see (2.15)).

3. **Linearisation of the equation of motion**
   The exact equations of motion from the above approximate Lagrangian density are fourth-order differential equations due to the derivative exchange terms. A part of the new densities ($C_{i\alpha}$ and $B_{i\alpha\mu}$) are responsible for this feature. An order of magnitude analysis of $B_{\alpha\mu}$ shows that these parts are small. If we suppose that a similar situation happens for all $C_{i\alpha}$ and $B_{i\alpha\mu}$, then neglecting these small parts from each new density will lead to second-order differential equation (Dirac equation). From the opposite point of view, we can obtain the approximate densities $C_{i\alpha}$ and $B_{i\alpha\mu}$ if we start from the Dirac equation.

4. **The approximate densities $C_{i\alpha}$ and $B_{i\alpha\mu}$**
   We calculate these densities by using the Gordon decomposition of the general Dirac equation (2.39) and with an approximate form of m^*, V^α and $T^{\alpha\beta}$ (see Eq. (2.43)).

2.5 Determination of Parameters

Before the fitting process (search the minimum error of the calculated observables), we need a trial input parameter set, which should make the iteration process in the Hartree code convergent. Until now, I have not been able to find the right trial parameters if I take into account the leading nonlinear terms ($\mathcal{L}^*_{non-lin}$). The reason is not clear. It could be that we should use not only the leading but also all nonlinear terms or our approximation gives the wrong nonlinear terms or that simply the right trial parameters have not been obtained yet. An investigation in this direction is, of course, necessary but it is still worthwhile to first pursue this study without nonlinear terms as a preliminary step, to examine how this approximation works. Neglecting nonlinear terms, in other words, corresponds to making the following approximation in Eq. (2.43) : $m^* \sim m_B$, V^ν=$T^{\nu\mu}$ $\sim$ 0. We call the parameters under this rough approximation LDZ1 and we will compare it with LDZ2 and study both numerically. LDZ2 denotes the parameters which for the case without exchange corrections. The corresponding Lagrangian were given in (2.49). Then we compare both of them with LZ and NLZ from Ref [7]. To make the result comparable to Refs. [2, 7], we follow their fitting procedure, choosing the same set of physical observables (the binding energies, diffraction radii and surface thicknesses of the ^{16}O,^{40}Ca,^{48}Ca,^{58}Ni,^{90}Zr,^{116}Sn,^{124}Sn, and ^{208}Pb) and weights (0.2% relative error for the binding energies, 0.5 % for the diffraction radii and 1.5% for the surface thicknesses) also using the constant gap pairing correlation [2, 7]. Our parameters are g_s, g_v, g_r, k_s, k_v and k_r (six parameters). In our approximation, we take m_s = 551.31 MeV, m_v = 780 MeV and m_r=763 MeV as fixed parameters.

2.6 Results and Discussions

In table 2.2, we collect our χ^2 results and compare to the linear and the nonlinear Hartree models [7]. Here LZ (a linear one) and NLZ (a nonlinear one) denote parameter sets from Refs. [7]. BE, DR and ST denote the binding energy, diffraction radii, and surface thicknesses. It will be helpful for the reader to collect the definiton of each parameter set which will be discussed in this section into one table as follows:

1. LZ : Walecka model, no nonlinear terms, exchange omitted
2. NLZ : Walecka model, with nonlinear terms, exchange omitted
3. LDZ1 : Point-coupling model, no nonlinear terms, exchange included

4. LDZ2 : Point-coupling model, no nonlinear terms, exchange omitted.

In LZ and NLZ one uses four and six free parameters respectively. Another interesting conclusion which can be found in Ref. [6] is "In the linear RMF model, the addition of two free parameters in the form of an omega and a rho meson mass (this parameter set is denoted L1 with $\chi^2/nucleus \sim 250$) and also the addition of other mesons or tensor couplings does not improve significantly the χ^2". Therefore we could say that the comparison of our approximation with the RMF model by using the LZ parameter set is still fair in the sense that if we use L1 as comparator, it still does not much change the conclusion. Global information which can be obtained from table 2.2 is that the parameter set with the exchange correction (LDZ1) gives a better χ^2 than the one without the exchange correction (LDZ2, LZ) in binding energies, surface thicknesses and diffraction radii, LZ has a better χ^2 in the diffraction radius than LDZ2, but basically they have the same quality of predictions, as we will see later. This fact gives us as an indication that large parts of the "long-range effect" or the effect beyond the second order approximation can be absorbed in the parameters k_i. If we compare LDZ1 (χ^2/nucleus $\sim$ 67.2) with a full Hartree-Fock result in Ref. [26] with χ^2/nucleus $\sim$ 20-46, it shows that our approximation works quite well. Comparing the global results in table 2.3 of LDZ1 with NLZ, most differences concern the surface thickness, but later we will see that after more systematic investigations in every observable, this is not really the case.

The values of our parameters sets can be seen in table 2.3. The values of the parameter set LDZ1 in table 2.3 are the values after redefinition (2.49), the original parameters can be obtained easily from these values with an inverse transformation. Comparing the coupling constants of LDZ2 and LDZ1 in table 2.3 with LZ (see the value in Refs. [7]), they have similar magnitude. Values of the parameters k_i not close to unity indicate that the long-range effect is strong. LDZ1 has smaller k_s and k_v values than LDZ2, with k_v even different in sign. LDZ1 has a larger k_r value then LDZ2. This shows that the exchange effect changes the relative magnitude of every contribution in the derivative terms.

χ^2	BE	DR	ST	Total
LZ	800.94	46.01	1668.99	2515.94
LDZ2	872.21	70.09	1250.96	2193.27
LDZ1	89.31	18.58	429.31	537.20
NLZ	23.89	18.77	29.25	71.92

Table 2.2: χ^2 results from various approximations. BE denotes the binding energies, DR the diffraction radii and ST the surface thicknesses.

Parameters	g_s	g_v	g_R	k_s	k_v	k_r
LDZ1	11.1437	13.8016	11.3544	0.2213	-0.2996	1.3419
LDZ2	11.4202	14.1580	11.3443	0.7998	0.8173	0.6999

Table 2.3: Values of the six free parameters after they are fitted, LDZ1 denotes the parameter set of the point coupling approximation which takes into account the exchange corrections and LDZ2 the parameter set without exchange corrections.

In figure 2.6 we compare the E/A and charge radius calculations of our work with the LDA calculation from Ref. [27]. We have better E/A results than the LDA for lighter nuclei and a similar result for heavier nuclei. For the charge radius we have a similar quality of results as the LDA calculation. Besides, the χ^2 of LDZ1 is not too far from Ref. [26]. This result also can be used as a rough probe to see how much relevant information is lost in our approximation.

Before we study the results in more detail, we will investigate the validity of the approximation which we already used in Eq. (2.43) by examining every contribution in its potential with the LDZ1 parameter set. Investigating two cases, ^{208}Pb and ^{16}O, the global behavior of the potentials should be adequately represented. The result can be seen in figure 2.7 for the ^{208}Pb case and figure 2.9 for the ^{16}O case. Figure 2.8. and figure 2.10. are the same figures but with a different scale. In figures 2.8 and 2.10, we show the behavior of the non-dominant contributions, which cannot be seen in the previous figures. From figures 2.7 and 2.9 it is clear that both nuclei have the same potential behaviour, i.e. the $\mathrm{Q_{s,v}} = (\text{-},+)\frac{g_{s,v}^2}{m_{s,v}^2}\rho_{s,v}$ give the dominant contribution in the potential ($\mathrm{Q_s}$ in an attractive part and $\mathrm{Q_v}$ in a repulsive part) if we compare them with the contribution from the isovector parts ($\mathrm{Q_{r,d}}$), the derivative parts ($\mathrm{dQ_i, i = s, v, r, d}$) and the tensor part ($\mathrm{Q_T}$). In figures 2.8 and 2.10, one can see that the isovector parts are more important than the derivative parts in Lead, but the situation is opposite in Oxygen, where the derivative parts dominate over the isovector parts. The fact that the dominant contribution comes from $\mathrm{Q_{s,v}}$ can be used to give a justification for our approximation in Eq. (2.43).

To see the difference among the four parameters more clearly in binding energies of finite nuclei, we use the error in the binding energies (EBE) and the two-neutron ($\mathrm{S_{2n}}$) and the two-proton ($\mathrm{S_{2p}}$) separation energies from some isotopic and isotonic chains. The error in the binding energy is defined as

$$\mathrm{EBE} = \frac{\mathrm{E_{th}} - \mathrm{E_{exp}}}{\mathrm{E_{exp}}}, \tag{2.68}$$

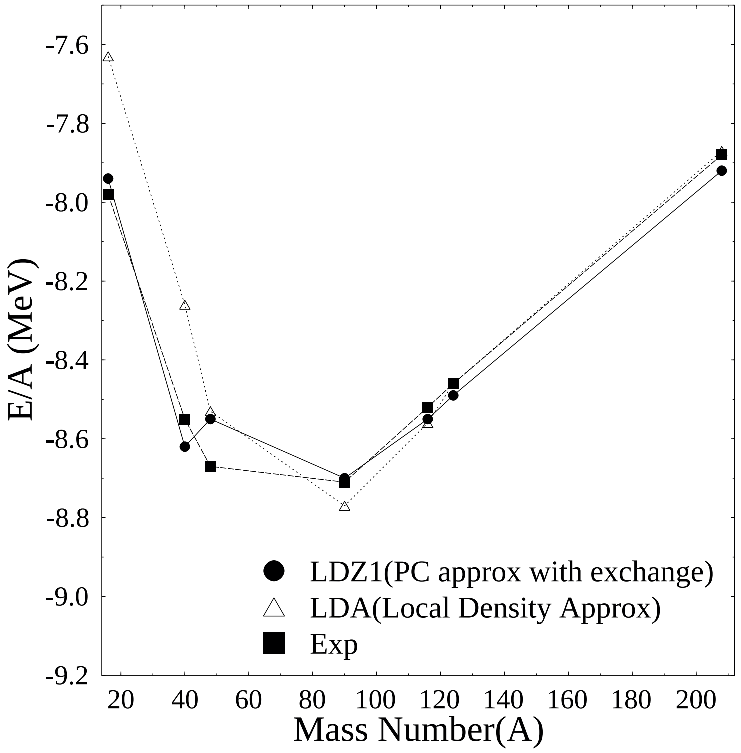

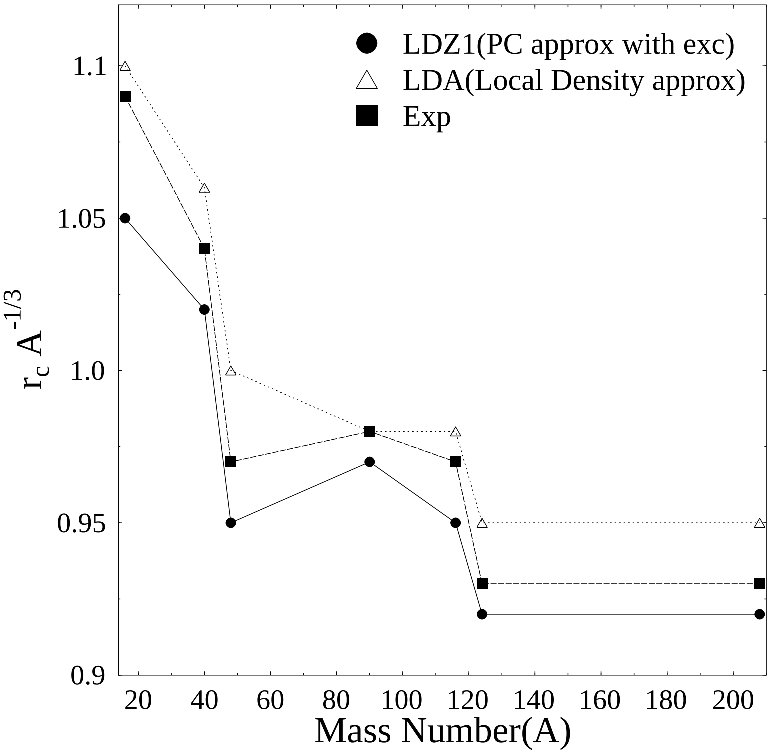

Figure 2.6: Comparison of binding energies per mass number and charge radii (r_c) of some spherical nuclei for LDZ1 with LDA calculations [27]. Lines in the figures are intended to guide the eye.

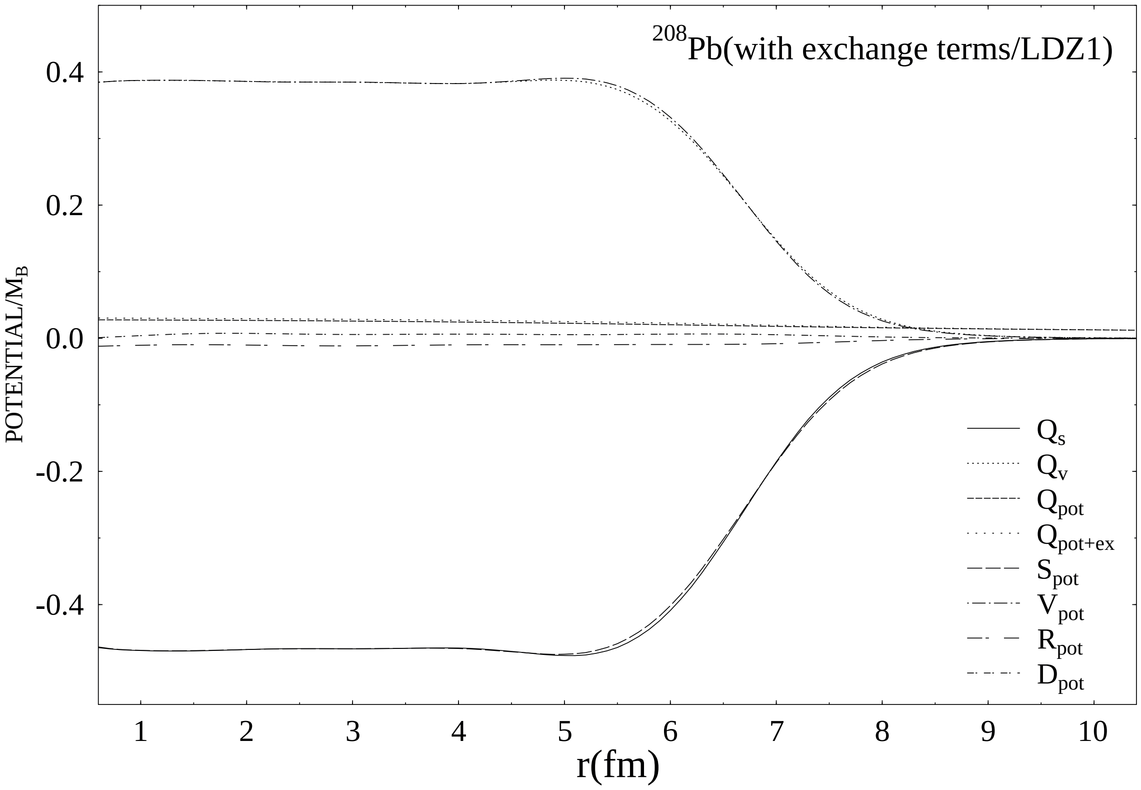

Figure 2.7: Every contribution in the scalar and the vector potential per nucleon mass as a function of radius (fm) in ^{208}Pb. Here we use the LDZ1 parameter set. The definitions are $\mathrm{Q_i} = \frac{s_i g_i^2}{m_i^2 m_B}\rho_i$, $\mathrm{dQ_i} = \frac{s_i g_i^2}{m_i^4 m_B}\Delta\rho_i$, $\mathrm{Q_t}$ = - $\frac{\theta_T}{m_B}\rho_i^T$, $I_{\mathrm{pot}} = \frac{V_I}{m_B}$, where "i" and "I" refer to the mesons s,v,r,d. V_I are the total potentials from meson I. $\mathrm{Q_{pot}}$ denotes the electromagnetic potential, g_i and θ_T are the coupling constants after redefinition. They represent effectively the contributions from the direct and exchange terms. s_i =1 for a repulsive potential and -1 for an attractive potential.

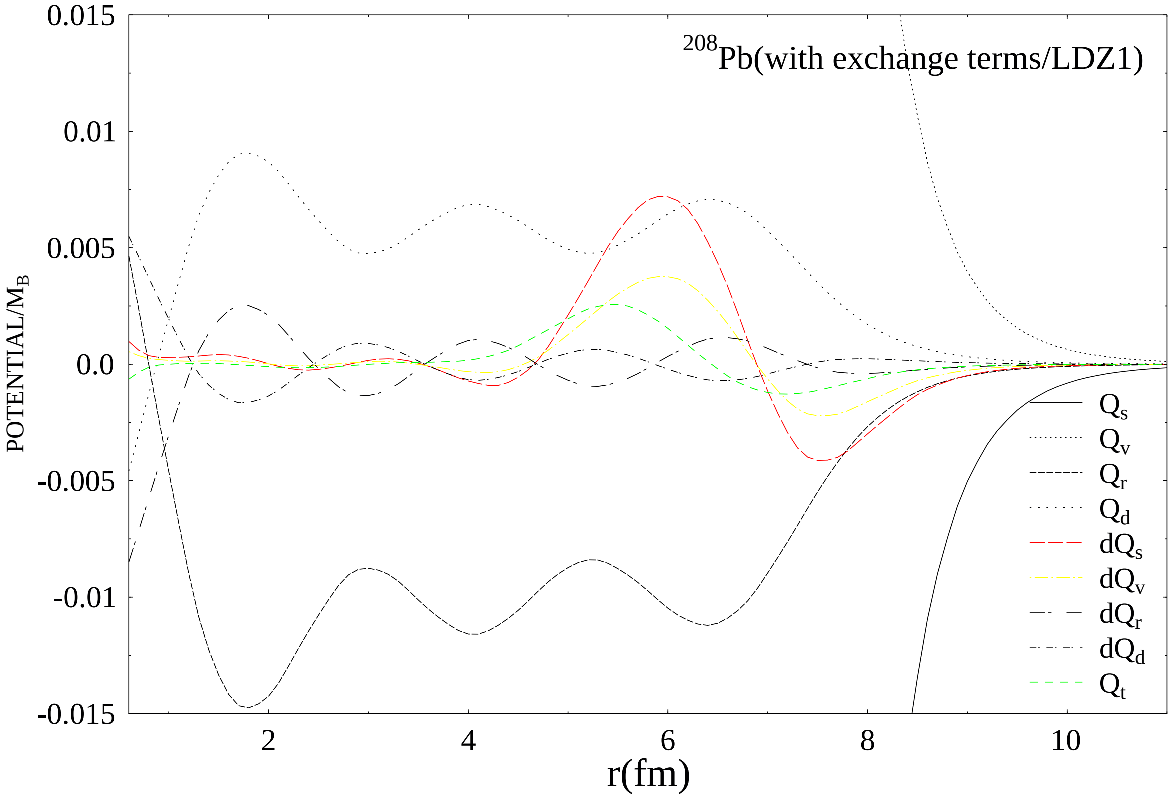

Figure 2.8: Same figure as figure 2.7 but with a different scale to show the minor contributions.

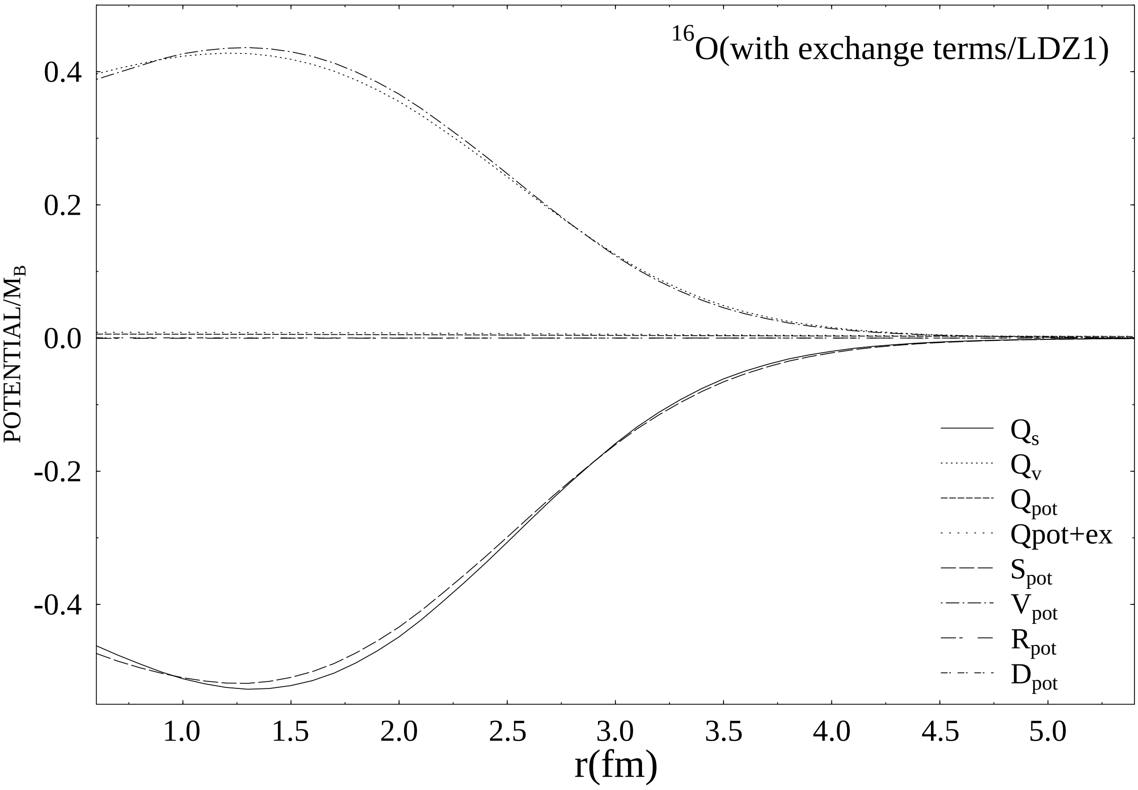

Figure 2.9: Same figure as figure 2.7, but for ^{16}O.

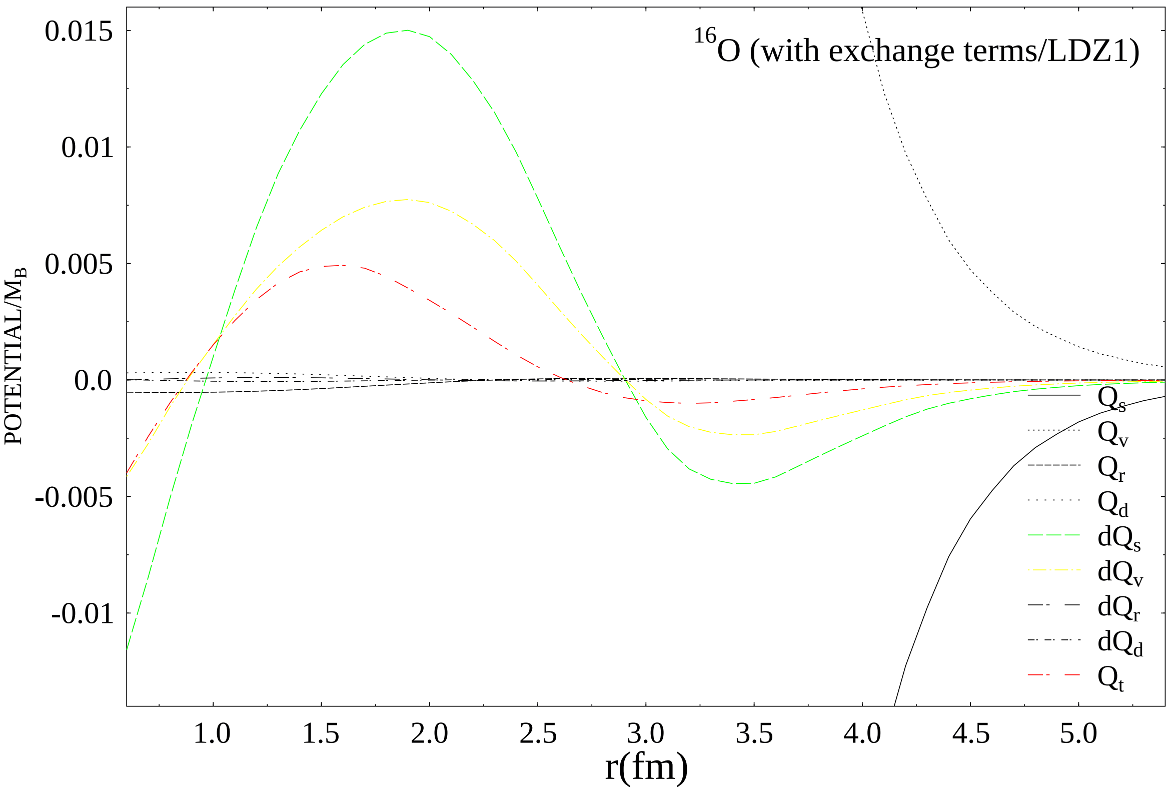

Figure 2.10: Same figure as figure 2.9 but with a different scale for the minor contributions.

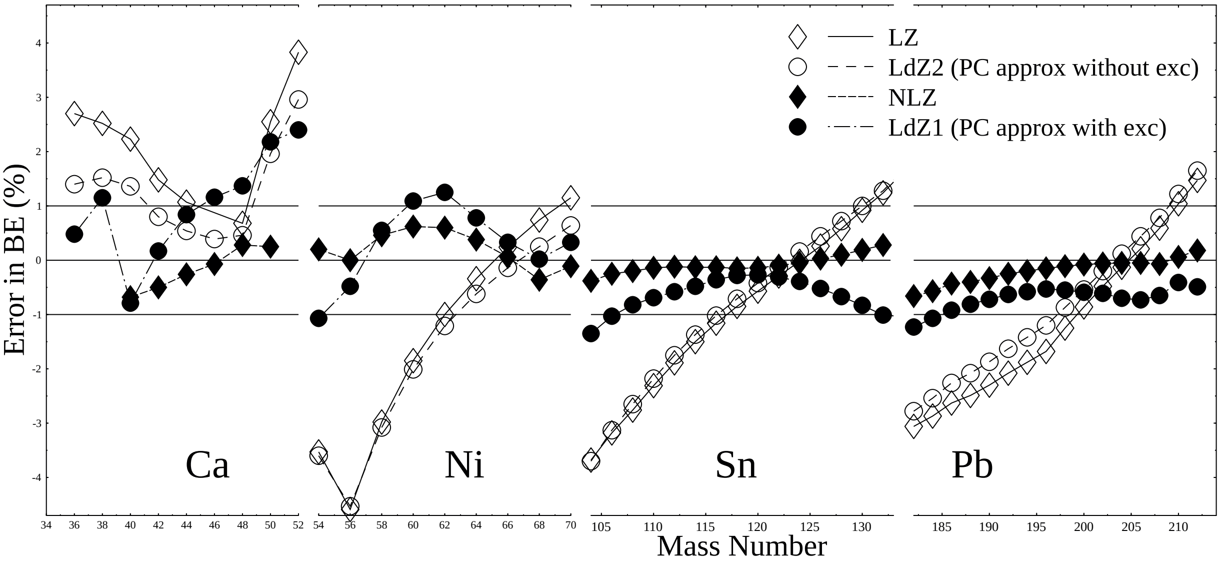

Figure 2.11: Error in the binding energies for the Ca, Ni, Sn and Pb isotopes.

while the S_{2p} and S_{2n} are defined as

$$S_{2n} = E(N, Z) - E(N - 2, Z), \tag{2.69}$$

and

$$S_{2p} = E(N, Z) - E(N, Z - 2) \tag{2.70}$$

respectively, with E(N,Z) the calculated binding energy. In figure 2.11 we give the EBE for the Pb, Sn, Ni and Ca isotopes, and the EBE for the N=82 and N=126 isotones in figure 2.12. As in the previous case, the lines in the figures appear only to guide the eye. From these figures, it is apparent that LDZ2 has the same trend as LZ in all cases with more than 1 % error. This can be understood due to the fact that these parameter sets have $\chi^2_{\rm BE}$ of the order of 800-900 (see table 2.2), so that it is clear that both of them have the same quality of prediction in EBE. Of course they could be similar in one observable but behave differently for the others, therefore we will investigate this fact later.

In the isotope chains, LDZ1 has better EBE results than LZ and LDZ2. LDZ1 has about ± 1 % error for the Ni, Sn, and Pb isotopes, but gives more than 1 % error in the larger neutron numbers of the Ca isotopes. In the isotonic chains, on the other hand, LDZ1 delivers worse predictions than LZ and LDZ2. This fact shows that even though LDZ1 has

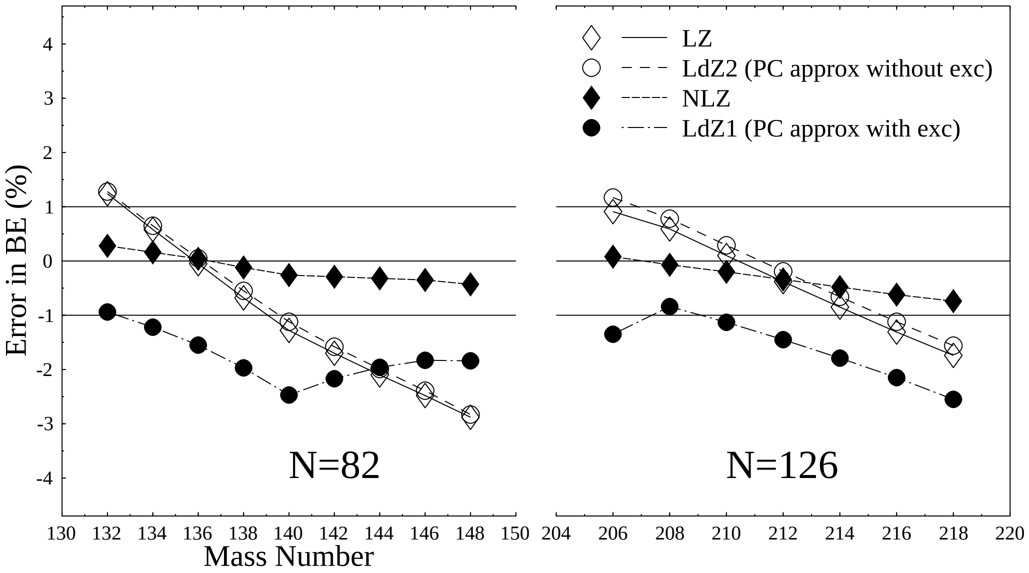

Figure 2.12: Error in the binding energies for the N=82 and N=126 isotones

better χ^2 than LZ and LDZ2 in binding energies, it does not mean it has better binding energy predictions for all spherical nuclei. We can also see that although the χ^2_{BE} of NLZ is not drastically different from that of LDZ1, NLZ yields much better predictions than LDZ1 for these isotopic trends.

Figure 2.13 shows that while in the heavier isotopes LDZ1 can reproduce the experimental data, this is not true for the isotones (in figure 2.14). This fact can be understood because LDZ1 has a relatively good EBE prediction in the isotopic chains but not isotonic chains (see once again figs 2.11 2.12). In general, the averages of S_{2n} and S_{2p} from LDZ1 are better than LDZ2 and LZ. This is due to the fact that LDZ1 gives better predictions in the isotopic cases and a little bit better trend of EBE in the isotonic cases than LZ and LDZ2. The same trend and quality of the S_{2n} and S_{2p} predictions from LZ and LDZ2 emphasize the EBE results that even though LZ and LDZ2 have slightly different χ^2, they have similar predictive power in binding energies. Here we can also see an important role of the nonlinear terms for the prediction of binding energies, because only NLZ can reproduce the S_{2n} and S_{2p} experimental data for almost all represented isotopes and isotones.

Basically we have not so different prediction qualities in binding energies from LDZ1 and LDZ2. This result is in agreement with Ref. [26]. The differences from Ref. [26] are that here we parameterized the same number of experimental observables as LZ, we took into account the pairing correlations and analysed the binding energies systematically. But

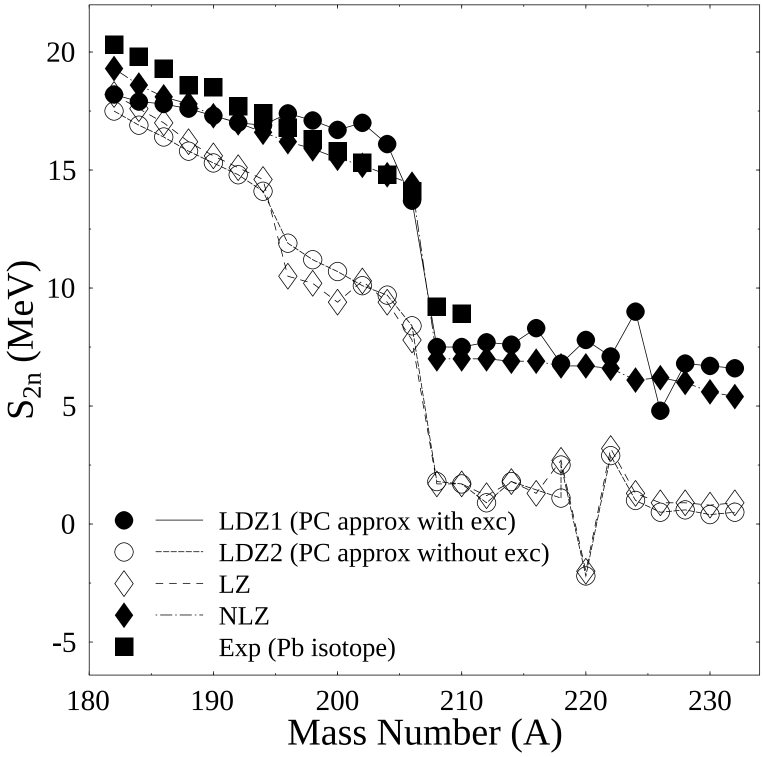

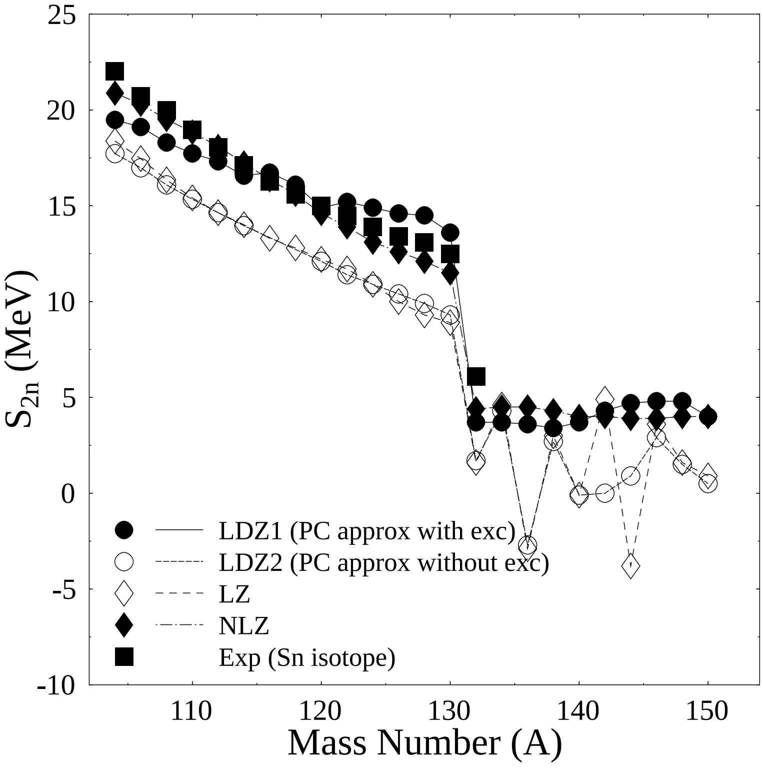

Figure 2.13: Two-neutron separation energies (S_{2n}) for the Sn and Pb isotopes.

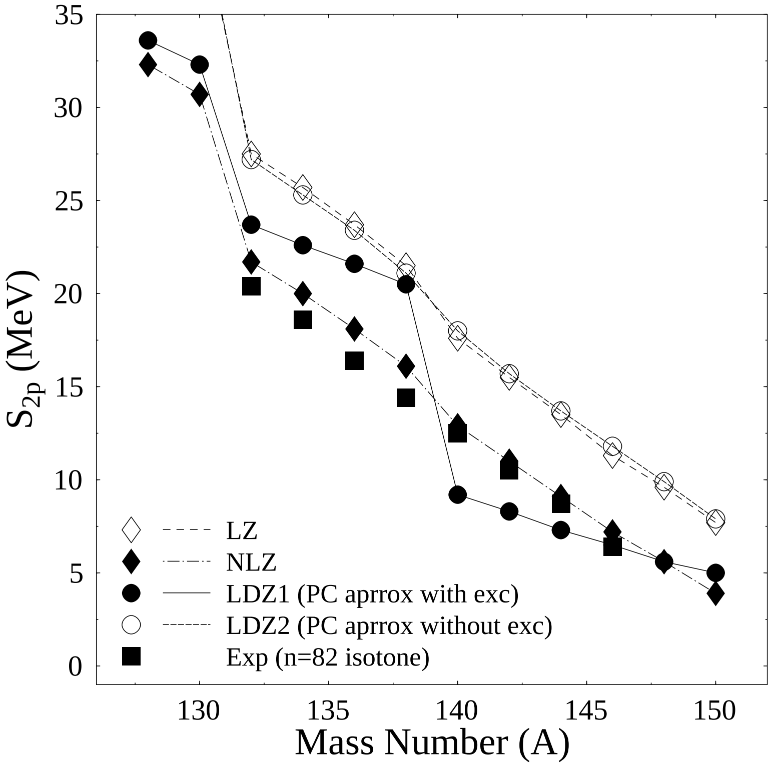

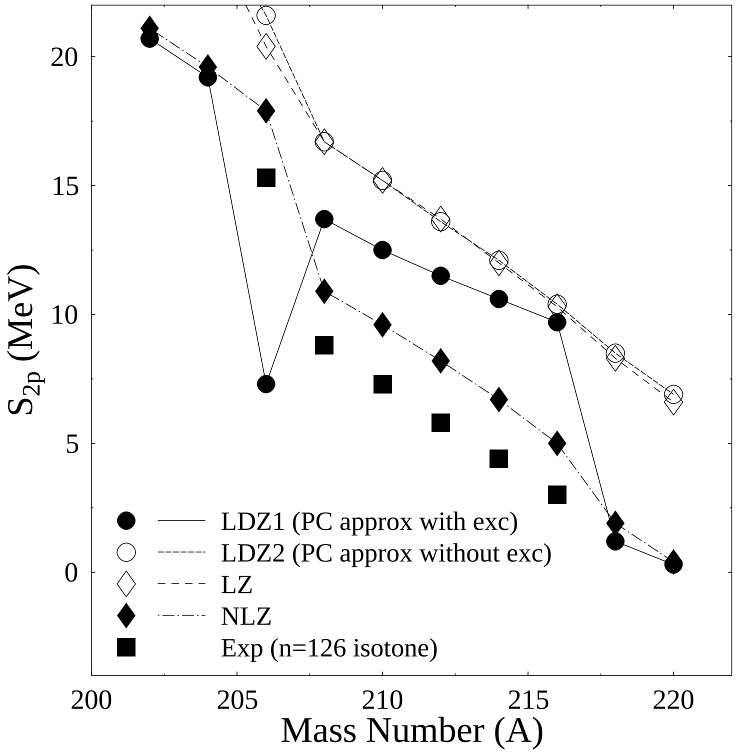

Figure 2.14: Two-proton separation energies (S_{2p}) for the N=82 and N=126 isotones.

instead of using exact finite range Fock terms as Ref. [26], we use a point-coupling-like approximation and only a rough approximation in the Fock terms of the derivative parts. We find also that the exchange correction plays a role for binding energies in the isotopic chains, but not for the isotonic chains. It is not clear whether this is a general feature or due to approximations. The insignificant difference in the binding energy predictions between LZ and LDZ2 gives an indication *that the long-range effects of meson propagators in binding energy predictions are already absorbed effectively into the coupling constants of any linear point-coupling model.*

As a next step, we show the predictions of the four parameter sets through observables which are extracted from scattering data, namely the diffraction radii and the surface thickness. Errors in the diffraction radius and the surface thicknesses are defined similarly as for the binding energies. Results for the diffraction radii (EDR) can be found in figure 2.15 and for the surface thickness (EST) in figure 2.16. Figure 2.15 shows that the parameter sets behave quite differently in each isotopic chain. LDZ1 and NLZ have an error of less than ± 2 %. In the Oxygen and Zirkonium isotopes LZ and LDZ2 have an error of more than ± 2 %. This result is expected as in ref [26] and can be understood because LDZ1 and NLZ have better χ^2 then LDZ2 and LZ. But because the difference is not really significant, we can say that basically they have similar predictions in EDR. It is shown that LDZ2 and LZ have a similar trend of the EST, namely, they have an EST of more than 20 % . LDZ1 has an EST value still in the range below 20 %. Here we can see clearly that the exchange effect has an important role in the surface thickness prediction but it is still a bad result if we compare with NLZ which has an EST value below 10 %. This confirms the result of ref. [26] that the relativistic linear HF calculation still cannot give acceptable surface thickness predictions. This figure shows us also that only models which include the nonlinearities can give acceptable surface thickness predictions.

To round off the above results we also calculated the charge distributions of ^{208}Pb and ^{16}O, shown in figure 2.17, and the single-particle spectra of ^{208}Pb and ^{16}O both for protons and neutrons, see figures 2.18 and 2.19. The error of the spin-orbit splitting can be found in figure 2.21. The experimental values of the single-particle spectra are from Ref. [36]. For the Oxygen case we obtain that LDZ1 has better charge density predictions then LDZ2 and LZ, but for the ^{208}Pb case it shows strong fluctuations in the surface part of the density and gives quite large a value of ρ_P(r) at r ≈ zero fermi. Here we cannot reproduce the result of Ref. [26] for the ^{208}Pb case. This fact is probably due to that we use a rough approximation for the exchange of the derivative terms.

For the single-particle spectra of protons and neutrons in ^{16}O, all parameter sets reproduce the experimental data. Only the $1S_{1/2}$ state is more deeply bound in experiment than NLZ. We can see also that LZ and LDZ2 show almost identical results. For the ^{208}Pb case, LZ and LDZ2 have the same trends. In the neutron case, LDZ1 gives a rather bad prediction

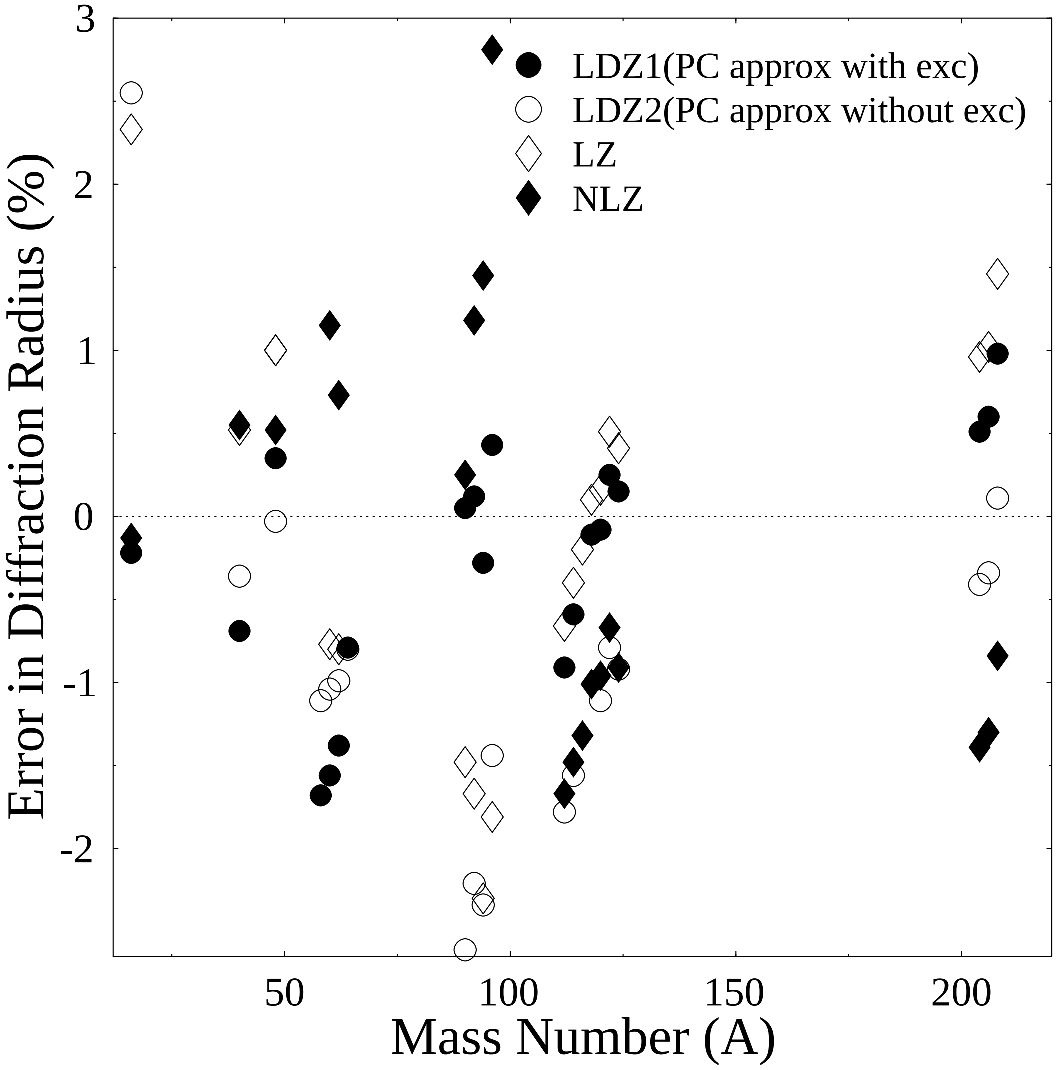

Figure 2.15: Errors in the diffraction radii for some spherical nuclei.

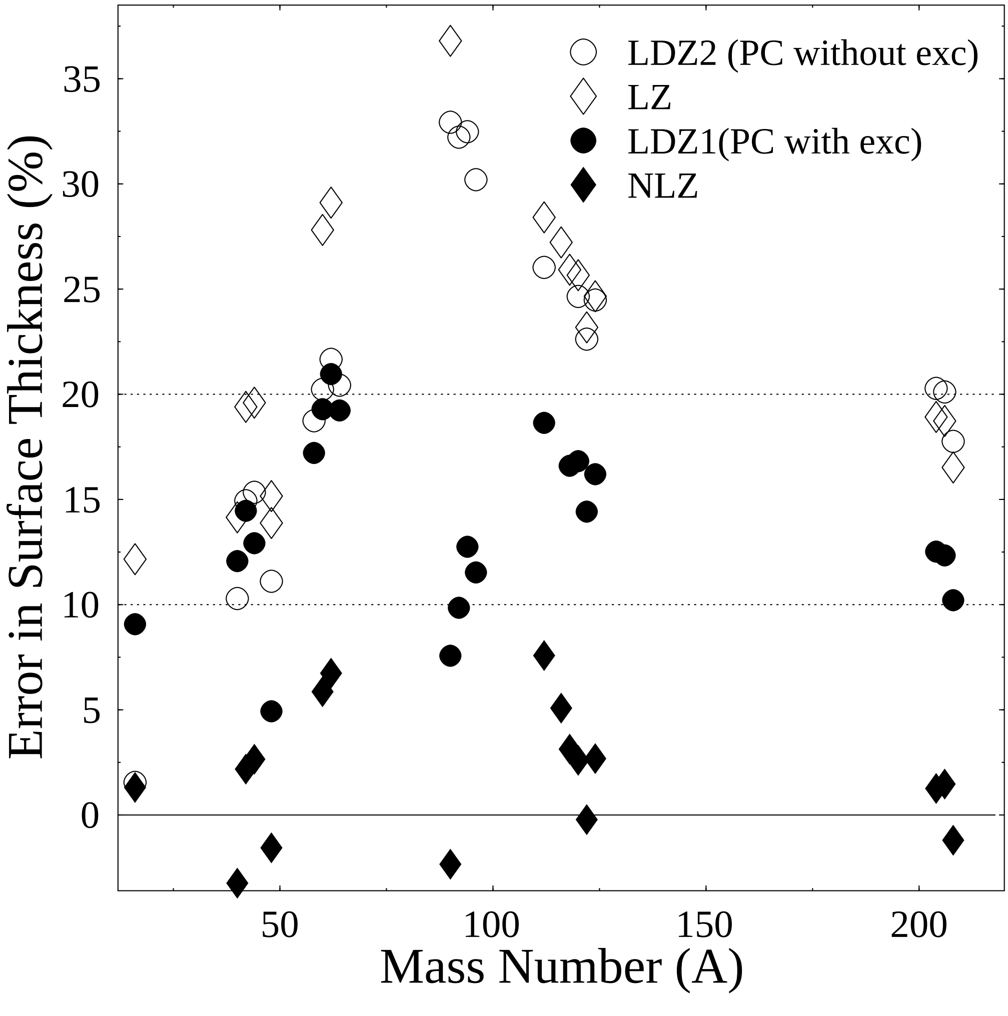

Figure 2.16: Error in the surface thicknessess for some spherical nuclei.

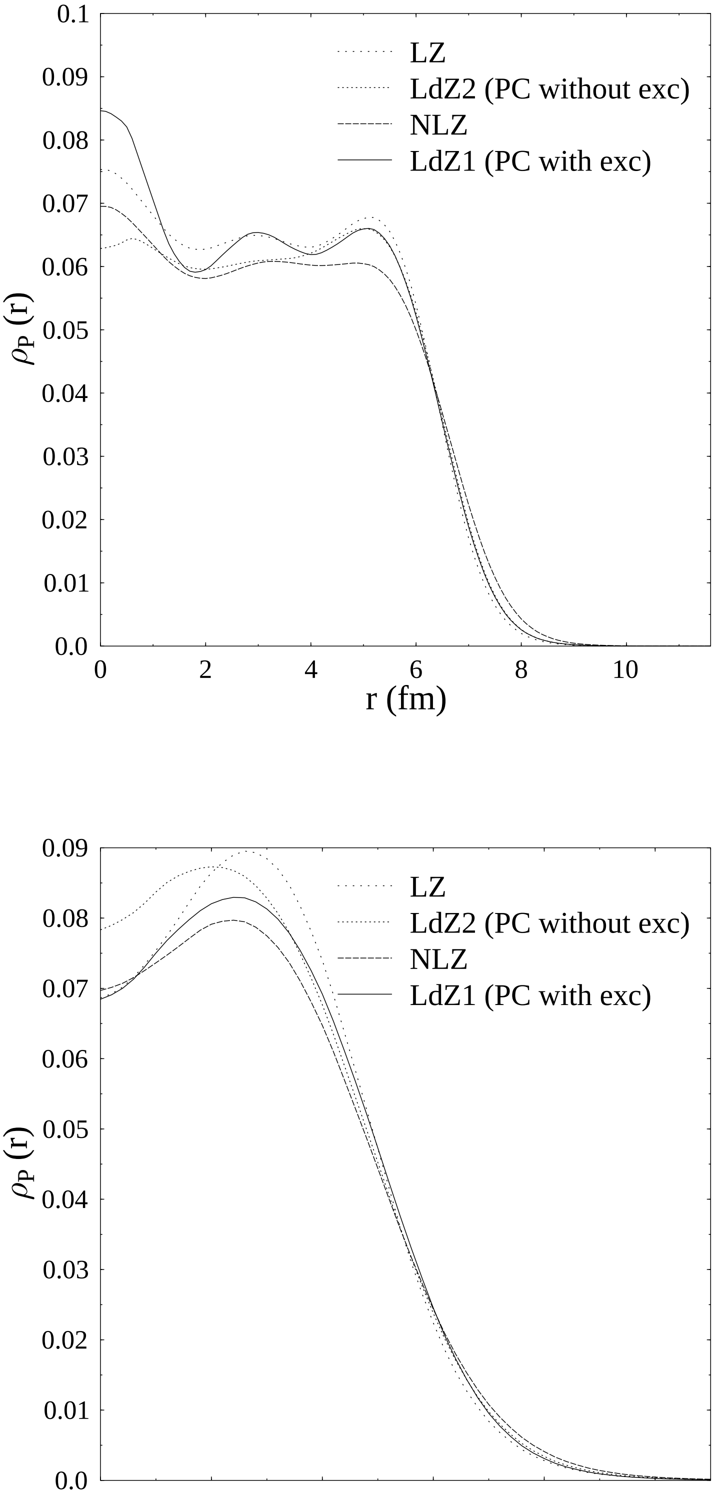

Figure 2.17: Radial charge density for ^{208}Pb and for ^{16}O.

parameter sets	$p_f(fm^{-1})$	E/A(MeV)	K(MeV)	M*/M	a_4(MeV)
LZ	1.3	-17.1	584.4	0.53	48.8
LDZ2	1.3	-16.7	553.0	0.54	48.9
LDZ1	1.3	-15.9	550.7	0.54	36.2
NLZ	1.3	-16.2	173.5	0.59	41.8

Table 2.4: Properties of nuclear matter from various approximations. Here p_f denotes the Fermi wave number, E/A the binding energy per nucleon, K the compressibility, M* the effective mass and a_4 the symmetry energy per nucleon

for the $1h_{9/2}$ state. Beside this state LDZ1 is intermediate in quality between LZ and LDZ2, on the one hand, and NLZ on the other. This also happens for the ^{208}Pb proton and for the ^{132}Sn cases. In general, LDZ1 gives better predictions for protons than for neutrons.

For the spin-orbit splitting, we use also the results of Ref. [20] for comparison. The definition of the error in spin-orbit splitting is the same as in the previous cases. For the neutron case, all models give a bad prediction for ^{90}Zr (2p) and ^{48}Ca(1d). LDZ2 and LZ only give acceptable results in ^{208}Pb(3p), LDZ1 and NLZ in $^{16}O(1p)$ and $^{40}Ca(1d)$ and NHM in ^{208}Pb(3p), $^{16}O(1p)$ and $^{40}Ca(1d)$. For protons, LDZ2 and LZ cannot give acceptable results. LDZ1 and NHM have three acceptable results while NLZ has four. All parameter sets cannot reproduce the experimental result of ^{48}Ca(1d) for protons. From this fact, it is clear that the exchange effect is important for the spin-orbit splitting prediction. We can also see clearly that the nonlinearity in any relativistic mean field model (here we use the NLZ and NHM models) appears necessary to give acceptable predictions in the spin-orbit splitting.

It was shown in Ref. [37] that the exchange effects improve the nuclear matter predictions of the linear Hartree model, therefore in figure 2.22 we calculate E/A vs p_f of symmetric nuclear matter for the four parameter sets. Other nuclear matter properties can be found in table 2.4. Our rough approximation cannot improve the nuclear matter predictions of the linear Hartree models (LDZ2, LZ). This fact demonstrates that it is necessary to refine the approximation or to solve the exact formulation if we want to see improvement in the nuclear matter prediction from the exchange effect.

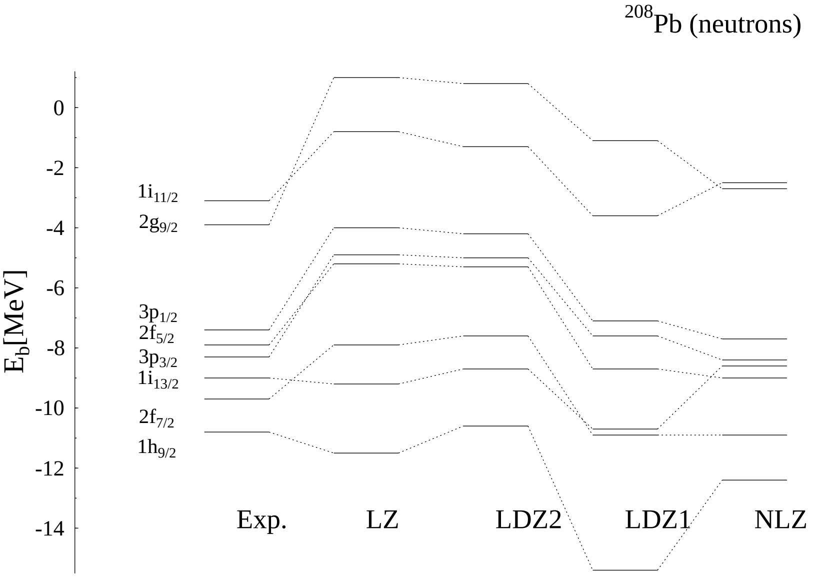

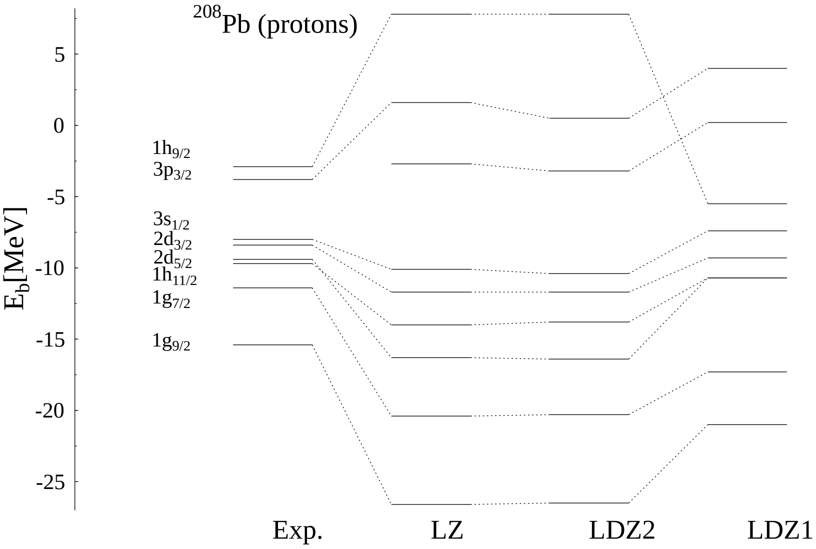

Figure 2.18: Single-particle spectra for ^{208}Pb (neutron) in the upper figure and for ^{208}Pb (proton) below.

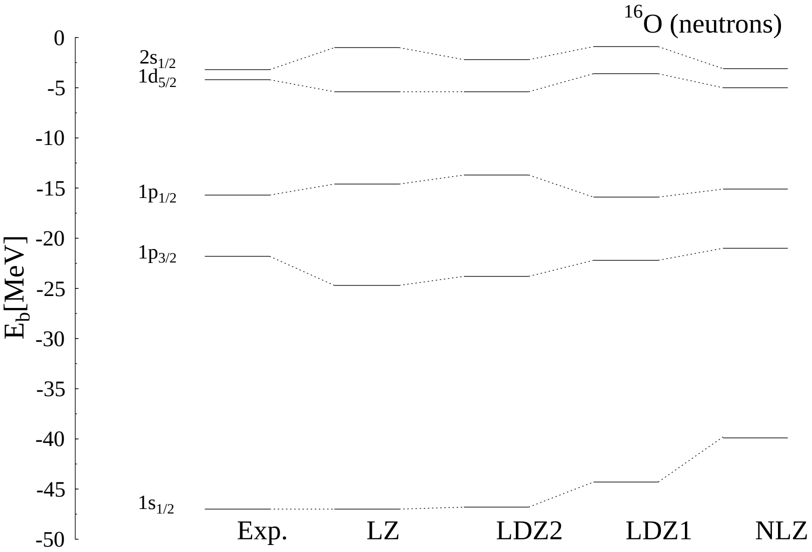

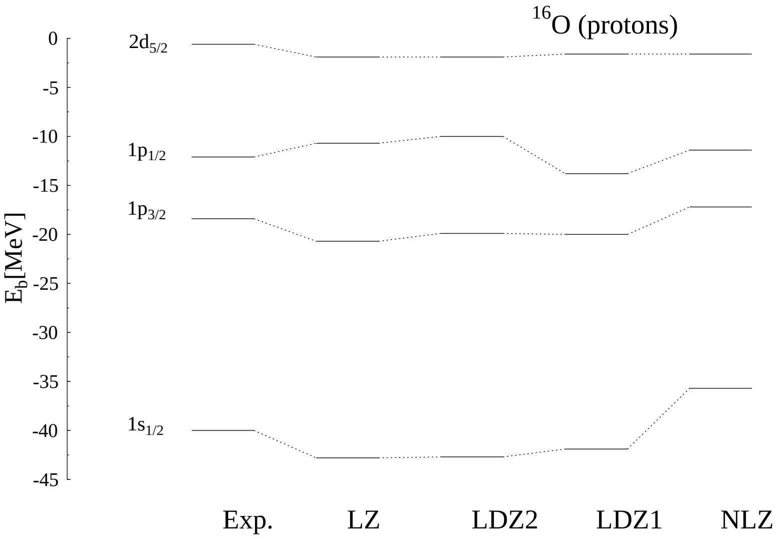

Figure 2.19: Single-particle spectra for ^{16}O (neutron) in the upper figure and for ^{16}O (proton) below.

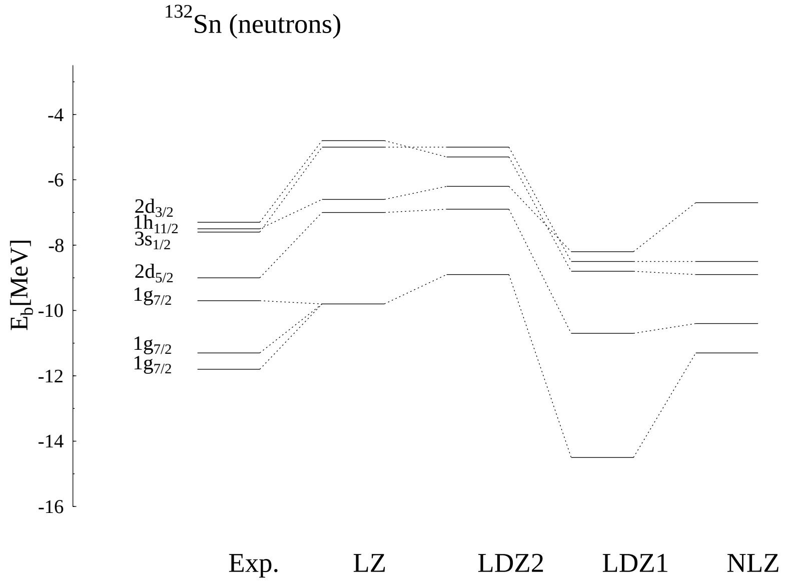

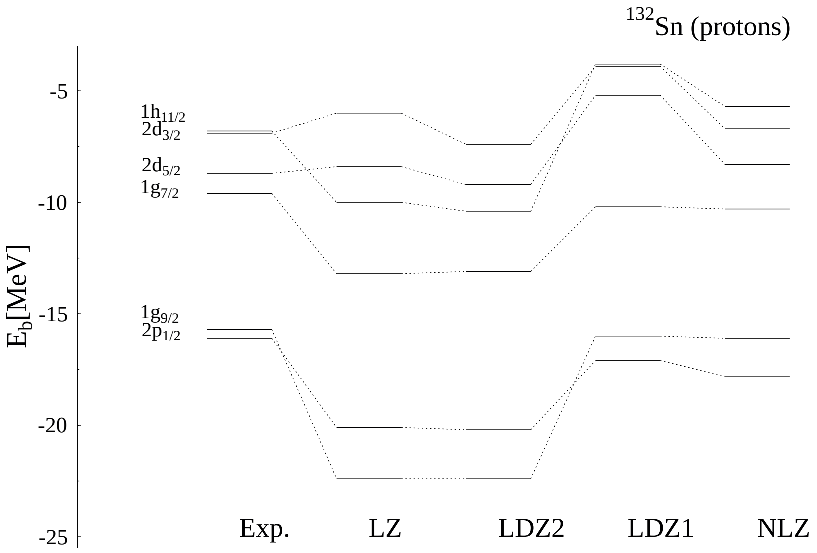

Figure 2.20: Single-particle spectra for ^{132}Sn (neutron) in the upper figure and for ^{132}Sn (proton) below.

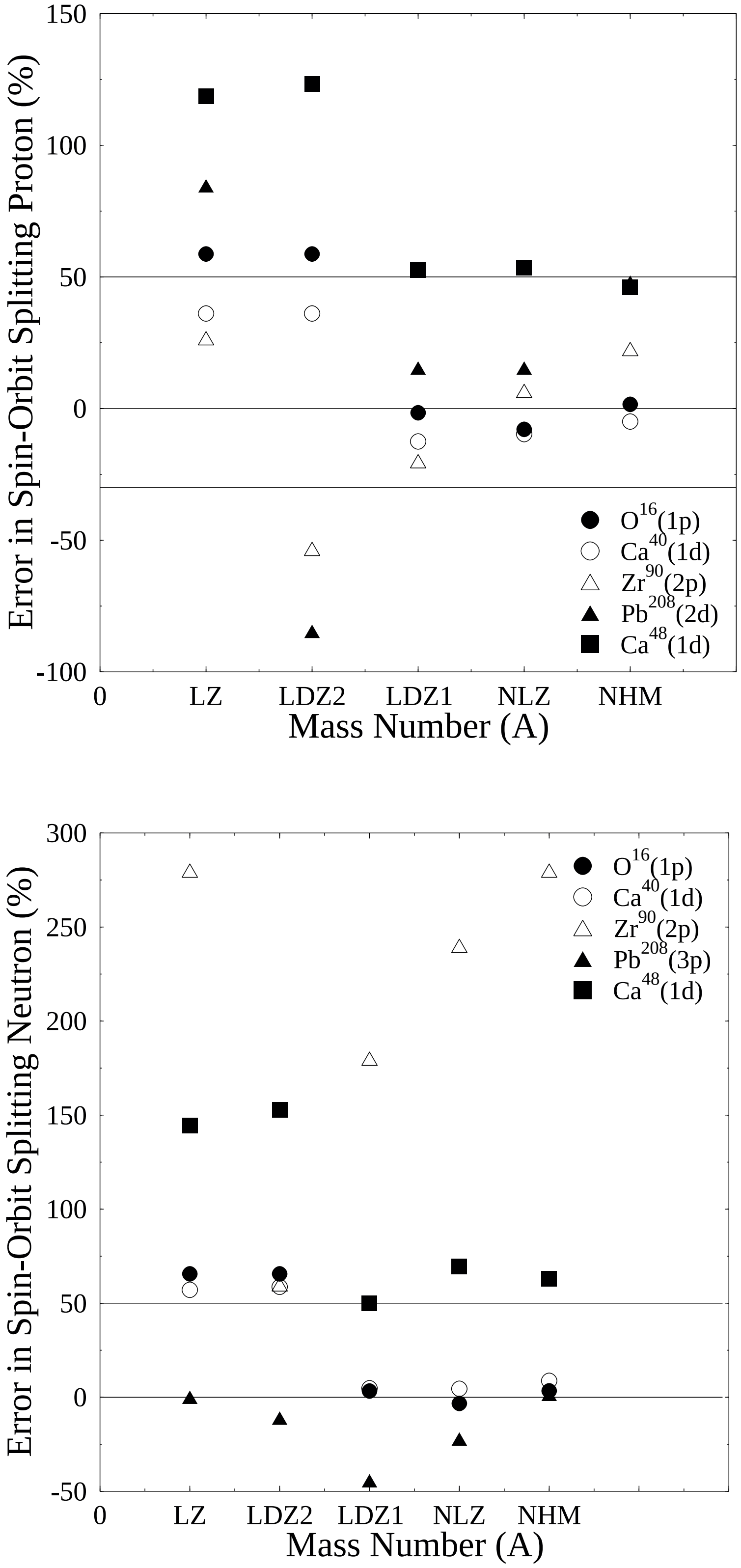

Figure 2.21: Error in the spin-orbit splitting for some spherical nuclei, the neutron case in the upper and the proton case in the lower figure.

In summary, we have shown that, formally, a Lagrangian densitiy $\mathcal{L}^{\mathrm{H}}$ can be determined in a relativistic linear point-coupling Hartree sense that is not equivalent to that determined in a relativistic linear point-coupling Hartree-Fock sense, $\mathcal{L}^{\mathrm{HF}}$. The significant difference is due to the exchange of the linear derivative terms which is created by the $C_{i\alpha}$ and $B_{i\alpha\mu}$ densities. By using Gordon decomposition, we can have another representation of these densities.*In this new representation, these densities can be separated into two parts. The role of the first part can be replaced effectively by tensor terms and all possible mixing nonlinear terms and the second part is genuine of these densities. This second part is responsible for the fourth-order differential equations and an order of magnitude analysis of the* $C_{i\alpha}$ *and* $B_{i\alpha\mu}$ *densities in the new representation shows that these parts are small.*

We have found that in the linear Hartree approximation, the long-range effect from heavy meson propagators does not give a distinct effect in predictions for finite nuclei, but on the other hand the local part of the exchange effectcan do so even using approximate $C_{i\alpha}$ and $B_{i\alpha\mu}$ (by neglecting the nonlinear contributions) densities. This was done by calculating the bulk properties of the ground states of some isotopes and isotones, single-particle spectra, spin-orbit splittings and saturated nuclear matter properties. The results were compared with the linear and nonlinear Hartree approximation from Ref. [7]. To show how effective our approximation is, we compared our result with LDA results [27], and also the $\chi^2/nucleus$ with the $\chi^2/nucleus$ of a full Hartree-Fock calculation [26]. The calculation in Ref. [26] used the same weight as Ref. [7] but fewer observables. We agree with [26] and [27] that both a linear RH and RHF calculation seem to indicate that some physics is still missing in the model.

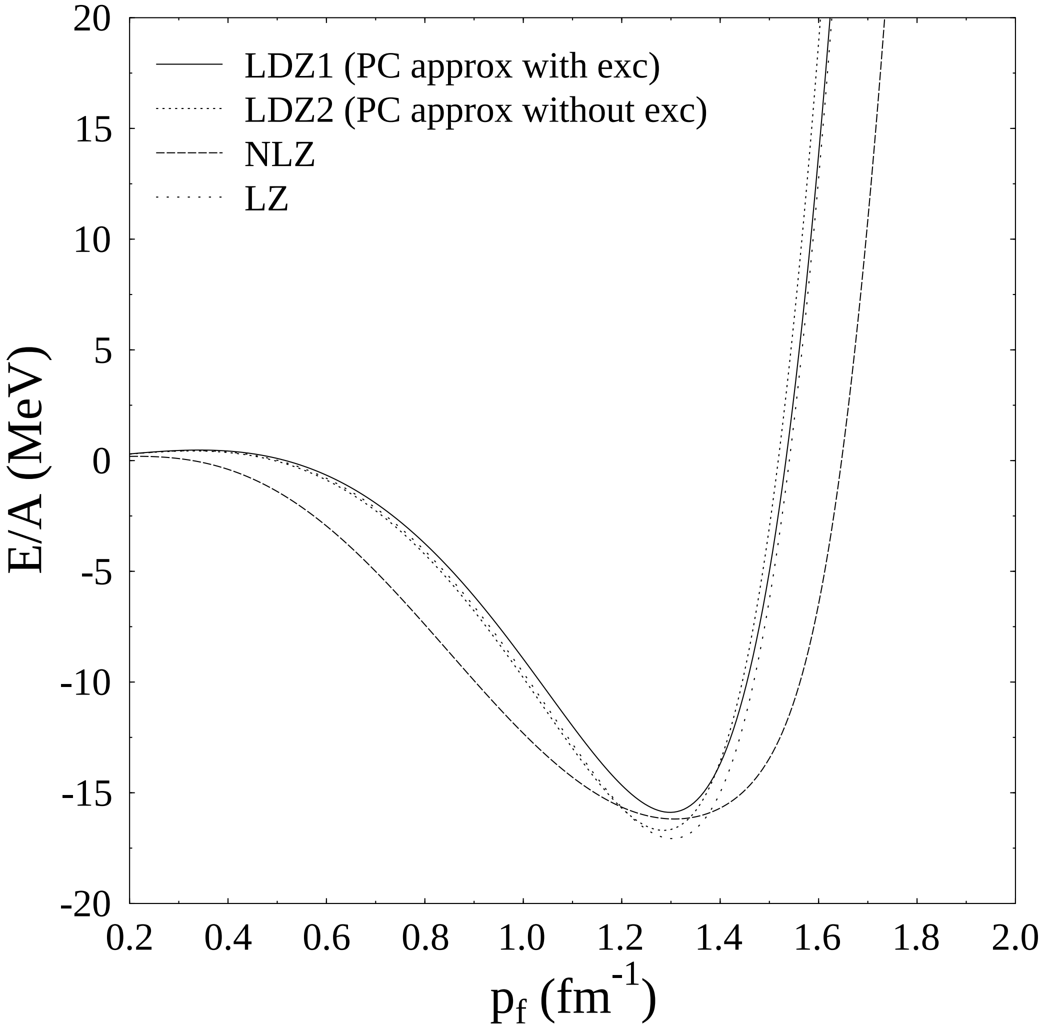

Figure 2.22: Binding energies per mass number of infinite symetric nuclear matter versus Fermi wave number.

–III–

NONLINEAR POINT-COUPLING(PC) MODEL

3.1 PC Model in the Hartree Level

To study the connection between the Walecka and the PC model, the point-coupling approximation must be fit now in the Hartree level but with the nonlinear terms included. Because in the form of our approximation the connection seems quite clear, we desire a parameter set with the same treatment as NLZ. The parameter set has scalar isoscalar nonlinear terms (LDZ2a). It should be emphasized here that our objective is quite different from other work ([20] and the new one [19]). We are not concerned with maximizing predictive power, but use experimental data only to study the connection of both models. Now, replacing the scalar meson nonlinear terms in the Walecka model

$$\mathcal{L}_{NL} = -\frac{1}{3}b_2\Phi_s^3 - \frac{1}{4}b_3\Phi_s^4 \tag{3.1}$$

with the very rough approximation

$$\begin{aligned} \mathcal{L}^a_{NL} &\approx -\frac{1}{3}b_2\Big(-\frac{g_s}{m_s^2}\rho_s\Big)^3 - \frac{1}{4}b_3\Big(-\frac{g_s}{m_s^2}\rho_s\Big)^4 \\ &\equiv -\frac{1}{3}C_2\rho_s^3 - \frac{1}{4}C_3\rho_s^4 \end{aligned} \tag{3.2}$$

and performing the point-coupling approximation for the linear one like in the previous chapter leads to a point coupling Lagrangian similar to Refs. [20, 19]. The difference is that in Refs. [20, 19] the vector isoscalar nonlinear term was included in their $\mathcal{L}_{NL}$, while they

Parameters	g_s	g_v	g_R	k_s	k_v	k_r	C_2	C_3
LDZ2a	9.5046	12.4295	8.9677	0.3112	-0.091	-4.1944	23.7337	-81.8440

Table 3.1: Values for the LDZ2a parameter set.

Parameters	g_s	g_v	g_R	m_s	$3b_2$	$4b_3$
NLZ	10.0553	12.9086	9.6988	488.67	-13.5072	-40.2243

Table 3.2: Values for the NLZ parameter set.

used the scalar isoscalar density term in the linear sector instead of the derivative of the vector isovector density, and it cannot be guaranteed that we have a parameter set with the right local minimum. In this point of view, essentially, the point coupling model can be seen as an approximation to the Walecka model, where the nonlinear potential of the Walecka model is replaced by a simple form of explicit density dependence. The nonlinear potential in the Walecka model actually is not only a function of the density but also of the derivative of the density in a complicated way. Surprisingly, this approximation works relatively well, which will be apparent in the following results.

3.2 Results

Parameter sets and fitting results can be seen in tables 3.1 and 3.3.

The coupling constants for LDZ2a and NLZ [7] in tables 3.1 and 3.2 have similar values. The values of the parameters k_i, which are not close to unity, indicate that the long-range effect seems to be significant. Table. 3.2 also shows that the main difference in χ^2 between LDZ2a and NLZ is in the surface thickness observables, leading to the speculation that the derivative part of the nonlinear terms, which is implicitly present in in the nonlinear part of the RMF, plays a role in this discrepancy.

χ^2	BE	DR	ST	Total
LDZ2a	27.65	6.57	75.79	110.01
NLZ	23.89	18.77	29.25	71.92

Table 3.3: χ^2 results from LDZ2a and NLZ. BE denotes the binding energies, DR the diffraction radii decomposed into contributions from the different observables, and ST the surface thickness. Details are given in the first chapter.

To see more detail let us compare the predictions of both models in some finite nuclear observables. First, we calculate the errors in the binding energies of some isotopes and isotones, second, we calculate the two-neutron separation energies for the Sn and Pb isotopes and the two-proton separation energies for the N=82 and N=126 isotones. Then we examine the errors in the diffraction radii, and surface thicknesses for some isotopes and finally we give also the spin-orbit splittings for selected nuclei. In addition we calculated the single-particle spectrum and the charge density of Lead.

We see from figs. 3.1 that NLDZ2a gives the error in the binding energy without too much difference in quality with NLZ. Together with the two-neutron and two-proton separation energies in figs. 3.2 and 3.3, LDZ2a still gives acceptable binding energy predictions. Fig. 3.4 shows that the error in the diffraction radii of LDZ2 is a little bit better than for NLZ. The error in the surface thickness for NLZ is less than 10 % and LDZ2 below 13 %, therefore the difference is not really significant as we expected in the beginning from the fit result. Figure 3.5 shows that similar to the previous result (without the nonlinear terms), the larger part of the difference in the charge density between the two models appears at small radii. From figs. 3.6 and 3.7, we can see clearly the role of the nonlinear terms to give correct single-particle spectra and spin-orbit splitting. This fact emphasizes the results of the previous chapter. The surprising feature, which can be seen from the above results is, NLZ has similar prediction quality in the shell structure and binding energy with LDZ2a where the nonlinear terms of the NLZ parameter set contain the σ meson, while the LDZa parameter set has a simple explicit scalar density-dependent nonlinear terms. *It seems that the nature of the finite nuclei observables and the fitting procedure make the binding energies and shell structure predictions insensitive to the difference of these nonlinear terms. The only clear difference of both models appears on the charge density. Finite range thus only affects the charge density.*

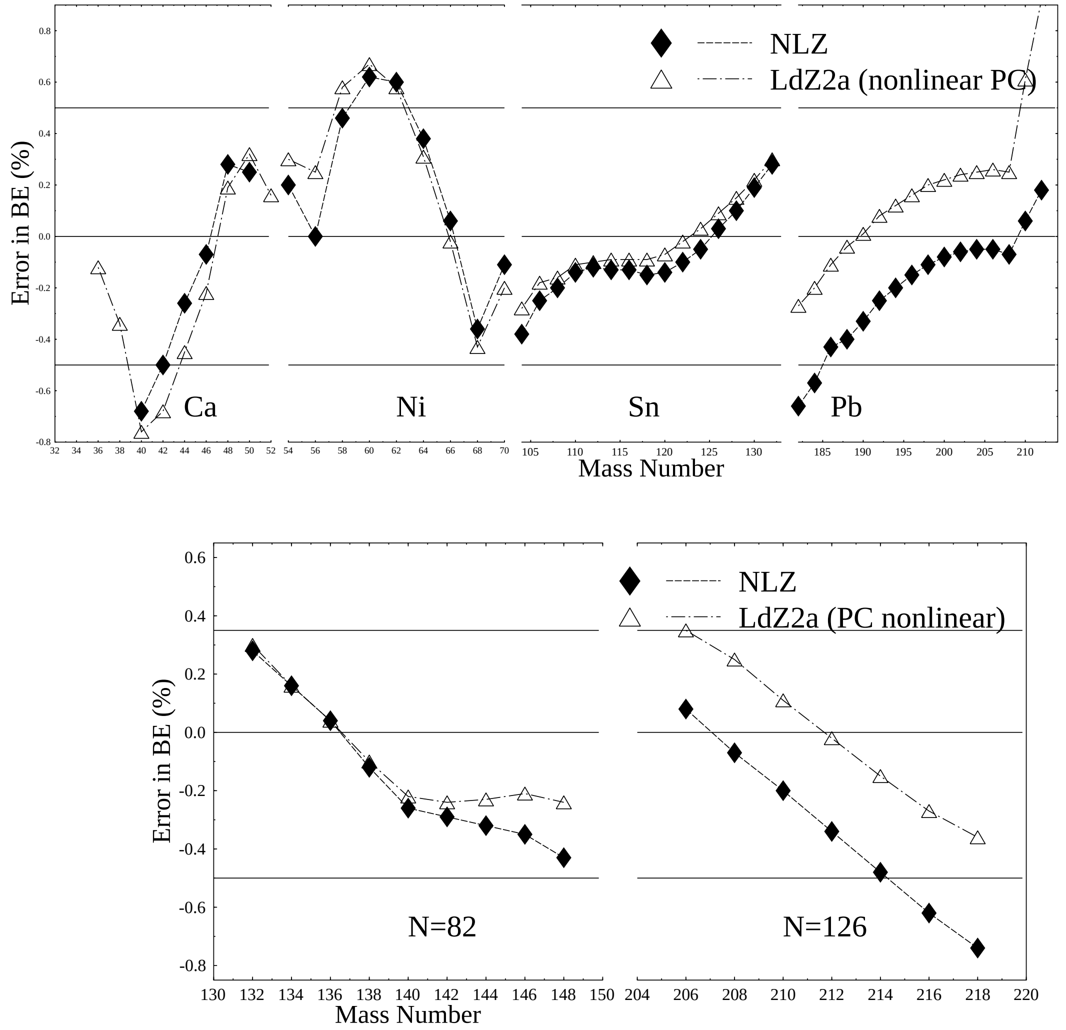

Figure 3.1: Error in the binding energies for the Ca, Ni, Sn, and Pb isotopes, respectively, in the upper figure, and the N=82 and N=126 isotones, respectively, in the lower figure with the parameter sets LDZ2a and NLZ.

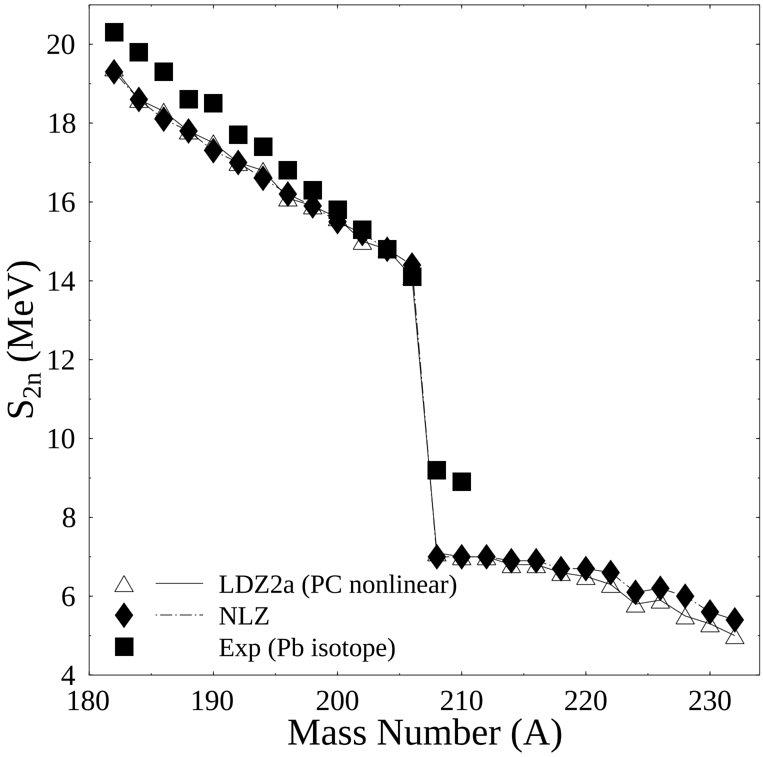

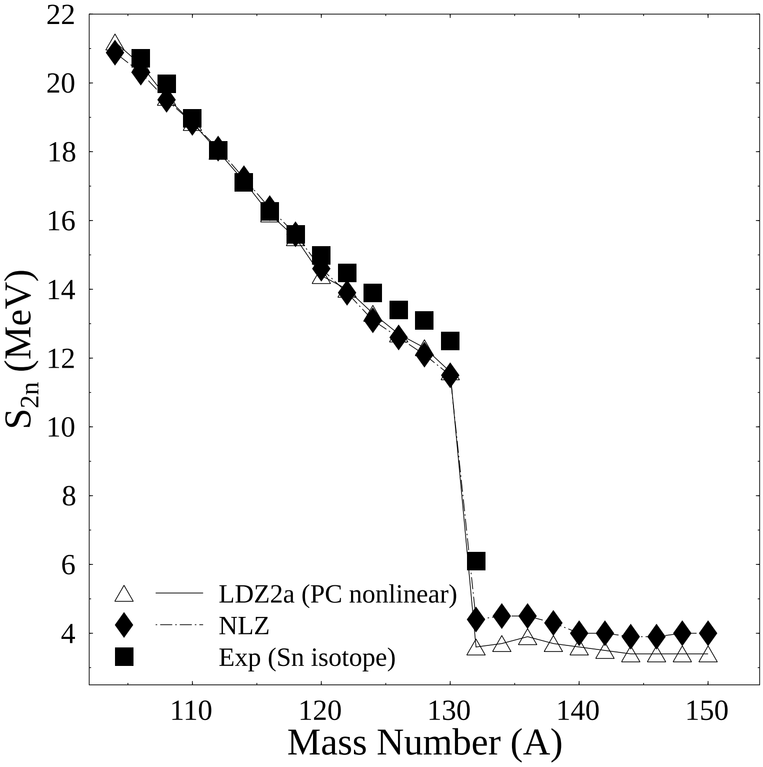

Figure 3.2: Two-neutron separation energies (S_{2n}) with the parameter sets LDZ2a and NLZ for the Sn and Pb isotopes.

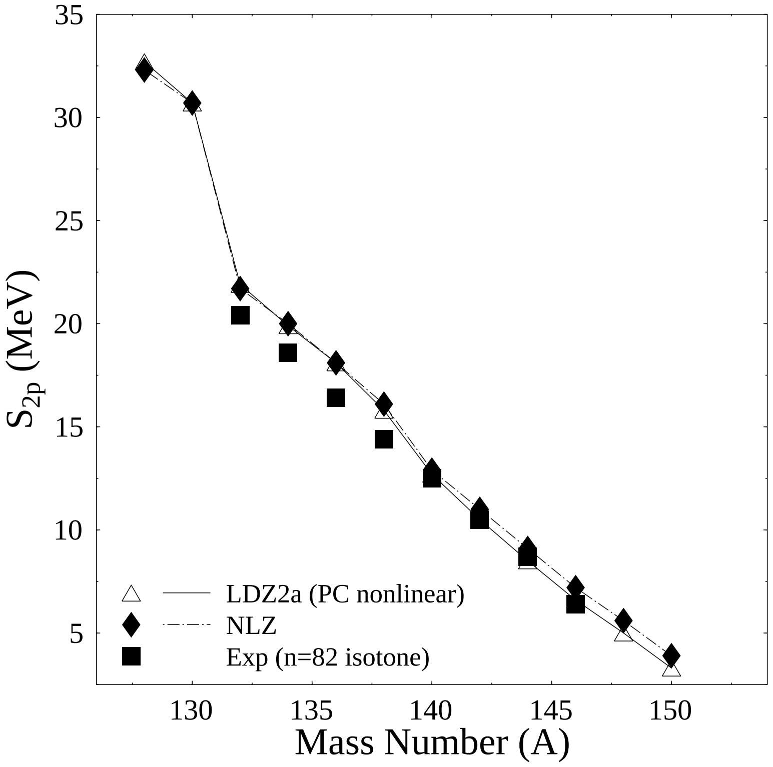

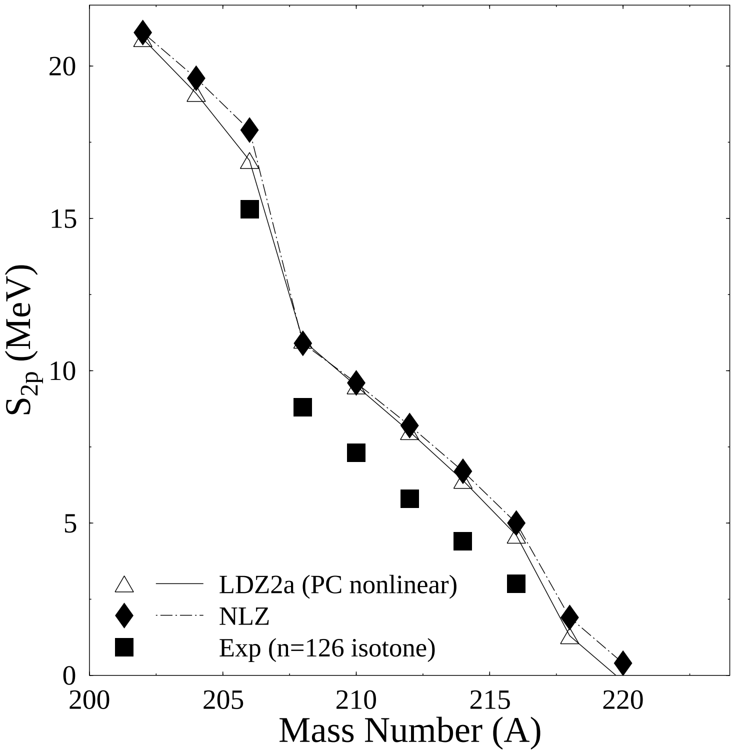

Figure 3.3: Two-proton separation energies (S_{2p}) for the N=82 and N=126 isotones with the parameter sets LDZ2a and NLZ.

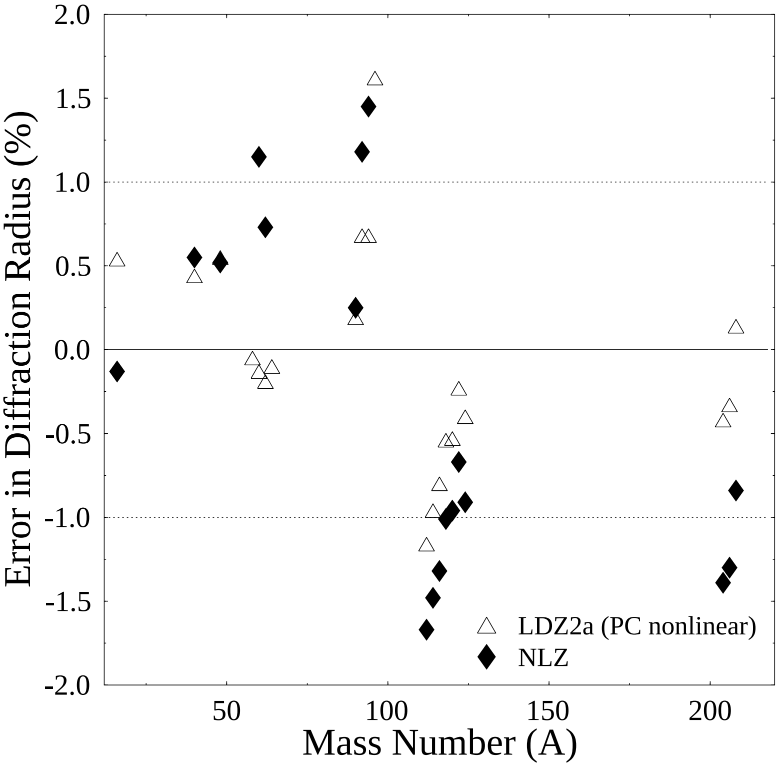

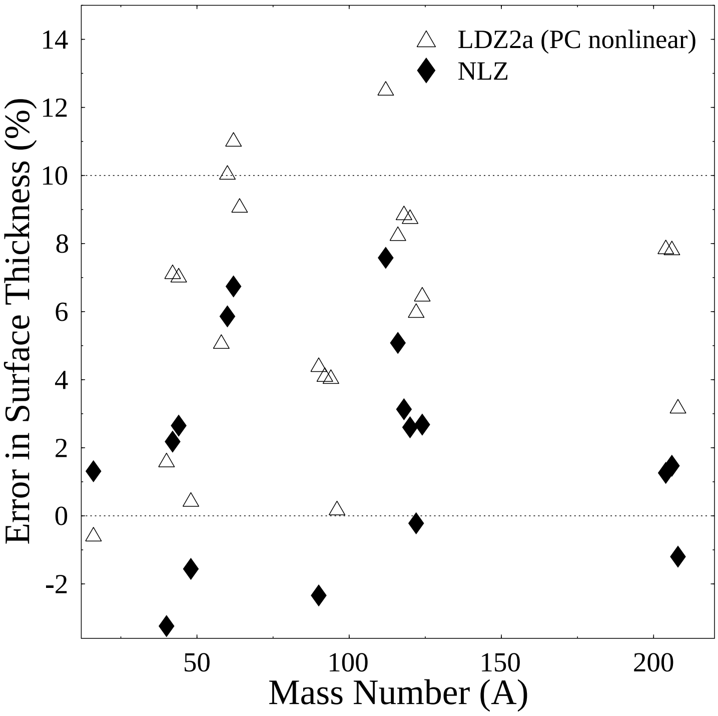

Figure 3.4: Error in the diffraction radii and surface thicknesses for some spherical nuclei with the LDZ2a and NLZ parameter sets.

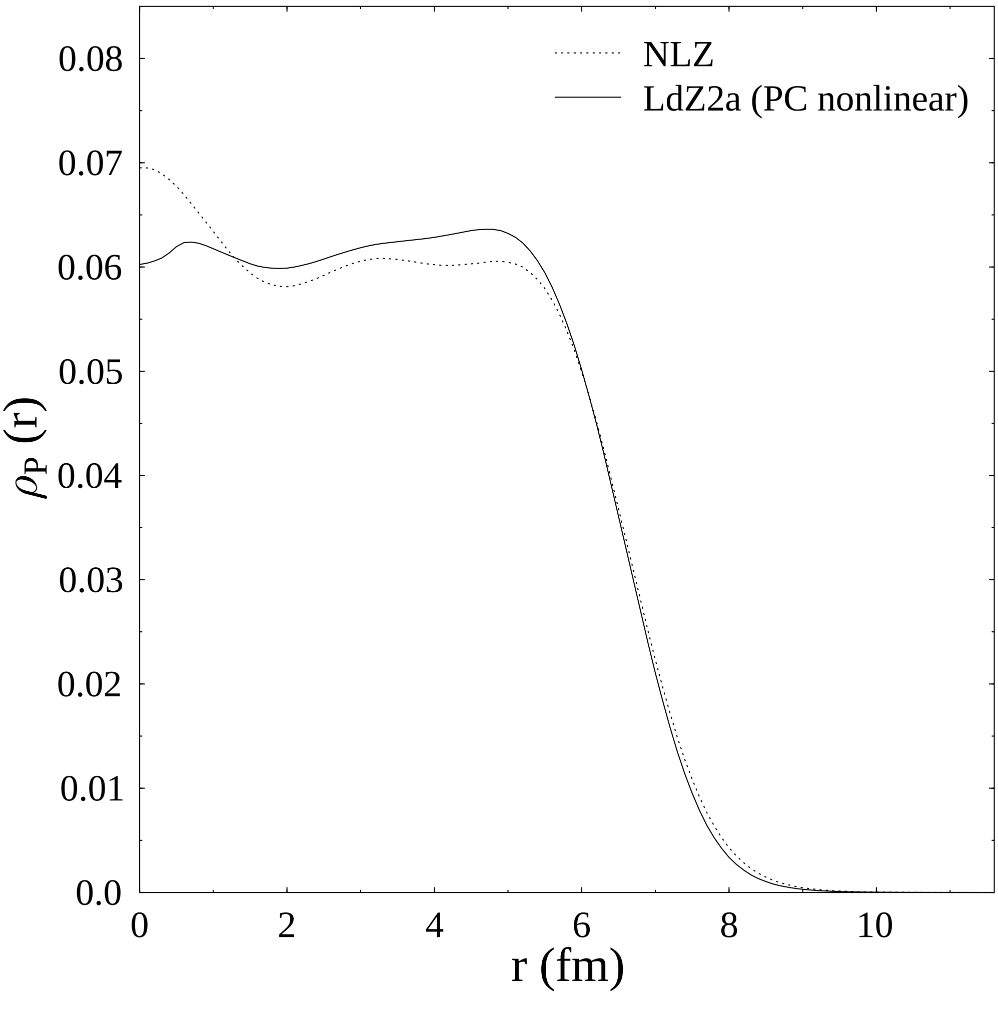

Figure 3.5: Charge density as a function of the radius for ^{208}Pb with the LDZ2a and NLZ parameter sets.

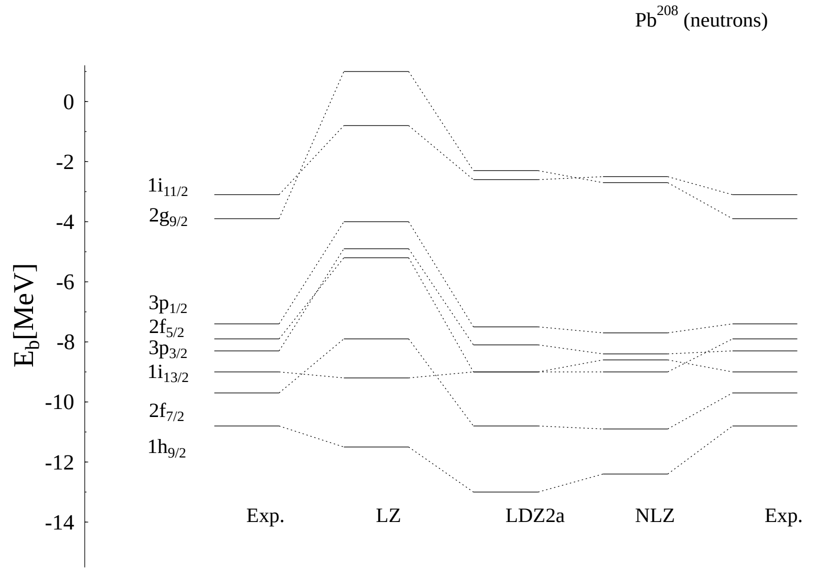

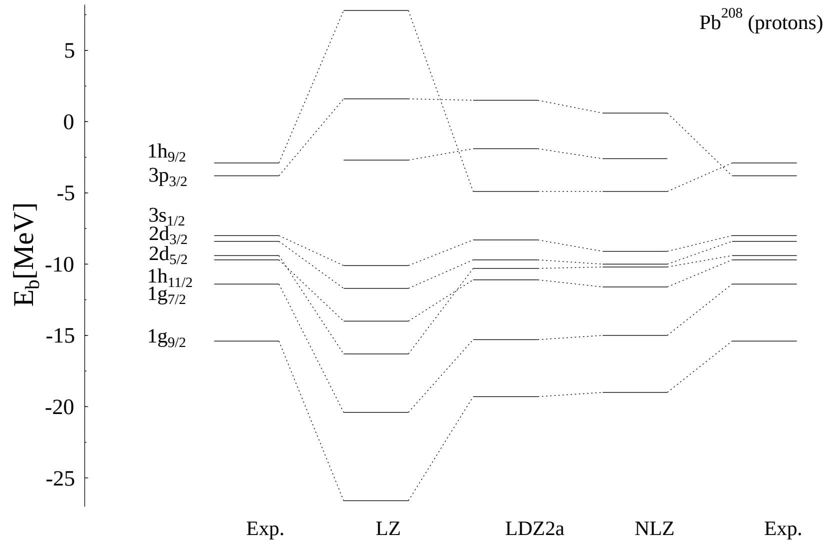

Figure 3.6: Single-particle spectra for ^{208}Pb (neutrons) in the upper figure and for ^{208}Pb (protons) in the lower figure, both with the LDZ2a and NLZ parameter sets. We give also experimental data (EXP), those for the standard linear parameter set (LZ) to emphasize the important role of nonlinear terms in this case.

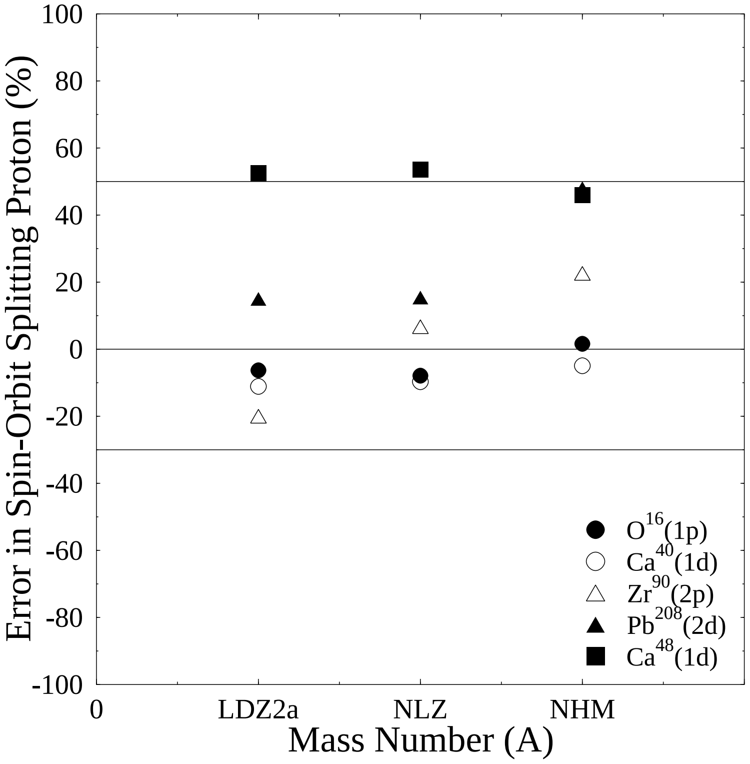

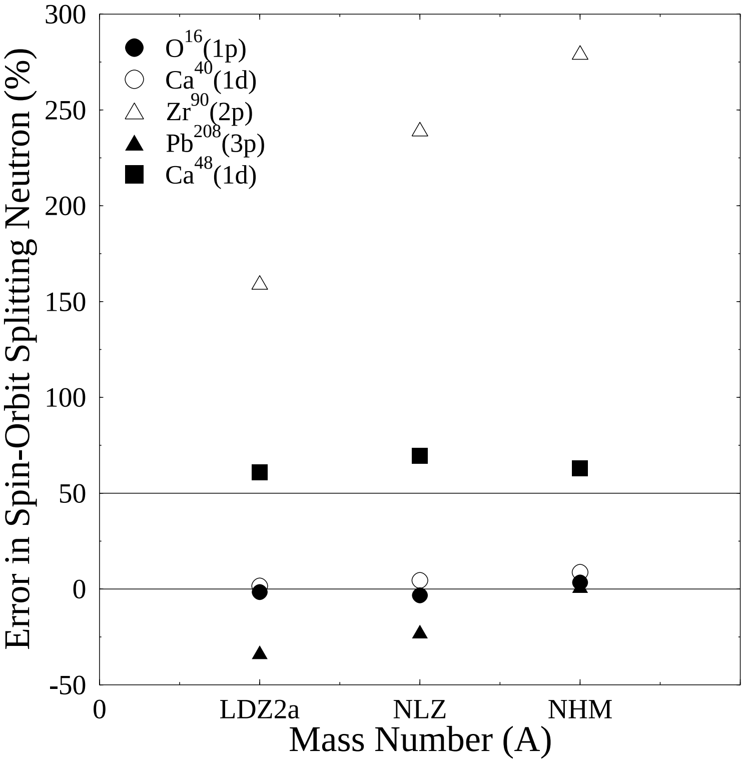

Figure 3.7: Error in the spin-orbit splitting for some spherical nuclei with the LDZ2a and NLZ parameter set, the neutron case in the upper figure and the proton case in the lower figure. In addition we give also the results of Ref [20](NHM).

3.3 Exchange Effect in the Nonlinear Terms (Qualitative Discussion)

Now we demonstrate qualitatively the exchange effect in the nonlinear Lagrangian density in Eq. (3.2). As before, the system is assumed to have good parity. A full exchange (without approximation) calculation for the nonlinear terms by using computational algebraic methods can be found in [50], but for simplicity without missing too much physical ingredient, here we only work with an approximation in nonlinear terms as follows :

$$\begin{aligned}
<: \hat{\bar{\psi}}\hat{\psi}\hat{\bar{\psi}}\hat{\psi}\hat{\bar{\psi}}\hat{\psi} :> &\simeq <: \hat{\bar{\psi}}\hat{\psi} :>^3 + 3\Delta_s <: \hat{\bar{\psi}}\hat{\psi} :> \\
<: \hat{\bar{\psi}}\Gamma^a\hat{\psi}\hat{\bar{\psi}}\Gamma_a\hat{\psi}\hat{\bar{\psi}}\Gamma^a\hat{\psi}\hat{\bar{\psi}}\Gamma_a\hat{\psi} :> &\simeq (<: \hat{\bar{\psi}}\Gamma^a\hat{\psi} :><: \hat{\bar{\psi}}\Gamma_a\hat{\psi} :>)^2 \\
&+ 6\Delta_a <: \hat{\bar{\psi}}\Gamma^a\hat{\psi} :><: \hat{\bar{\psi}}\Gamma_a\hat{\psi} :> \\
\Delta_a &= <: \hat{\bar{\psi}}\Gamma^a\hat{\psi}\hat{\bar{\psi}}\Gamma_a\hat{\psi} :> - <: \hat{\bar{\psi}}\Gamma^a\hat{\psi} :><: \hat{\bar{\psi}}\Gamma_a\hat{\psi} :>, \qquad (3.3)
\end{aligned}$$

where Γ_a=1 or $\Gamma_a = \gamma_\mu$. It is clear that here we neglected the contributions from the third and fourth-order Fierz transformation and also Δ_a^2 terms. Then we follow appendix A to obtain

$$\begin{aligned}
<: \hat{\mathcal{L}}^a_{NL} :> &\simeq -\frac{1}{3}C_2[(1-\frac{3}{8})\rho_s^3 - \frac{3}{8}\rho_s J_v^\mu J_{v\mu} - \frac{3}{8}\rho_s \vec{\rho}_{ts}^{\,2} - \frac{3}{8}\rho_s \vec{J}_{tv}^\mu \vec{J}_{tv\mu} \\
&- \frac{3}{16}\rho_s J_T^{\mu\nu} J_{T\mu\nu} - \frac{3}{16}\rho_s \vec{J}_{TT}^{\mu\nu} \vec{J}_{TT\mu\nu}] \\
&- \frac{1}{4}C_3[(1-\frac{6}{8})\rho_s^4 - \frac{6}{8}\rho_s^2 J_v^\mu J_{v\mu} - \frac{6}{8}\rho_s^2 \vec{\rho}_{ts}^{\,2} - \frac{6}{8}\rho_s^2 \vec{J}_{tv}^\mu \vec{J}_{tv\mu} \\
&- \frac{6}{16}\rho_s^2 J_T^{\mu\nu} J_{T\mu\nu} - \frac{6}{16}\rho_s^2 \vec{J}_{TT}^{\mu\nu} \vec{J}_{TT\mu\nu}]. \qquad (3.4)
\end{aligned}$$

It is known from the previous chapter that the isovector terms and the tensor term only give minor contributions; if we neglect them, only two terms in line one and line three in Eq. (3.4) survive. It is obvious now, that if the exchange corrections from the nonlinear terms are taken into account, we obtain a mixing among all possible density-dependent contributions. Looking at the Rusnak-Furnstahl model in Ref. [21] which, beside the standard form of the point-coupling model also contains the tensor terms, mixing terms in the nonlinear part between the scalar isoscalar and vector isoscalar densities, and also a nonlinear contribution in the form of a derivative of densities, it is understandable from our point of view, why they claimed that the exchange effect is effectively absorbed in the coupling constants of their model. But if we want to have a more refined model with tensor and isovector nonlinearities taken into account without added parameters, it seems that the exact forms of the exchange of the nonlinear terms should be used.

–IV–

NONRELATIVISTIC REDUCTION

The nonrelativistic Skyrme model has been successfully applied in nuclear structure calculations for many years [47, 34]. The Skyrme potential takes the form of zero-range terms representing an expansion in the nucleon density and momentum, effectively containing finite range due to momentum dependence. This model is constructed for use in Hartree-Fock calculations. Like the RMF model, the parameters of the potential are adjusted to experimental data both in nuclear matter and in finite nuclei.

The connection between this model and the RMF model was done by several authors, without [39, 40] and with the nonlinear terms [2, 41], but they did not take into account tensor and space components of the vector potential contributions. The nonlinearities in ρ_0 alone of the RMF and Skyrme models are hard to compare because the δU' (the meson dependent nonlinear potential of the RMF model) is a quite involved function of ρ_0 [2]. The role of the tensor coupling of the isoscalar vector meson to the nucleon in the framework of effective field theories was investigated in Ref. [42], while the relativistic spin-orbit field in finite nuclei and superdeformed nuclei was examined in Refs. [46, 45]. The effect of the tensor coupling to enhance the role of the vector mean field in leading order of the spin-orbit correction to the nonrelativistic single-nucleon energy in the Zimányi model has also been investigated [44]. The second-order form of the Dirac equation with local potential has been discussed in reference [48]. It has been shown [43] with the Skyrme model that a tensor and a time-reversal noninvariant force turns out to be necessary in studying the properties of odd nuclei. In the previous chapter, the role of the exchange effects was also investigated in the framework of the point-coupling approximation. It seems that the largest part of the role of exchange effects in the linear model can be effectively replaced by the tensor and nonlinear terms in Hartree calculations.

It is obvious from previous chapters that the investigation of the role of nonlinear terms of the relativistic model in the nonrelativistic limit is quite important. This investigation seems not really completely done in previous work [2, 41] because, as we mentioned previously, it is difficult to write down explicitly the density dependence of the RMF nonlinear terms. This problem does not appear if we use the point-coupling model, because in the point-coupling model the nonlinear terms are explicitly density dependent. Therefore it is quite worthwhile to study the connection between the point-coupling model and the nonrelativistic Skyrme model. In this context, we study not only the role of the linear terms but also the nonlinear terms of both models in the nonrelativistic limit. The complete discussion about the point-coupling model can be found in Ref. [19]. It consists of a careful way to obtain a new parameter set for the point-coupling model which is guaranteed to correspond to the right local minimum by combining different methods for the χ^2 minimization. This parameter set was applied to a wide area in nuclear theory, from spherical finite nuclei, deformed nuclei (more than one-dimensional calculations), odd nuclei, superheavy elements, potential energy surfaces, nuclear matter, neutron matter, up to exotic nuclei [19]. In the calculations we use the method put forward by Reinhard [2] to reduce the model into a nonrelativistic form. We use the NHM [20] and some variant of the LDZ parameter sets simply because they have only few parameters and not too many terms, so that we can study the effects more clearly.

We organize this chapter as follow : In section 2 we briefly review the Schrödinger equation. In section 3 we give the Schrödinger form of the Dirac equation. Section 4 contains results and the discussion is given in section 5.

4.1 Schrödinger Equation

In the nonrelativistic field theory, it is customary to adopt the Schrödinger field for a massive particle regardless of its spin. The spin structure is not usually built into the free Lagrangian, but is taken into account only in the interaction Lagrangian. Consequently the free part of the stress tensor is always symmetric [51]. However, as is demonstrated in refs. [51, 52], if we break the Schrödinger equation into two equations containing only first-order derivatives, we can represent the spin content explicitly. The stress tensor calculated from it is in general not symmetric, but can be symmetrized by standard methods as is shown in ref. [51]. Reducing the Schrödinger equation into two first-order equations not only represents its spin content explicitly, but also gives the Landé factor g = 2 [51, 53]. The spin-orbit coupling is obtained by introducing a central potential U(r). It means that these two effects are not necessarily a consequence of the relativistic invariance but rather of the field equation of the first-order. In the following we will use the results of Ref. [51]

as follows:

$$\Psi(x) = \begin{pmatrix} \psi(x) \\ \chi(x) \end{pmatrix}, \tag{4.1}$$

and the classical Lagrangian density is defined as

$$\begin{aligned} \mathcal{L} &= i\psi^\dagger(x)\dot{\psi}(x) - \psi^\dagger(x)V(r)\psi(x) + i\psi^\dagger(x)\vec{\sigma}.\vec{\nabla}\chi(x) \\ &+ i\chi^\dagger(x)\vec{\sigma}.\vec{\nabla}\psi(x) + \chi^\dagger(x)(2m - U(r))\chi(x) \end{aligned} \tag{4.2}$$

where V(r) and U(r) are central potentials. The quantization of this Lagrangian can be done and will give a nonlocal correction in the equation of state which depends on the form of the potentials, but for the moment the extension into this direction is not necessary for our purpose. From Eq. (4.2), we can obtain

$$i\dot{\psi}(x) = ([V(r) - \vec{\nabla} \cdot f(r)\vec{\nabla}] + \frac{1}{r}\frac{df}{dr}\vec{\sigma} \cdot \vec{L})\psi(x) \tag{4.3}$$

and

$$\chi(x) = -if(r)\vec{\sigma} \cdot \vec{\nabla}\psi(x), \tag{4.4}$$

with f(r) = $(2m - U(r))^{-1}$. If 2m >> $|U(r)|$ then

$$\frac{df(r)}{dr} = \frac{1}{4m^2}\frac{dU(r)}{dr} + ... \tag{4.5}$$

Eq.(4.3) shows that the nonrelativistic Schrödinger equation with potentials V(r) and U(r) gives a spin-orbit coupling. There is no reason to assume that the two potentials should be the same. As long as the χ field is given in the form of Eq. (4.2), independent of the form of f(r), the spin orbit coupling will appear. In the next section we will give the Schrödinger form of the Dirac equation. It also yields two different potentials, the only difference with the nonrelativistic one being that they are energy dependent. The normalisation of the wave function is

$$N = \int d^3x(\psi^\dagger(x)\psi(x) + \chi^\dagger(x)\chi(x)). \tag{4.6}$$

If we compare it with the normalisation definition in Ref. [2] as

$$N = \int d^3x\phi^{\mathrm{class}\dagger}(x)\phi^{\mathrm{class}}(x), \tag{4.7}$$

we will obtain ϕ^{class} of the nonrelativistic Schrödinger equation as $\phi^{\mathrm{class}} = \hat{T}^{1/2}\psi$ with

$$\hat{T}^{1/2} = (1 - \vec{\sigma} \cdot \vec{\nabla}f^2(r)\vec{\sigma} \cdot \vec{\nabla})^{1/2}. \tag{4.8}$$

The last term can be interpreted as a spin effect in the normalisation.

4.2 Dirac Equation

In this section we will derive the second-order form of the Dirac equation. We start from

$$[\gamma_\mu \partial^\mu + i(m^* + \gamma_\alpha V^\alpha + \sigma_{\alpha\beta}T^{\alpha\beta})]\Psi = 0, \tag{4.9}$$

where

$$\gamma_\mu V^\mu = \begin{pmatrix} V_0 & -\vec{\sigma}\cdot\vec{V} \\ \vec{\sigma}\cdot\vec{V} & -V_0 \end{pmatrix}, \tag{4.10}$$

$$\sigma_{\mu\nu}T^{\nu\mu} \approx i\gamma_0\gamma_i T^{0i} = \begin{pmatrix} 0 & i\vec{\sigma}\cdot\vec{T} \\ i\vec{\sigma}\cdot\vec{T} & 0 \end{pmatrix}. \tag{4.11}$$

Here we neglected the time-reversal noninvariant tensor term $(i\gamma_i\gamma_j T^{ij})$ due to its smallness. If we assumed from the beginning that the system does not "change sign" under time reversal, this term and the space component of the vector part would vanish, but at the moment we will still retain the space component of the vector part to study the role of this term. If we define

$$\begin{aligned} \vec{\Omega} &\equiv \vec{T} + i\vec{V} \\ B(\epsilon`; r) &= (2m_B + \epsilon` + S - V_0)^{-1} \\ \epsilon` &= (\epsilon - m_B), \end{aligned} \tag{4.12}$$

and ϵ is the Dirac energy, then by using the same procedure as in Ref. [2], we arrive at the following expression :

$$< \hat{H} - \epsilon > \; = \; \int d^3x (\varphi^{\mathrm{up}\dagger}(S + V_0 - \vec{\sigma}\cdot(\vec{\nabla} - \vec{\Omega})B\vec{\sigma}\cdot(\vec{\nabla} + \vec{\Omega}^*) - \epsilon`)\varphi^{\mathrm{up}}, \tag{4.13}$$

where φ^{up} is upper component of Ψ. If we compare eq. (4.13), with eq. (4.3) we can see that

$$\begin{aligned} \psi &\longrightarrow \varphi^{\mathrm{up}} \\ V(r) &\longrightarrow S(r) + V_0(r) + g(\Omega, \vec{\nabla}; r) \\ f(r) &\longrightarrow B(\epsilon`; r), \end{aligned} \tag{4.14}$$

where the function $g(\Omega, \vec{\nabla}; r)$ comes from the third term of Eq. (4.13). As we mentioned in the previous chapter, in contrast to a nonrelativistic equation, from a Dirac equation we obtain V(r) and U(r) with an energy dependence $(\epsilon`)$. In order to estimate the convergence of the classical expansion, we take the NHM model [20] as example and as in Ref. [2] we assume the energy ϵ' $\sim$ -0.03 m_B. From the model, we can also obtain

$$\begin{aligned} S+V_0 &\sim -0.08\ m_B, \\ S-V_0 &\sim -0.8\ m_B, \\ B_0p^2 &\sim 0.05\ m_B, \\ B_0^3p^4/\epsilon &\sim 0.07, \end{aligned} \tag{4.15}$$

with

$$B_0 \sim (1.2m_B)^{-1}, \tag{4.16}$$

and estimate that $|\vec{\Omega}| \sim$ p. These properties fullfill the allowed range of Reinhard's order-of-magnitude estimation of every term in the effective Hamiltonian, which will be used as the criterion of the approximation [2]. We may thus assume that this behaviour is fullfilled by any point-coupling model. From the above numbers, we can also see that the point-coupling model gives automatically a weak V(r) but a strong U(r) like the RMF. This fact may therefore be identified as another feature of the relativistic model [55]. Using the normalisation in Eq. (4.7), we will have $\varphi^{\rm class} = \hat{I}^{1/2}\varphi^{\rm up}$ with

$$I^{1/2} = \left(1 - \vec{\sigma}\cdot(\vec{\nabla}-\vec{\Omega})B^2\vec{\sigma}\cdot(\vec{\nabla}+\vec{\Omega}^*)\right)^{1/2}, \tag{4.17}$$

and writing Eq. (4.13) as

$$< \hat{H} - \epsilon > = \int d^3x \varphi^{\rm class\dagger}(H_{\rm eff}^{\rm class} - \epsilon‘)\varphi^{\rm class}, \tag{4.18}$$

yields

$$H_{\rm eff}^{\rm class} = I^{-1/2}[S+V_0 - \vec{\sigma}\cdot(\vec{\nabla}-\vec{\Omega})[B(\epsilon‘)+\epsilon‘B^2(\epsilon‘)]\vec{\sigma}\cdot(\vec{\nabla}+\vec{\Omega}^*)]I^{-1/2}. \tag{4.19}$$

Now we are ready to approximate Eq. (4.19). The first step is to neglect the $\epsilon‘$ dependence in Eq. (4.19), which comes from the B and $\epsilon‘B^2$ terms. The last term gives contributions in order more than v^4, where v is the absolute velocity of the nucleons. From the previous discussion, we know that the v (or momentum) expansion seems convergent, therefore we can neglect this term in (4.19). The way to expand the $\epsilon‘$ dependence from B is not trivial [2, 21]. Here we only choose one form from Ref. [21] as follows :

$$\begin{aligned} B &\approx B_0 - \epsilon‘B_0^2, \\ B_0 &= (2m_B + S - V_0)^{-1}, \end{aligned} \tag{4.20}$$

because with this approximation we still have the opportunity later to study the isospin effect. Then Eq. (4.19) can be written as

$$H_{\text{eff}}^{\text{class}} \approx H_{\text{eff}}^{\text{class(2)}} + H_{\text{eff}}^{\text{class(4)}}. \tag{4.21}$$

The first term gives a contribution in order of v^2 and the second term gives a contribution in order of v^4. The results are

$$H_{\text{eff}}^{\text{class(2)}} = S + V_0 + \vec{\sigma}\cdot\vec{\Omega}B_0\vec{\sigma}\cdot\vec{\Omega}^* + \vec{\sigma}\cdot\vec{\Omega}B_0\vec{\sigma}\cdot\vec{\nabla} - \vec{\sigma}\cdot\vec{\nabla}B_0\vec{\sigma}\cdot\vec{\Omega}^* - \vec{\sigma}\cdot\vec{\nabla}B_0\vec{\sigma}\cdot\vec{\nabla}, \tag{4.22}$$

and defining

$$\hat{C} \equiv \vec{\sigma}\cdot\vec{\Omega}B_0^2\vec{\sigma}\cdot\vec{\Omega}^* + \vec{\sigma}\cdot\vec{\Omega}B_0^2\vec{\sigma}\cdot\vec{\nabla} - \vec{\sigma}\cdot\vec{\nabla}B_0^2\vec{\sigma}\cdot\vec{\Omega}^* - \vec{\sigma}\cdot\vec{\nabla}B_0^2\vec{\sigma}\cdot\vec{\nabla}, \tag{4.23}$$

$$\begin{aligned} H_{\text{eff}}^{\text{class(4)}} &= \vec{\sigma}\cdot\vec{\Omega}B_0^2(S+V_0)\vec{\sigma}\cdot\vec{\Omega}^* + \vec{\sigma}\cdot\vec{\Omega}B_0^2(S+V_0)\vec{\sigma}\cdot\vec{\nabla} - \vec{\sigma}\cdot\vec{\nabla}B_0^2(S+V_0)\vec{\sigma}\cdot\vec{\Omega}^* \\ &- \vec{\sigma}\cdot\vec{\nabla}B_0^2(S+V_0)\vec{\sigma}\cdot\vec{\nabla} - \frac{1}{2}\{\hat{C}, H_{\text{eff}}^{\text{class(2)}}\}. \end{aligned} \tag{4.24}$$

The last term in Eq. (4.24) is an anticommutator between $\hat{C}$ and $H_{\text{eff}}^{\text{class(2)}}$. If we set $\vec{\Omega}$=0 in Eq (4.24), the equation is nothing else but Eq. (90) in appendix A of Ref. [2]. It is clear that $\vec{\Omega}$ gives corrections with and without $\vec{\nabla}$ operator. The contribution containing a $\vec{\nabla}$ operator and arising from $\vec{V}$ (the space component of the vector potential) plays no significant role in the spherical system, because we will see later that after we make a gauge transformation in the wave function these terms will be absorbed in phase factors. The only effect of these terms are small corrections in S, V_O, T_r and B_O because S, V_O, T_r and B_O are functions of the densities, which are in turn functions of the wave functions. But the $g(\vec{\nabla})$ contribution from the T(tensor) will give an enhancement in the spin-orbit potential. An interesting discussion about the role of $H_{\text{eff}}^{\text{class(4)}}$ with $\vec{\Omega}$=0 in the spin-orbit potential can be seen in Ref. [2]. In this work, we will work only up to order v^2. We do that in order to avoid any complications due to the ϵ‘ dependence in the ρ_s and $\vec{j}_T$ calculations appearing in order v^4. In addition we assume that the system fulfills spherical symmetry. Therefore we have

$$\begin{aligned} H_{\text{eff}}^{\text{class}} &= (S + V_0 + B_0(T_r^2 + V_r^2) + \vec{p}B_0\vec{p} + \frac{1}{r}((\frac{dB_0}{dr}) - 2T_rB_0)\vec{\sigma}\cdot\vec{L} \\ &- i\frac{\partial}{\partial r}(B_0V_r) - \frac{\partial}{\partial r}(B_0T_r) - 2iB_0\frac{V_r}{r}\vec{r}\cdot\vec{p}, \end{aligned} \tag{4.25}$$

with $\vec{p} = -i\vec{\nabla}$, $T_r = \vec{r}.\vec{T}$ and $V_r = \vec{r}.\vec{V}$. Here we find a similar Hamiltonian form (with $\vec{r}.\vec{p}$ terms) as in reference [48], but we will show later that the $\vec{r}.\vec{p}$ term will vanish after a gauge tranformation. It is shown also that in Eq. (4.25) the tensor terms enhance the spin-orbit coupling. Now let us write :

$$(H_{\text{eff}}^{\text{class}} - \epsilon')\varphi^{\text{class}} = 0 \tag{4.26}$$

and $\varphi^{\text{class}} \equiv$ K(r) ψ (r) and take [48]

$$K(r) \equiv \exp(-i \int_0^1 V_r(tr) r dt) \tag{4.27}$$

If we substitute Eq. (4.27) into Eq. (4.26) then we will have

$$(\tilde{H}_{\text{eff}}^{\text{class}} - \epsilon')\psi = 0 \tag{4.28}$$

with

$$\tilde{H}_{\text{eff}}^{\text{class}} = (S + V_0 + B_0 T_r^2 + \vec{p} B_0 \vec{p} + \frac{1}{r}((\frac{dB_0}{dr}) - 2T_r B_0)\vec{\sigma}.\vec{L} - \frac{\partial}{\partial r}(B_0 T_r)) \tag{4.29}$$

Since S, V_O, T_r and B_O are functions of the densities and the densities are functions of the wave functions, it seems necessary to check how the densities change through the transformations. First, we calculate the densities (ρ_s, $\vec{j}_T$)

$$\rho_s = \sum_\alpha W_\alpha (\varphi^{\text{up}\dagger}\varphi^{\text{up}} - \varphi^{\text{low}\dagger}\varphi^{\text{low}}) \tag{4.30}$$

and

$$\vec{j}_T = i \sum_\alpha W_\alpha (\varphi^{\text{up}\dagger}\vec{\sigma}\varphi^{\text{up}} - \varphi^{\text{low}\dagger}\vec{\sigma}\varphi^{\text{low}}), \tag{4.31}$$

A straight-forward calculation up to order v^2 yields the above densities as functions of the nonrelativistic densities (τ and $\vec{J}$) as

$$\begin{aligned} \rho_s &= \rho_0 - 2B_0^2(\tau - \vec{\nabla} \cdot \vec{J}) \\ &- 2B_0^2 \vec{T} \cdot \vec{\nabla}\rho_0 - 2B_0^2 \rho_0 (\vec{T})^2, \end{aligned} \tag{4.32}$$

and

$$\vec{j}_T = B_0(\vec{\nabla}\rho_0 + 2\rho_0 \vec{T}) - 2B_0 \vec{J}. \tag{4.33}$$

The last two terms in ρ_s are due to the tensor effect. One can find the definition of ρ_0, τ and $\vec{J}$ in Ref. [2], but for the convenience of the reader we write them explicitly as

$$\begin{aligned} \rho_0 &= \sum_\alpha W_\alpha \varphi^{\text{class}\dagger}\varphi^{\text{class}} \\ \tau &= \sum_\alpha W_\alpha (\vec{\nabla}\varphi^{\text{class}\dagger}).\vec{\nabla}\varphi^{\text{class}} \\ \vec{\nabla} \cdot \vec{J} &= -i \sum_\alpha W_\alpha (\vec{\nabla}\varphi^{\text{class}\dagger}).(\vec{\nabla} \times \vec{\sigma})\varphi^{\text{class}}. \end{aligned} \tag{4.34}$$

We see that the forms of ρ_0 and $\vec{J}$ are not changed under the transformation in Eq. (4.27), but the kinetic term τ acquires an additional contribution, which has a form like $V_r^2\rho_0$. We estimate roughly by taking only the first leading term: $V_r^2\rho_0 \sim \frac{g_v^4}{m_v^4}\vec{j}_v^2\rho_0$, here $\vec{j}_v$ is a vector density, which is defined as

$$\vec{j}_v = \sum_\alpha W_\alpha(\varphi^{\text{up}\dagger}\vec{\sigma}\varphi^{\text{up}} + \varphi^{\text{low}\dagger}\vec{\sigma}\varphi^{\text{low}}). \tag{4.35}$$

We can also expand this density into a non-relativistic density like ρ_s and $\vec{j}_T$. The expansion depends on the density content of the potential $\vec{V}$ and consists of the following nonrelativistic densities:

$$\begin{aligned}\vec{j} &= \frac{i}{2}\sum_\alpha w_\alpha[(\vec{\nabla}\varphi^{\text{class}\dagger})\varphi^{\text{class}} - \varphi^{\text{class}\dagger}(\vec{\nabla}\varphi^{\text{class}})]\\ \vec{T}^2 &= \sum_\alpha w_\alpha[\varphi^{\text{class}\dagger}(\vec{\nabla}\times\vec{\sigma})\varphi^{\text{class}}].\end{aligned} \tag{4.36}$$

These densities change sign under a time reversal.

From Eq. (4.35) we can estimate roughly that $\vec{j}_v \sim 2\,B_0(\vec{j}+\vec{T}^2)$, and from Eq. (4.36) that $\vec{j}_v$ and $\vec{T}^2$ are of order v, therefore $V_r^2\rho_0 \sim \frac{g_v^4}{m_v^4}v^2 4B_0^2\rho_0^3 \sim \frac{g_v^4}{m_v^4}\rho_0^2 4B_0^2\tau \sim 0.3\ \tau$; because this term has a smaller value than the previous one, we can neglect it. Thus in a spherically symmetric system, after a gauge transformation (Eq. (4.27)), the space-component contribution of the vector potential is absorbed into a phase factor, where it seems to give no significant physical effect in $\tilde{H}_{\text{eff}}^{\text{class}}$. Therefore from now on we neglect the space component of the vector term from our discussion and the essential contributions of the potential up to second order in v can be written as :

$$\begin{aligned}V^{\text{cent}} &\equiv S + V_0 + B_0T_r^2 - \frac{\partial}{\partial r}(B_0T_r)\\ \vec{W} &\equiv (\vec{\nabla}B_0) - 2B_0\vec{T}\\ B_0^{-1} &\equiv 2m_{\text{eff}}\end{aligned} \tag{4.37}$$

with (4.29) written as

$$H_{\text{eff}}^{\text{class}} = \vec{p}\frac{1}{2m_{eff}}\vec{p} + V^{\text{cent}} + \vec{W}.(\vec{p}\times\vec{\sigma}). \tag{4.38}$$

This equation will serve to compare the nonrelativistic reductions of the models.

4.2.1 Summary of the Approximations in this Section

Because it will be useful for the reader, here I summarize the approximations which have been done in this chapter.

1. **The time-reversal non-invariant tensor term**
   We neglected it from the Dirac equation due to its smallness.
2. **Approximation in inverse "effective mass" B**
   We neglected $\epsilon` B^2$ terms and B $\approx B_0$ - $\epsilon` B_0^2$ from Eq (4.24), i.e, we neglected contributions in order more than v^4.
3. **Eliminating $\epsilon`$ dependence in the densities and currents**
   To avoid complications due to the $\epsilon`$ dependence in the densities and currents, the contributions from the terms in order v^4 are neglected and the system is assumed to have spherical symmetry.
4. **The space component of vector contribution**
   It is shown that it does not give a significant effect in the effective Hamiltonian for spherical symmetry so that it is neglected.
5. **Effective mass**
   Later, in model comparisons (Eq. (4.45)), we will approximate the effective mass in the effective Hamiltonian by $m_{\text{eff}} \approx m_B + \frac{1}{2}(\tilde{\alpha}_s(\rho_0) - \tilde{\alpha}_v(\rho_0))\rho_0$ to obtain the explicit form of the effective Hamiltonian.

4.3 Comparisons of the Models

We will now compare the Skyrme model with the nonrelativistic reduction expansion up to order v^2 of the linear Walecka model and the point-coupling model. For the linear Walecka model it was already calculated in Ref. [2], so that we can take the results from there, here we only need to calculate for the point-coupling model and to analyse the results.

First the calculation is done without the isospin effect, which will be taken into account later only in the spin-orbit calculation, because it is significant only in this sector. The starting point is the following Lagrangian density

$$\begin{aligned}
\mathcal{L} &\equiv \mathcal{L}_{\text{NHM}} + \mathcal{L}_T \\
\mathcal{L}_{\text{NHM}} &= \mathcal{L}_{\text{free}} - \sum_{i=s,o} (\frac{1}{2}\alpha_i\rho_i^2 + \frac{1}{2}\delta_i\rho_i\triangle\rho_i + \frac{1}{4}\gamma_i\rho_i^4) - \frac{1}{3}\beta_s\rho_s^3
\end{aligned}$$

$$\begin{aligned}
\mathcal{L}_{\mathrm{free}} &= \sum_{\alpha=A} \bar{\Psi}_\alpha (i\gamma_\mu \partial^\mu - m_B)\Psi_\alpha \\
\mathcal{L}_T &= -\frac{1}{2}\Theta_T \rho_0 \vec{\nabla}.\vec{j}_T \equiv \frac{1}{2}\Theta_T \rho_0 \rho_0^T
\end{aligned} \tag{4.39}$$

For $\mathcal{L}_T = 0$, $\mathcal{L}$ represents the NHM parametrization, if $\gamma_s = 0$, it represents the LDZ2a, and if $\beta_s = \gamma_i = 0$ LDZ2. If $\mathcal{L}_T$ is not equal to zero and $\beta_s = \gamma_i = 0$ then LDZ1 is obtained. $\mathcal{L}$ in this form leads to

$$\begin{aligned}
S &\approx \tilde{\alpha}_s(\rho_0)\rho_0 + \delta_s \Delta\rho_0 + \frac{\Theta_T}{4m_{\mathrm{eff}}^2}\left[\frac{\partial}{\partial\rho_0}(\tilde{\alpha}_s(\rho_0)\rho_0)\right](\vec{\nabla}\rho_0)^2 - \frac{1}{2m_{\mathrm{eff}}^2}\left[\frac{\partial}{\partial\rho_0}(\tilde{\alpha}_s(\rho_0)\rho_0)\right](\tau - \vec{\nabla}.\vec{J}) \\
V_0 &\approx \tilde{\alpha}_v(\rho_0)\rho_0 + (\delta_v + \frac{\Theta_T}{4m_{\mathrm{eff}}})\Delta\rho_0 - \frac{\Theta_T}{4m_{\mathrm{eff}}^2}(\frac{\partial m_{\mathrm{eff}}}{\partial\rho_0})(\vec{\nabla}\rho_0)^2 - (\frac{\Theta_T}{2\mathrm{m}_{\mathrm{eff}}})\vec{\nabla}.\vec{J} \\
&+ \frac{\Theta_T}{2\mathrm{m}_{\mathrm{eff}}^2}(\frac{\partial m_{\mathrm{eff}}}{\partial\rho_0})\vec{\nabla}\rho_0 \cdot \vec{J} \\
\vec{T} &= -\frac{\Theta_T}{2}\vec{\nabla}\rho_0.
\end{aligned} \tag{4.40}$$

with

$$\begin{aligned}
\tilde{\alpha}_s &= \alpha_s + \beta_s\rho_0 + \gamma_s {\rho_0}^2 \\
\tilde{\alpha}_v &= \alpha_v + \gamma_v {\rho_0}^2
\end{aligned} \tag{4.41}$$

and the effective mass becomes

$$\begin{aligned}
2m_{\mathrm{eff}} &= 2m_B + (\tilde{\alpha}_s(\rho_0) - \tilde{\alpha}_v(\rho_0))\rho_0 + (\delta_s - \delta_v - \frac{\Theta_T}{4m_{\mathrm{eff}}})\Delta\rho_0 \\
&- \frac{1}{2m_{\mathrm{eff}}^2}\left[\frac{\partial}{\partial\rho_0}(\tilde{\alpha}_s(\rho_0)\rho_0)\right]\tau - \frac{\Theta_T}{2m_{\mathrm{eff}}^2}(\frac{\partial m_{\mathrm{eff}}}{\partial\rho_0})\vec{\nabla}\rho_0.\vec{J} \\
&+ \frac{\Theta_T}{4m_{\mathrm{eff}}^2}\left[\frac{\partial}{\partial\rho_0}(\tilde{\alpha}_s(\rho_0)\rho_0) + (\frac{\partial m_{\mathrm{eff}}}{\partial\rho_0})\right](\vec{\nabla}\rho_0)^2 \\
&+ \frac{1}{2m_{\mathrm{eff}}^2}\left[\frac{\partial}{\partial\rho_0}(\tilde{\alpha}_s(\rho_0)\rho_0) + \Theta_T m_{\mathrm{eff}}\right]\vec{\nabla}\cdot\vec{J}
\end{aligned} \tag{4.42}$$

Notice that the above equation is equivalent to the self-consistency condition for the effective mass m_{eff} in any mean-field model. Solving this equation yields m_{eff}, from which the central potential and the spin-orbit potential can be calculated through the following equations:

$$\begin{aligned}
V^{\mathrm{cent}} &= (\tilde{\alpha}_s(\rho_0) + \tilde{\alpha}_v(\rho_0))\rho_0 + (\delta_s + \delta_v)\Delta\rho_0 \\
&- \frac{1}{2m_{\mathrm{eff}}^2}\left[\frac{\partial}{\partial\rho_0}(\tilde{\alpha}_s(\rho_0)\rho_0)\right]\tau + \frac{\Theta_T}{2m_{\mathrm{eff}}^2}(\frac{\partial m_{\mathrm{eff}}}{\partial\rho_0})\vec{\nabla}\rho_0 \cdot \vec{J}
\end{aligned}$$

$$
\begin{aligned}
&+ \quad \frac{\Theta_T}{4m_{\text{eff}}^2}[\frac{\partial}{\partial\rho_0}(\tilde{\alpha}_s(\rho_0)\rho_0) + \frac{1}{2}\Theta_T m_{\text{eff}}](\vec{\nabla}\rho_0)^2 \\
&+ \quad \frac{1}{2m_{\text{eff}}^2}[\frac{\partial}{\partial\rho_0}(\tilde{\alpha}_s(\rho_0)\rho_0) - \Theta_T m_{\text{eff}}]\vec{\nabla}\cdot\vec{J} \qquad (4.43)
\end{aligned}
$$

and

$$\vec{W}(r) = -\frac{1}{2m_{\text{eff}}^2}[(\frac{\partial m_{\text{eff}}}{\partial\rho_0}) - \Theta_T m_{\text{eff}}]\vec{\nabla}\rho_0. \qquad (4.44)$$

To see $H_{\text{eff}}^{\text{class}}$ more explicitly, unfortunately, we must break the self-consistency condition in Eq. (4.42) with the following approximation

$$m_{\text{eff}} \approx m_B + \frac{1}{2}(\tilde{\alpha}_s(\rho_0) - \tilde{\alpha}_v(\rho_0))\rho_0; \qquad (4.45)$$

substituting Eq. (4.40) into eq. (4.38) leads to

$$
\begin{aligned}
H_{\text{eff}}^{\text{class}} &= C_1\rho_0 + C_2\Delta\rho_0 + C_3\vec{\nabla}\rho_0\cdot\vec{J} + C_4(\frac{d\rho_0}{dr})^2 + C_5\tau + C_6\vec{\nabla}.\vec{J} \\
&+ \vec{p}C_7\vec{p} + C_8(\frac{1}{r}\frac{d\rho_0}{dr})\vec{\sigma}\cdot\vec{L} \qquad (4.46)
\end{aligned}
$$

where for the linear point-coupling model without exchange (LDZ2)

$$
\begin{aligned}
C_1 &= (\frac{{g_v}^2}{{m_v}^2} - \frac{{g_s}^2}{{m_s}^2}) \\
C_2 &= (\frac{{g_v}^2 k_v}{{m_v}^4} - \frac{{g_s}^2 k_s}{{m_s}^4}) \\
C_3 &= C_4 = 0 \\
C_5 &= -C_6 = \frac{\frac{{g_s}^2}{{m_s}^2}}{2(m_B - \frac{1}{2}(\frac{{g_s}^2}{{m_s}^2} + \frac{{g_v}^2}{{m_v}^2})\rho_0)^2} \\
C_7 &= \frac{1}{2(m_B - \frac{1}{2}(\frac{{g_s}^2}{{m_s}^2} + \frac{{g_v}^2}{{m_v}^2})\rho_0)} \\
C_8 &= \frac{(\frac{{g_s}^2}{{m_s}^2} + \frac{{g_v}^2}{{m_v}^2})}{4(m_B - \frac{1}{2}(\frac{{g_s}^2}{{m_s}^2} + \frac{{g_v}^2}{{m_v}^2})\rho_0)^2}, \qquad (4.47)
\end{aligned}
$$

while for the linear point-coupling model with exchange (LDZ1)

$$C_1 = (\frac{{g_v}^2}{{m_v}^2} - \frac{{g_s}^2}{{m_s}^2})$$

$$\begin{aligned}
C_2 &= (\frac{{g_v}^2 k_v}{{m_v}^4} - \frac{{g_s}^2 k_s}{{m_s}^4}) \\
C_3 &= -\frac{\Theta_T(\frac{{g_s}^2}{{m_s}^2} + \frac{{g_v}^2}{{m_v}^2})}{4(m_B - \frac{1}{2}(\frac{{g_s}^2}{{m_s}^2} + \frac{{g_v}^2}{{m_v}^2})\rho_0)^2} \\
C_4 &= \frac{\Theta_T(-\frac{{g_s}^2}{{m_s}^2} + \frac{1}{4}\Theta_T(2m_B - \rho_0(\frac{{g_s}^2}{{m_s}^2} + \frac{{g_v}^2}{{m_v}^2})))}{4(m_B - \frac{1}{2}(\frac{{g_s}^2}{{m_s}^2} + \frac{{g_v}^2}{{m_v}^2})\rho_0)^2} \\
C_5 &= \frac{\frac{{g_s}^2}{{m_s}^2}}{2(m_B - \frac{1}{2}(\frac{{g_s}^2}{{m_s}^2} + \frac{{g_v}^2}{{m_v}^2})\rho_0)^2} \\
C_6 &= \frac{(-\frac{{g_s}^2}{{m_s}^2} - \Theta_T(2m_B - \rho_0(\frac{{g_s}^2}{{m_s}^2} + \frac{{g_v}^2}{{m_v}^2})))}{4(m_B - \frac{1}{2}(\frac{{g_s}^2}{{m_s}^2} + \frac{{g_v}^2}{{m_v}^2})\rho_0)^2} \\
C_7 &= \frac{1}{2(m_B - \frac{1}{2}(\frac{{g_s}^2}{{m_s}^2} + \frac{{g_v}^2}{m_v})\rho_0)} \\
C_8 &= \frac{(\frac{{g_s}^2}{{m_s}^2} + \frac{{g_v}^2}{{m_v}^2} - \Theta_T(2m_B - \rho_0(\frac{{g_s}^2}{{m_s}^2} + \frac{{g_v}^2}{{m_v}^2})))}{4(m_B - \frac{1}{2}(\frac{{g_s}^2}{{m_s}^2} + \frac{{g_v}^2}{{m_v}^2})\rho_0)^2},
\end{aligned} \tag{4.48}$$

for the NHM parametrization

$$\begin{aligned}
C_1 &= (\alpha_s + \alpha_v + \beta_s\rho_0 + (\gamma_s + \gamma_v)\rho_0^2) \\
C_2 &= \delta_s + \delta_v \\
C_3 &= C_4 = 0 \\
C_5 &= -C_6 = -\frac{2(\alpha_s + 2\beta_s\rho_0 + 3\gamma_s\rho_0^2)}{(2m_B + (\alpha_s - \alpha_v + \beta_s\rho_0 + (\gamma_s - \gamma_v)\rho_0)\rho_0^2)^2} \\
C_7 &= \frac{1}{(2m_B + (\alpha_s - \alpha_v + \beta_s\rho_0 + (\gamma_s - \gamma_v)\rho_0^2)\rho_0)} \\
C_8 &= -\frac{(\alpha_s - \alpha_v + 2\beta_s\rho_0 + 3(\gamma_s - \gamma_v)\rho_0^2)}{(2m_B + (\alpha_s - \alpha_v + \beta_s\rho_0 + (\gamma_s - \gamma_v)\rho_0^2)\rho_0)^2},
\end{aligned} \tag{4.49}$$

while finally for LDZ2a, the results are similar with NHM, except that for this parameter set, γ_v =0 and α_i is replaced by $s_i\frac{{g_i}^2}{{m_i}^2}$ and δ_i by $s_i\frac{{g_i}^2 k_i}{{m_i}^4}$, where s_i is equal to +1 for v and -1 for s.

For comparison we take the RMF and Skyrme Hartree-Fock model results from Ref. [2]. For the linear RMF model (LZ), this is

$$C_1 = (\frac{{g_v}^2}{{m_v}^2} - \frac{{g_s}^2}{{m_s}^2})$$

$$\begin{aligned}
C_2 &= (\frac{{g_v}^2}{{m_v}^4} - \frac{{g_s}^2}{{m_s}^4}) \\
C_3 &= C_4 = 0 \\
C_5 &= -C_6 = \frac{\frac{{g_s}^2}{{m_s}^2}}{2(m_B - \frac{1}{2}(\frac{{g_s}^2}{{m_s}^2} + \frac{{g_v}^2}{{m_v}^2})\rho_0)^2} \\
C_7 &= \frac{1}{2(m_B - \frac{1}{2}(\frac{{g_s}^2}{{m_s}^2} + \frac{{g_v}^2}{m_v})\rho_0)} \\
C_8 &= \frac{(\frac{{g_s}^2}{{m_s}^2} + \frac{{g_v}^2}{{m_v}^2})}{4(m_B - \frac{1}{2}(\frac{{g_s}^2}{{m_s}^2} + \frac{{g_v}^2}{{m_v}^2})\rho_0)^2},
\end{aligned} \tag{4.50}$$

and for the Skyrme Hartree-Fock model :

$$\begin{aligned}
C_1 &= \frac{3}{4}t_0 + (\frac{2+\alpha}{16}t_3{\rho_0}^\alpha) \\
C_2 &= -\frac{9t_1 - 5t_2}{32} \\
C_3 &= C_4 = 0 \\
C_5 &= \frac{3t_1 + 5t_2}{16} \\
C_6 &= -C_8 = -3/4t_4 \\
C_7 &= \frac{1}{2m_B} + \frac{3t_1 + 5t_2}{16}\rho_0.
\end{aligned} \tag{4.51}$$

4.4 Discussion

In this subsection, we qualitatively analyse the results from the previous subsection.

4.4.1 LZ and LDZ2 (Linear Parameter Sets)

Except for C_2, the C_i in LZ and LDZ2 are identical. In C_2, LZ has k_i=1 but LDZ2 has $k_i \neq 1$. Referring to chapter 1, remember that this fact actually gives no qualitative physical difference in the nonrelativistic limit. It appears only as a matter of how to represent the approximation in LDZ2, which has as a consequence that some part of the long-range effect still remains in the nonrelativistic limit. Therefore we can say that in the nonrelativistic limit, LZ and LDZ2 are identical.

4.4.2 Linear (LDZ2 or LZ) vs Nonlinear (LDZ2a and NHM) Parameter Sets

On the other hand if γ_v equals zero then NHM and LDZ2a become identical. Comparing LDZ2 (or LZ) and LDZ2a (or NHM), there are three similar points, namely: both parameter sets give $C_3 = C_4 = 0$, $C_5 = -C_6$, and C_2 is density-independent (constant). The denominators of C_5, C_6 and C_8, in both parameter sets, have a very weak density-dependence, whereas the numerators for LDZ2a are density dependent, therefore the difference between LDZ2 and LDZ2a is in C_5, C_6 and C_8. For LDZ2, these have constant values but for LDZ2a they are density dependent. Setting $g_s \approx g_v$ and $m_s \approx m_v$ in both parameter sets leads to $C_8 \approx -C_6$. In LDZ2a C_1 is density dependent, but in LDZ2 C_1 is constant. It is obvious in Eq. (4.49) that the role of γ_v is not only to enhance the nonlinearity in C_1 but give a nonlinearity enhancement also in the spin-orbit coupling (C_8).

4.4.3 PC vs Skyrme Hartree-Fock (SHF) model

Like LDZ2a, the Skyrme (SHF) model has density-dependence in C_1, $C_3 = C_4 = 0$ and also C_2 is density independent. SHF has $C_8 = -C_6$ but $C_5 \neq -C_6$. Now LDZ1, due to the enhancement from the tensor term, has C_3, $C_4 \neq 0$ and like SHF, this parameter set has $C_5 \neq -C_6$. As we mentioned previously, the tensor term in LDZ1 enhances also the spin-orbit term (C_8) due to the additional density-dependent term in C_8. The other density-dependent term in LDZ1 is C_6. From the above results, it seems to me that if one wants to have a correct spin-orbit splitting, one needs to have a correct density dependence in $\vec{W}$, because only models with an additional density dependence in C_8 (LDZ2a and NHM obtain this part from nonlinear terms and LDZ1 from the tensor term) give acceptable spin-orbit predictions. To combine an acceptable binding energy and surface thickness prediction one needs to have density dependence in C_1 (NHM and LDZ2a). For constant C_1, nonzero values of C_3 and C_4 and also a density dependence in C_6 like LDZ1 can help the prediction of binding energy and surface thickness a bit, but the results are still far from acceptable, because we see from the first chapter that LDZ1 has a problem in the prediction of binding energies in isotonic chains and a much larger χ^2 of the surface thickness than models with the nonlinearity.

4.4.4 Possible Enhancement in Nonlinear Terms and Isospin Effect

Taking into account the exchange correction in the nonlinear terms, after a straightforward calculation in the effective Hamiltonian, instead of C_2 all C_i are seen to be density dependent (since the explicit form does not provide particular insight, I omit presenting it here). If we calculate by using the model of Rusnak and Furnstahl (R-F) [21] with the derivative nonlinear terms taken into account. we will obtain C_2 also density dependent.

Generally the spin-orbit potential can be written as

$$\vec{W}_q = b_4 \vec{\nabla}\rho_0 + b_4' \vec{\nabla}\rho_q + c_1 \vec{J} + c_1' \vec{J}_q. \tag{4.52}$$

We will once again use the NHM model without the exchange terms and take the contribution of isovector terms into account to study how the isospin effect enhances the spin-orbit potential. In the same way as before

$$\begin{aligned} b_4 &= -\frac{A(\rho_0)}{(2m_q + A'(\rho_0)\rho_0 + B\rho_q)^2}, \\ b_4{}^{\prime} &= -\frac{B}{(2m_q + A'(\rho_0)\rho_0 + B\rho_q)^2}, \\ c_1 &= 0, \qquad c_1' = 0, \end{aligned} \tag{4.53}$$

with

$$\begin{aligned} A(\rho_0) &= (\alpha_s - \alpha_{ts} - \alpha_v + \alpha_{tv}) + 2\beta_s\rho_0 + 3(\gamma_s - \gamma_v)\rho_0^2, \\ A'(\rho_0) &= (\alpha_s - \alpha_{ts} - \alpha_v + \alpha_{tv}) + \beta_s\rho_0 + (\gamma_s - \gamma_v)\rho_0^2, \\ B &= \alpha_{ts} - \alpha_{tv}. \end{aligned} \tag{4.54}$$

From the previous chapter we can see that if we take into account the tensor term (R-F model [21] or LDZ1 for example) there will be a small correction in b_4 and b_4' due to the tensor contribution in this part, and if we take into account the exchange corrections, we will have not only enhancements in b_4 and b_4' but also c_1 and c_1' are not zero, due to the contribution of the tensor terms which come from the Fierz Transformation. Once again it must be said that these corrections are small.

This discussion makes clear that the density dependence in the C_i can be created by the tensor and the nonlinear terms. But in contrast to the nonlinear terms, the tensor terms alone seem not to be adequate to yield acceptable results in the finite nuclear observables. Therefore, *it seems quite obvious from this qualitative analysis in the nonrelativistic limit that the role of the nonlinear terms to describe finite nuclei is highly significant.*

–V–

SUPERHEAVY NUCLEI

The study of the possible existence of shell-stabilized superheavy elements (SHE) is important for heavy ion physics([57] and Refs. therein). The earliest calculations extrapolating nuclear shell structure to superheavy systems by using the shell correction method can be seen from the Frankfurt group in Refs. [60, 61, 62, 63] and the others in [58, 59, 66, 67]. They predicted spherical proton shell closures at Z=114 and Z=126 and the spherical neutron shell closure at N=184. Experimental progress on this topic can be found in Refs. [68, 69, 70, 71, 72, 73, 74]. Self-consistent mean-field models (relativistic and nonrelativistic) have been used for the investigation of superheavy nuclei [14, 75, 9, 10, 11, 76, 13, 27, 18, 49, 57].

Especially interesting results can be found in Ref. [13], showing that different types of self-consistent models do not give a unique shell closure prediction for superheavy nuclei. The relativistic models were represented by the NLZ, PL40, NL-SH and TM1 parameter sets. NLZ, PL40 and NL-SH gave the same shell closure prediction, namely Z=120 and N=172 but the TM1 parameter set did not predict strong shell structure for spherical superheavy nuclei. The nonrelativistic models were represented by the Skyrme model with the SKM*, SKP, SKx and SLy6 parameter sets. SKM* and SKP predicted Z=126 and N=184, SKI4 predicted Z=114 and N=184, but SKI1, SKI3 and SLy6 did not predict strong shell structure for spherical superheavy nuclei.

In Ref. [18], Bender et al. have investigated systematically the shell structure of the superheavy nuclei using the self-consistent mean-field models. They focused on differences in the isospin dependence of the spin-orbit interaction and the effective mass between the models and their influence on the single-particle spectra. Their findings have given a strong argument for Z=120 and N=172 to be the next spherical doubly magic superheavy nucleus, but until now, the precise microscopic origin of this discrepancy is still not clear.

The underlying models do not only differ in their representation of the effective nucleon-nucleon interaction and their treatment of relativity but also with respect to their many-body character [27].

In this chapter we will analyse the role of the nonlinear terms in the binding energies and the single-particle spectra of heavy and superheavy nuclei by using the nonrelativistic reduction results from the previous chapter. The result of this analysis will be used to restudy the discrepancy of predictions for superheavy nuclei between relativistic and nonrelativistic models.

5.1 Results and Discussion

Before we go into superheavy nuclei, let us focus once again on the differences and the similarities between the linear (LZ and LDZ2) and nonlinear parameter sets (NLZ and LDZ2a). We can see from the previous chapters that parameter sets with nonlinear terms come much closer to experimental data. The parameter sets without nonlinear terms fail to give acceptable predictions. This applies not only to the binding energies, but also to the shell structure predictions (single-particle spectra and/or spin orbit splitting). The two nonlinear models (NLZ and LDZ2a) have similar behaviour in binding energies and shell structure predictions. There are of course some differences in detail between both parameter sets, but it seems that the difference is not big enough to distinguish the predictive capability of both parameter sets. The same situation occurs also between the two linear parameter sets (LZ and LDZ2). In the nonrelativistic limit we know that the LDZ2 and LZ parameter sets have identical form in every constant in the effective Hamiltonian, concluding that, due to the nature of the finite nuclear observables and the "magic of the fitting procedure", the different behaviour of both models at short distance (or high momentum) does not emerge or cannot be seen from those observables. In the nonlinear case, the nonlinear terms of the NLZ parameter set contain the σ meson, while the LDZa parameter set has simple explicit scalar density-dependent nonlinear terms. I do not intend to interpret the above fact as meaning that the replacement of two types of nonlinear terms has no physical effects, but with the same argument as before, namely that the nature of the finite nuclei observables and the fitting procedure make the binding energies and shell structure predictions insensitive to the difference of these nonlinear terms. It is clear from the previous discussion that the LDZ2 and LDZ2a parameter sets yield different predictions and in the nonrelativistic limit contain different forms of some constants. Thus it is quite reasonable to interpret *the difference of those constants in the nonrelativistic limit as the key feature leading to different predictions in finite nuclei.*

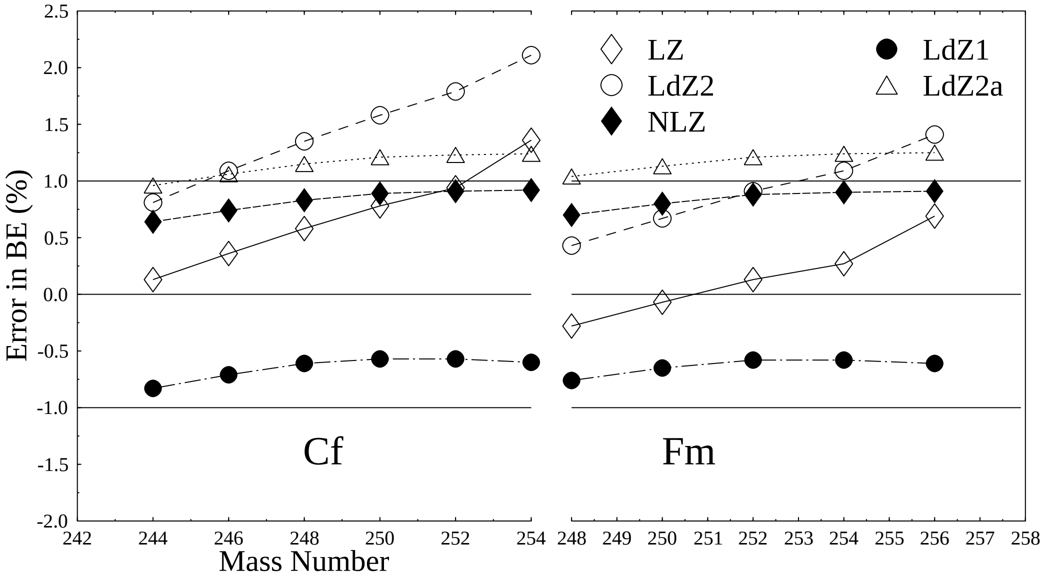

Figure 5.1: Error in the binding energies for Cf and Fm isotopic chains.

5.1.1 Nonlinear Effects in the Heavy and Superheavy Regions

Now we check whether the differences and the similarities of the linear and nonlinear parameter sets still remain in the heavy and two superheavy nuclei, namely Z=114, N= 184 and Z= 120 N=172. First we study the binding energies of two heavy nuclei isotopic chains, namely the Californium and Fermium isotopes. Figure 5.1 shows that all parameter sets except LDZ2 show about 1 % error in the binding energies, but each of them has a different trend. The trend difference can be seen more clearly in the two-neutron separation energies of figure 5.2. We see from figure 5.2 that the linear models without exchange (LDZ2 and LZ) show a quite different trend from NLZ, and LDZ2a (PC model with standard nonlinear terms) has almost the same trend as the standard parameter set NLZ. The LDZ1 parameter set (a linear PC model but with exchange contribution) has a different trend from NLZ but is quite acceptable. LDZ2a has a similar trend as NLZ and LDZ2 has as LZ. These results emphasize the results from the previous chapter. The different behaviour due to the nonlinear effect not only appears in the binding energies but is also reflected in the charge densities. In the superheavy region, this is still the same, as is clear from figure 5.3.

From the previous chapter, it is known that in contrast to the sets NLZ, LDZ1, and LDZ2a, LZ and LDZ2 do not give an acceptable spin-orbit splitting. From the point of view of

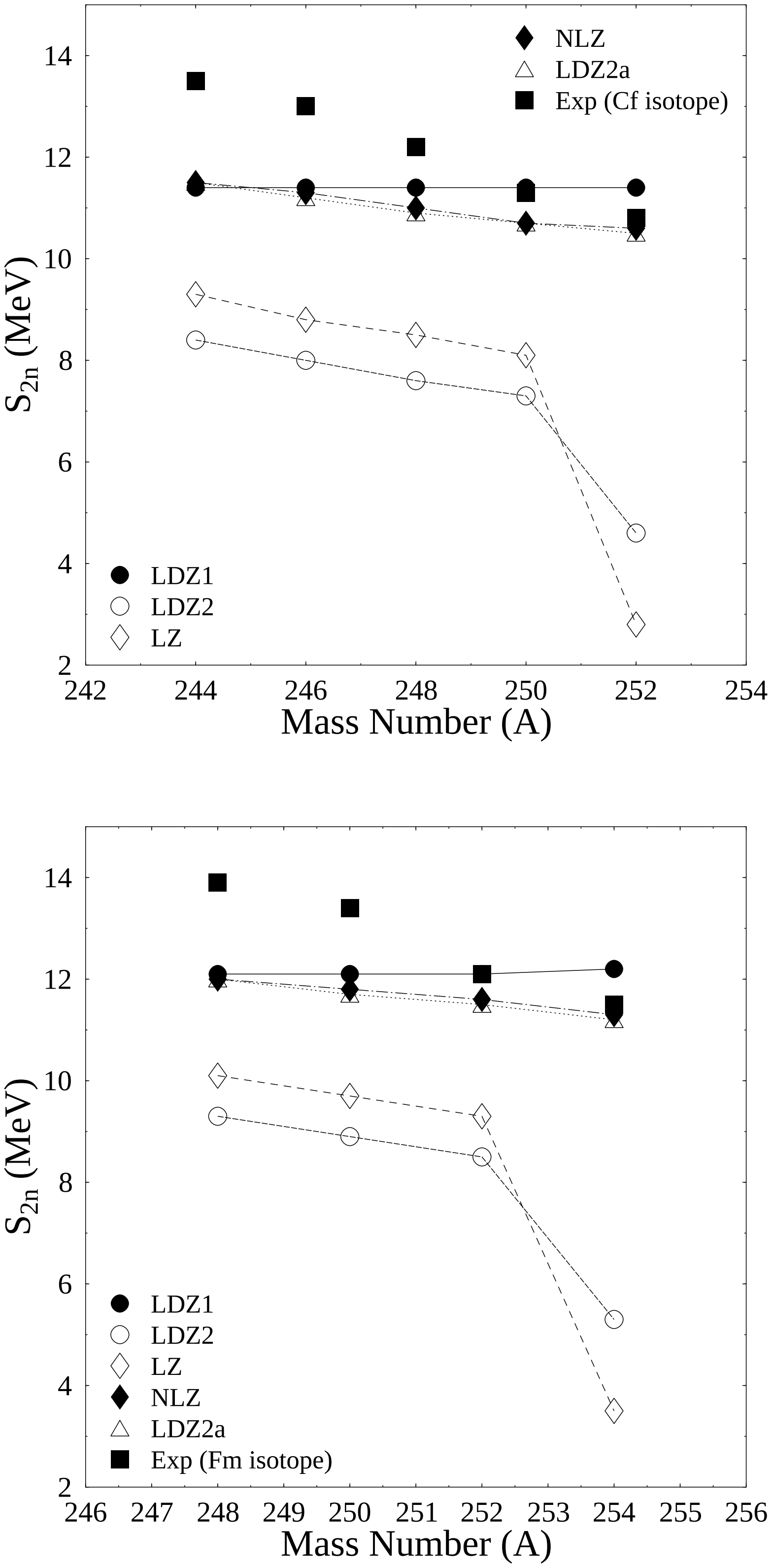

Figure 5.2: Two-neutron separation energies (S_{2n}) for Cf and Fm isotopic chains.

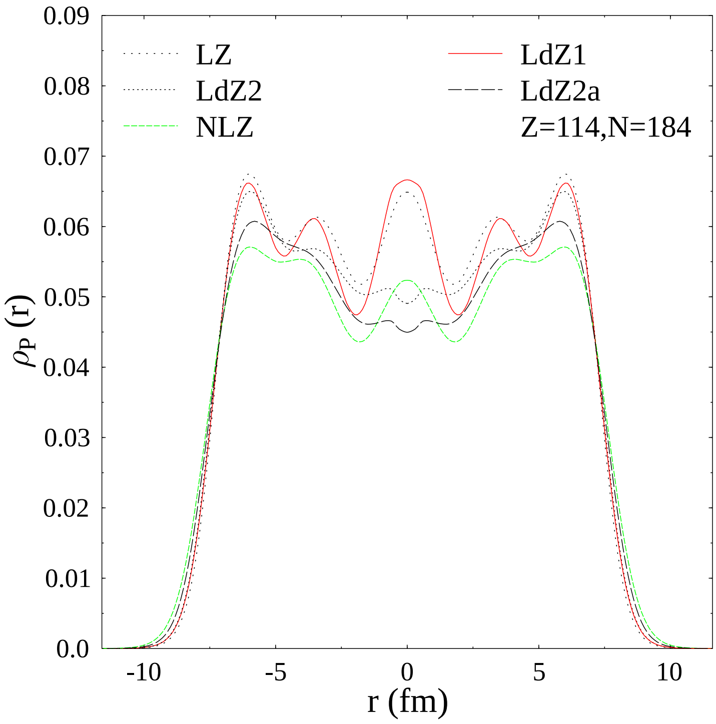

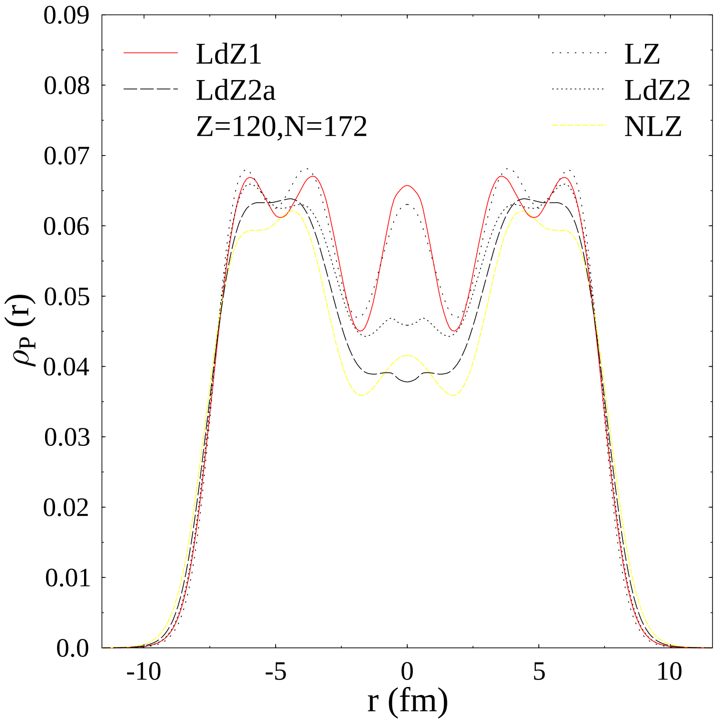

Figure 5.3: The charge density as a function of the radius for Z=114, N=184 and Z=120, N=172.

the nonrelativistic limit, the LZ and LDZ2 parameter sets do not have density dependence in the spin-orbit potential, while LDZ1 and LDZ2a have a small one, but the density dependence in the spin-orbit potential behaviour of LDZ1 is different from that of LDZ2a, because they appear from different sources. This fact is a consequence of the correct spacing of single-particle spectra predicted by the model. The single-particle spectra seem most important for the stability of superheavy nuclei [14, 75, 9, 10, 11, 76, 13, 27, 18, 49, 57]. Therefore only models with acceptable single-particle spectra could give a correct prediction of superheavy nuclei. Figures 5.4 and 5.5 show that for LDZ2, LZ and LDZ1 not only the spacing but also the position of the single-particle states is different from NLZ in the super heavy region, but it is interesting that, even though LDZ2a has not quite the same spacing as NLZ, it still predicts similar behaviour of the single-particle spectra.

5.1.2 Shell Closures Predictions in Superheavy Nuclei

Therefore we expect that LDZ2a yields similar predictions for spherical shell closures in superheavy nuclei as NLZ. A direct measure of a shell closure is the observation of a sudden jump in the two-nucleon separation energies for protons and neutrons, easily visible in the "two-nucleon gaps" [13]. The definition of the two-nucleon gaps is as follow :

$$\begin{aligned} \delta_{2\mathrm{p}}(N,Z) &= 2B(N,Z) - B(N,Z-2) - B(N,Z+2) \\ \delta_{2\mathrm{n}}(N,Z) &= 2B(N,Z) - B(N-2,Z) - B(N+2,Z). \end{aligned} \tag{5.1}$$

These expressions correspond to the second differences in the binding energy and will show a maximum where the two-nucleon separation energies have a jump. One important thing to remember is that a guarantee for spherical shape can only be given for doubly magic nuclei where protons as well a neutrons experience a spherical shell closure. Singly magic nuclei have a good chance to stay spherical, but can deform occasionally [13]. The result can be seen in figure 5.6. We see that LDZ2a gives a spherical proton shell closure at Z=120 and a spherical neutron shell closure at N=184. There is a signal of a spherical neutron shell closure developing at N=172, but it is weak. There is still some difference in this prediction from NLZ, but globally the trends are similar.

We showed in chapter four that for the point coupling model (LDZ2a parameter set) in the nonrelativistic limit the nonlinear terms automatically give a contribution in the form of a small nonlinearity (density dependence) in V_{cent} and $W_{\mathrm{L-S}}$. Because the correct form of V_{cent} has a connection to correct binding energies and the correct form of $W_{\mathrm{L-S}}$ to correct shell structure, it appears that to predict spherical shell closures in superheavy nuclei from the relativistic model the inclusion of the correct form of the nonlinear terms is necessary.

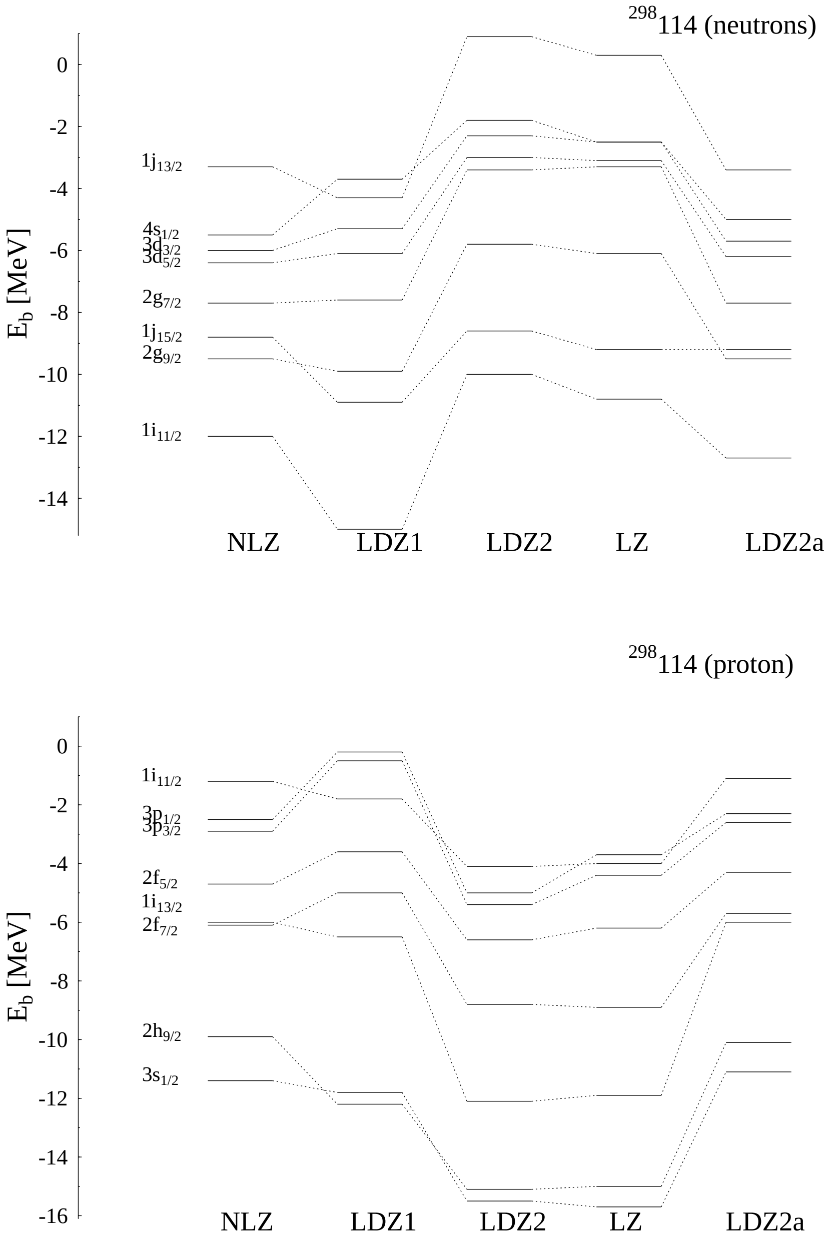

Figure 5.4: Single-particle spectra for Z=114 (neutrons) in the upper figure and for Z=114 (protrons) in the lower figure.

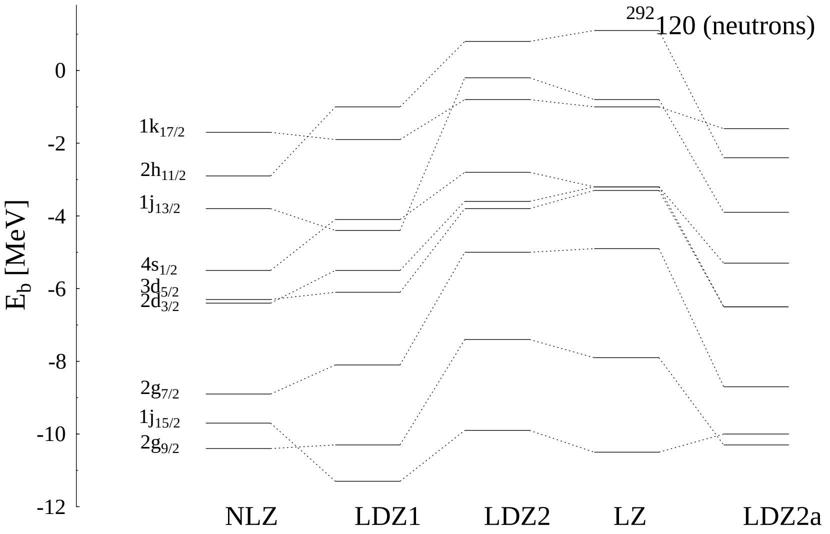

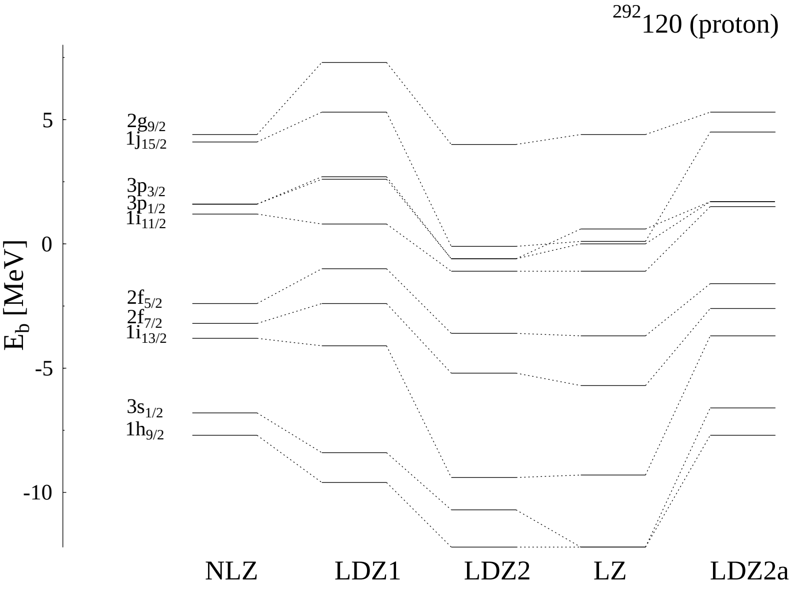

Figure 5.5: Single-particle spectra for Z=120 (neutrons) in the upper figure and for Z=120 (protrons) in the lower figure.

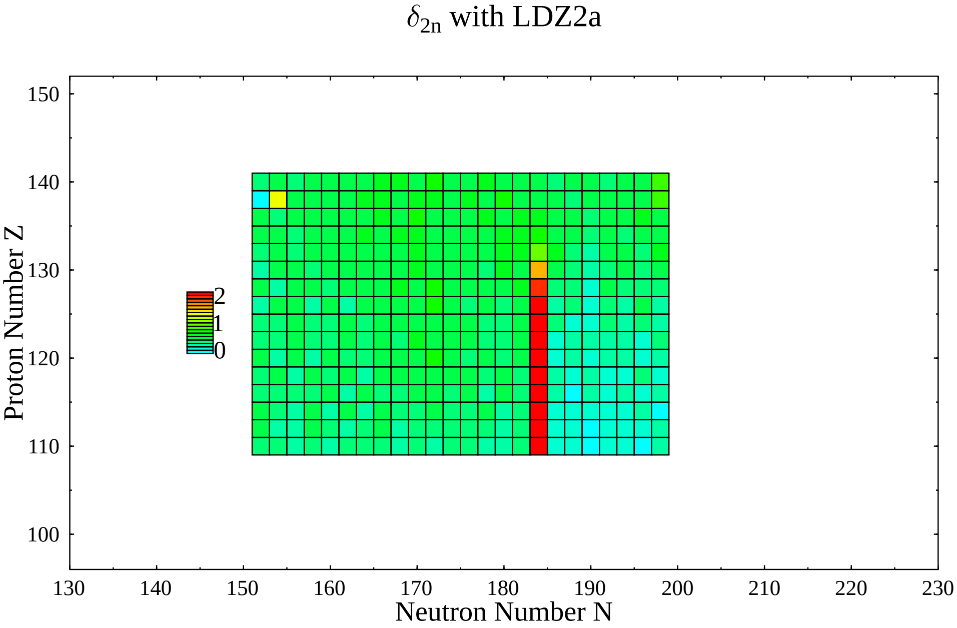

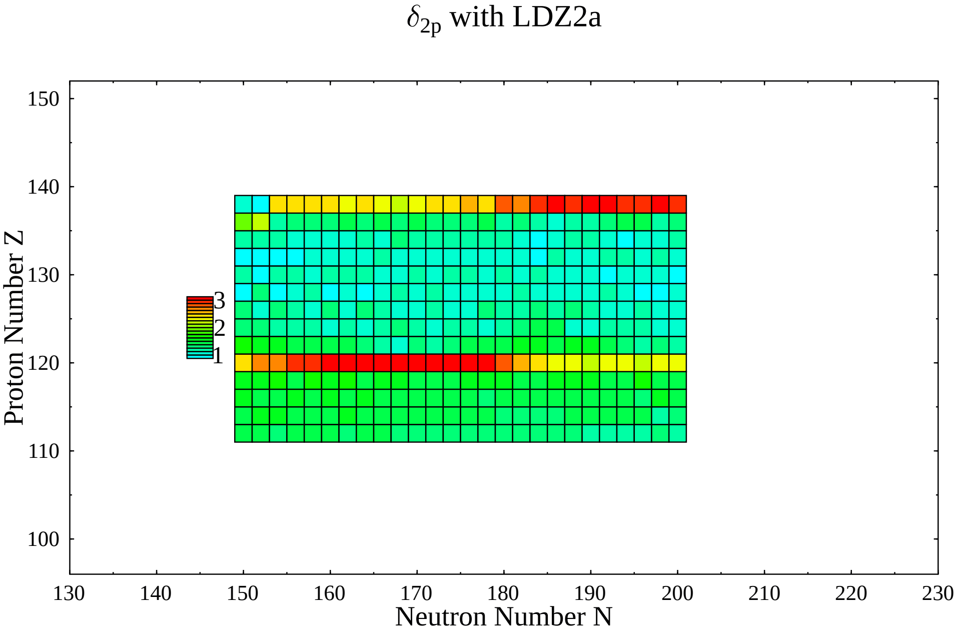

Figure 5.6: Second differences of binding energy with respect to proton (δ_{2p}) and neutron number (δ_{2n}) in the superheavy region for the parameter set LDZ2a, plotted in a grayscale as shown to the left (value in MeV).

5.1.3 Nonrelativistic Limit of the PC vs Skyrme Model (Essential Points)

Now we are ready to analyse the discrepancy between the predictions of the PC model and the Skyrme-force model from the point of view of the nonrelativistic limit.

1. **The significant differences in $V_{\rm cent}$ are in C_1:**
   (a) the Skyrme model has:
   $$C_1 \quad \sim \quad a_1 + a_2\rho_0^\alpha \tag{5.2}$$
   (b) while the parameter set LDZ2a has:
   $$C_1 \quad \sim \quad a_3 + a_4\rho_0 + a_5\rho_0^2. \tag{5.3}$$
   $a_1..a_5$ are constant. With these forms both models yield good predictions for the binding energies. We see that the constants (a_2 and α) or (a_4 and a_5) play a crucial role, because without these constants there never result acceptable binding energy predictions, as discussed previously. The other basic consideration from the nonrelativistic Skyrme model point of view is as follows: there must be a minimum in E/A vs k_f and a correct incompressibility value of nuclear matter in connection with acceptable binding energies in finite nuclei. This can be achieved in the Skyrme model only if we introduce the constants a_2 and α.

2. **The significant differences in $W_{\rm L-S}$ are in C_8**
   (a) the Skyrme model has:
   $$C_8 \quad \sim \quad b_1 \tag{5.4}$$
   (b) while the parameter set LDZ2a has:
   $$C_8 \quad \sim \quad b_3 + b_4\rho_0 + b_5\rho_0^2 + \text{isospin} \quad \text{contributions}. \tag{5.5}$$
   Here $b_1..b_5$ are constant. With the form (5.4) the Skyrme model does not yield really satisfactory shell structure [18, 49, 57]. As we see LDZ2a yields an acceptable prediction for the shell structure. An extension of the Skyrme model with an enhancement in $W_{\rm L-S}$ by isospin contributions has already been done (SKI3-4) [18] and [13]. By introducing isospin contributions into the spin-orbit potential, like in the RMF model, SKI3-4 do reproduce the isotope shift of the rms radii in the heavy Pb

isotopes, but these parameter sets still yield different shell closures in superheavies than the RMF model. On the other hand, in relativistic PC models, the role of b_4 and b_5 seems important to reproduce acceptable single-particle spectra. Therefore possibly the enhancement of SKI3-4 with nonlinear terms (density dependent) can give even more improvement in their shell structure predictions.

5.1.4 Skyrme Force Inspired by the PC Model

The above discussion is only qualitative; a quantitative calculation using the Skyrme model not only with isospin terms but also with density dependent terms in the spin-orbit potential is strongly suggested. A density-dependent ansatz in the spin-orbit potential has been introduced in Ref [77], but unfortunately this reference does not give a parameter set for this type of Skyrme model and the form of the spin-orbit potential is quite different from the one predicted by the point-coupling model. The energy density which reproduces the spin-orbit potential predicted by the point-coupling model is given by

$$\varepsilon(r) \equiv \varepsilon^0(r) + \frac{1}{2}(W_1\rho + W_2\rho^2)(\vec{J}_n.\vec{\nabla}\rho_p + \vec{J}_p.\vec{\nabla}\rho_n + \sum_q \vec{J}_q.\vec{\nabla}\rho_q), \tag{5.6}$$

$\varepsilon^0(r)$ is the energy density in the absence of the new terms and $\vec{J}_q$ is the neutron or proton spin-current density. From $\varepsilon(r)$ we find for the central potential

$$\begin{aligned} U_q(r) &= U_q^0(r) - \frac{1}{2}(W_1\rho + W_2\rho^2)\vec{\nabla}.\vec{J} \\ &+ \frac{1}{2}(W_1 + 2W_2\rho)(2\vec{J}_q.\vec{\nabla}\rho_q - \vec{J}.\vec{\nabla}\rho - 2\vec{J}.\vec{\nabla}\rho_q - 2\vec{J}_q.\vec{\nabla}\rho), \end{aligned} \tag{5.7}$$

and for the spin-orbit potential

$$\vec{W}_q(r) = \frac{1}{2}\vec{W}_q^0(r) + \frac{1}{2}(W_1\rho\vec{\nabla}\rho + W_2\rho^2\vec{\nabla}\rho). \tag{5.8}$$

Where $\vec{W}_q^0(r)$ is the spin-orbit potential and $U_q^0(r)$ the central potential in the absence of the new terms.

–VI–

CONCLUSION AND OUTLOOK

6.1 Conclusion

We have fitted parameter sets in two approximations, i.e. a linear point-coupling approximation with and without the exchange corrections by using the same procedure as Ref. [7]. We used the parameter sets to calculate the error in binding energies and the two-proton (two-neutron) separation energies of some isotopic and isotonic chains. We also calculated the error of the diffraction radii and surface thicknesses of some isotopes. The spin-orbit splitting, single-particle spectra, and nuclear matter properties also were calculated. The predictive power of both parameter sets is reflected by the above results and was compared to that of the standard parameter sets LZ and NLZ. We also compared with LDA results [27] and also the $\chi^2/nucleus$ of the above parameter sets with the $\chi^2/nucleus$ of a full Hartree-Fock calculation [26].

We have found that due to the nature of the finite nucleus observables and the "magic of the fitting process" the difference between the RMF model and the point-coupling model in short distance (or high momentum) does not emerge or cannot be seen obviously from the predictive power of both models for finite nuclei. On the other hand, if we take into account the exchange effects, distinctions in predictive power appear. We conclude that the exchange effect cannot be absorbed into the coupling constants of the linear RMF or PC model. The linear RH and RHF calculation seems to indicate that some physics is still missing in the model and the nonlinear terms are needed to cure this. An investigation of these nonlinear terms on a more fundamental level is necessary to explore more deeply the nature of finite nuclei from the point of view of relativistic models and to understand the relativistic models by themselves.

We have derived the effective Hamiltonian of the nonlinear point-coupling model in the nonrelativistic limit, using it to analyse the previous results. It becomes clear that the role of the nonlinearity in the PC model is important not only for the bulk properties but also for the shell structure. Different from the nonrelativistic models, the nonlinearity in the relativistic models automatically yields contributions in the form of a weak density dependence not only in the central potential but also in the spin-orbit potential. The central potential affects the bulk and surface properties while the spin-orbit potential is crucial for the shell structure of finite nuclei. We have also used these results to analyse superheavy nuclei and then suggested a modification in the Skyrme model with a density-dependent spin-orbit potential inspired by the PC model.

6.2 Outlook

Three things are quite important to investigate in the future before turning to the Hartree-Fock-Bogoliubov calculations: first, the role of nonlinear exchange terms, second, the most effective form of the nonlinear terms and third, the exact treatment of derivative exchange terms. The reason to do the third one is clear and the following argumentation can be used to illuminate why the first and the second investigations in my opinion are also important.

Let us consider the following case: I fitted $\mathcal{L}_{\mathrm{L}}^{\mathrm{HF}}$ from chapter one, plus

$$\mathcal{L}_{\mathrm{NL}}^{\mathrm{a}} = -\frac{1}{3}C_2\rho_s^3 - \frac{1}{4}C_3\rho_s^4, \tag{6.1}$$

where $\mathcal{L}_{\mathrm{NL}}^{\mathrm{a}}$ simulates all effects beyond linear PC Hartree Fock. We also regard this parameter set (Test-NLa) as a nonlinear PC Hartree Fock ignoring the exchange from the nonlinear terms.

Parameters	g_s	g_v	g_R	k_s	k_v	k_r	C_2	C_3
set a	9.4586	12.3756	9.4586	0.3123	-0.1556	0.1145	24.1679	-83.3120
LDZ2a	9.5046	12.4295	8.9677	0.3112	-0.091	-4.1944	23.7337	-81.8440

Table 6.1: Value of the Test-NLa and the LDZ2a parameter set.

There is still improvement comparing set a with LDZ2a in the surface thicknesses, but not too significant. If we compare with the standard parameter set NLZ, it seems some effort is still needed to improve the surface thickness predictions. Possibly taking into

Parameters	g_s	g_v	g_R	k_s	k_v	k_r	C_2	C_3	C^b
set b	9.516	12.502	10.775	0.276	-0.077	0.043	24.146	-87.6741	-0.4170

Table 6.2: Parameter value of the Test-NLb.

χ^2	BE	DR	ST	Total
set a	21.93	6.91	59.51	88.35
set b	19.32	9.71	41.00	70.00
LDZ2a	27.65	6.57	75.79	110.01
NLZ	23.89	18.77	29.25	71.92

Table 6.3: χ^2 results from the Test-NLa, Test-NLb, LDZ2a, and NLZ. BE denotes the binding energies, DR the diffraction radius and ST the surface thickness contributions

account the nonlinear exchange terms may give better results without adding new free parameters. Therefore an investigation of the necessity for the nonlinear exchange terms is quite important.

As we have discussed previously, the significant difference between the RMF model and the PC model appears quite significantly in the surface thickness observables. I suspect that this is due to the advantages of the mesonic nonlinear terms, which already include implicitly the contribution of the derivative nonlinear terms from the PC model point of view. As a preliminary test, I added one more term (with one more free parameter) in $\mathcal{L}^{\mathrm{a}}_{\mathrm{NL}}$ as

$$\mathcal{L}^{\mathrm{b}}_{\mathrm{NL}} = \mathcal{L}^{\mathrm{a}}_{\mathrm{NL}} + C^b {\rho_s}^2 \Delta \rho_s \tag{6.2}$$

The parameter count of the Test-NLb is equal to that of the conventional PC model. In this version the exchange of linear terms is taken into account and a derivative nonlinear term is used instead of the vector nonlinear term. the Test-NLb gives more improvement in surface thickness than the Test-NLa. This is still a preliminary test, but motivates an investigation to search more effective nonlinear terms than the standard ones in the PC model. This is clearly of paramount interest.

–A–

FIERZ TRANSFORMATION (FT)

The complete derivation of the FT for the spinor in the second order case can be found in the text books, for example in Ref. [56]. The extension to higher order can be found in Ref. [50]. For the isospin case in second order one can derive it straightforwardly. Here we give the FT in second order taking into account isospin effects.

The result can be written as

$$\bar{\Psi}_\alpha(x_1)\Gamma^i\Psi_\beta(x_3)\bar{\Psi}_\beta(x_2)\Gamma_i\Psi_\alpha(x_4) = \sum_j C_{ji}\bar{\Psi}_\alpha(x_1)\Gamma^j\Psi_\alpha(x_4)\bar{\Psi}_\beta(x_2)\Gamma_j\Psi_\beta(x_3), \tag{A.1}$$

where Γ_i denotes one of the operator combinations constructed from the Dirac matrices and the isospin, and the constants C_{ji} are written in the following table

C_{ji}	Γ_i=1	Γ_i =γ_μ	Γ_i=$\gamma_\mu\vec{\tau}$
Γ_j =1	$\frac{1}{8}$	$\frac{4}{8}$	$\frac{12}{8}$
Γ_j=$\vec{\tau}$	$\frac{1}{8}$	$\frac{4}{8}$	-$\frac{4}{8}$
Γ_j=γ_μ	$\frac{1}{8}$	-$\frac{2}{8}$	-$\frac{6}{8}$
Γ_j=$\gamma_\mu\vec{\tau}$	$\frac{1}{8}$	-$\frac{2}{8}$	$\frac{2}{8}$
Γ_j=$\sigma_{\mu\nu}$	$\frac{1}{16}$	0	0
Γ_j=$\sigma_{\mu\nu}\vec{\tau}$	$\frac{1}{16}$	0	0
Γ_j=γ_5	$\frac{1}{8}$	-$\frac{4}{8}$	-$\frac{12}{8}$
Γ_j=$\gamma_5\vec{\tau}$	$\frac{1}{8}$	-$\frac{4}{8}$	$\frac{4}{8}$
Γ_j=$\gamma_5\gamma_\mu$	$\frac{1}{8}$	$\frac{2}{8}$	$\frac{6}{8}$
Γ_j=$\gamma_5\gamma_\mu\vec{\tau}$	$\frac{1}{8}$	$\frac{2}{8}$	-$\frac{2}{8}$

In the practical calculation, we will neglect terms with γ_5, as for spherical nuclei the parity is assumed to be a good quantum number.

–B–

EXCHANGE PART FROM THE DERIVATIVE LAGRANGIAN DENSITY

To derive the approximation for the exchange part from the derivative Lagrangian density, we use the Gordon decomposition [38]. The derivation is straightforward, as one can see for the scalar case in section 1. In this Appendix, we collect all of the results of this approximation.

1. the Scalar Case

$$\tilde{\mathcal{L}}_S^{lin} = -\frac{1}{2}\partial_\mu \rho_s \partial^\mu \rho_s + 2m_B^2 \rho_s^2 - 2m_B^2 J_v^\mu J_{v\mu} - 2m_B J_v^\mu \partial^\nu (J_{T\nu\mu}) - \frac{1}{2}\partial^\nu (J_{T\nu\mu}) \partial_\sigma (J_T{}^{\sigma\mu}) \quad \text{(B.1)}$$

and

$$\begin{aligned} \tilde{\mathcal{L}}_S^{non-lin} &= -\frac{4m_B \tilde{g}_s^2}{m_s^2}\rho_s^3 + \frac{2\tilde{g}_s^4}{m_s^4}\rho_s^4 + 4m_B \frac{\tilde{g}_s^2}{m_s^2}\rho_s J_v^\mu J_{v\mu} \\ &+ 2(\frac{\tilde{g}_s^2}{m_s^2}\rho_s J_v^\mu \partial^\nu (J_{T\nu\mu}) + \frac{\tilde{g}_v^2}{m_v^2}\rho_s J_{T\nu\mu}\partial^\nu (J_v^\mu)) - \frac{2\tilde{g}_s^4}{m_s^4}\rho_s^2 J_v^\mu J_{v\mu} + ..., \end{aligned} \quad \text{(B.2)}$$

2. the Vector Case

$$\tilde{\mathcal{L}}_V^{lin} = -\frac{1}{2}\partial_\mu J_v^\nu \partial^\mu J_{v\nu} + 2m_B^2 J_v^\nu J_{v\nu} \quad \text{(B.3)}$$

$$\tilde{\mathcal{L}}_V^{non-lin} = -\frac{2\tilde{g}_v^4}{m_v^4}(J_v^\nu J_{v\nu})^2 - 4m_B \frac{\tilde{g}_s^2}{m_s^2}\rho_s J_v^\mu J_{v\mu} + \frac{2\tilde{g}_s^4}{m_s^4}\rho_s^2 J_v^\mu J_{v\mu} + \frac{2\tilde{g}_s^2}{m_s^2}\rho_s \partial^\nu (J_{T\nu\mu} J_v^\mu) + ..., \quad \text{(B.4)}$$

3. the Tensor Case

$$\tilde{\mathcal{L}}_T^{lin} = \frac{1}{2}\partial_\mu (J_T^{\alpha\beta})\partial^\mu (J_{T\alpha\beta}) \tag{B.5}$$

4. the Scalar-Isovector Case

$$\tilde{\mathcal{L}}_{tS}^{lin} = -\frac{1}{2}\partial_\mu \vec{\rho}_{ts}\partial^\mu \vec{\rho}_{ts} + 2m_B^2 \vec{\rho}_{ts}^{\,2} - 2m_B^2 \vec{J}_{tv}^{\mu} \vec{J}_{tv\mu} - 2m_B \vec{J}_{tv}^{\mu}\partial^\nu (\vec{J}_{tT\nu\mu}) - \frac{1}{2}\partial^\nu (\vec{J}_{tT\nu\mu})\partial_\sigma (\vec{J}_{tT}^{\sigma\mu}) \tag{B.6}$$

$$\begin{aligned} \tilde{\mathcal{L}}_{tS}^{non-lin} &= +4\frac{\tilde{g}_s^2}{m_s^2} m_B \rho_s (\vec{J}_{tv}^{\mu}\vec{J}_{tv\mu} - \vec{\rho}_{ts}^{\,2}) - 2\frac{\tilde{g}_s^4}{m_s^4}\rho_s^2 (\vec{J}_{tv}^{\mu}\vec{J}_{tv\mu} - \vec{\rho}_{ts}^{\,2}) \\ &+ 2\frac{\tilde{g}_s^2}{m_s^2}\partial^\sigma (\vec{J}_{tT\sigma\mu})\rho_s \vec{J}_{tv}^{\mu} + \frac{\tilde{g}_v^2}{m_v^2}\vec{\rho}_{ts}\vec{J}_{tT\sigma\mu}\partial^\sigma (J_v^\mu) + \ldots \end{aligned} \tag{B.7}$$

5. the Vector-Isovector Case

$$\tilde{\mathcal{L}}_{tV}^{lin} = -\frac{1}{2}\partial_\mu \vec{J}_{tv}^{\nu}\partial^\mu \vec{J}_{tv\nu} + 2m_B^2 \vec{J}_{tv}^{\nu}\vec{J}_{tv\nu} \tag{B.8}$$

$$\tilde{\mathcal{L}}_{tV}^{non-lin} = -4m_B\frac{\tilde{g}_s^2}{m_s^2}\vec{J}_{tv}^{\nu}\vec{J}_{tv\nu}\rho_s + 2\frac{\tilde{g}_s^4}{m_s^4}\rho_s^2 \vec{J}_{tv}^{\nu}\vec{J}_{tv\nu} - 2\frac{\tilde{g}_v^4}{m_v^4}(\vec{J}_{tv}^{\nu}J_{v\nu})^2 + \frac{2\tilde{g}_s^2}{m_s^2}\rho_s\partial^\nu (\vec{J}_{TT\nu\mu}\vec{J}_{tv}^{\mu}) + \ldots \tag{B.9}$$

6. the Tensor-Isovector Case

$$\tilde{\mathcal{L}}_{tT}^{lin} = \frac{1}{2}\partial_\mu (\vec{J}_{tT}^{\alpha\beta})\partial^\mu (\vec{J}_{tT\alpha\beta}) \tag{B.10}$$

where

$$\begin{aligned} \rho_s(x) &= \sum_\alpha \bar{\Psi}_\alpha \Psi_\alpha \\ J_v^\mu(x) &= \sum_\alpha \bar{\Psi}_\alpha \gamma^\mu \Psi_\alpha \end{aligned}$$

$$\begin{aligned}
\vec{\rho}_{ts}(x) &= \sum_{\alpha} \bar{\Psi}_\alpha \vec{\tau} \Psi_\alpha \\
\vec{J}^{\mu}_{tv}(x) &= \sum_{\alpha} \bar{\Psi}_\alpha \gamma^\mu \vec{\tau} \Psi_\alpha \\
J^{\nu\mu}_{T}(x) &= \sum_{\alpha} \bar{\Psi}_\alpha \sigma^{\nu\mu} \Psi_\alpha \\
\vec{J}^{\nu\mu}_{tT}(x) &= \sum_{\alpha} \bar{\Psi}_\alpha \sigma^{\nu\mu} \vec{\tau} \Psi_\alpha .
\end{aligned} \qquad \text{(B.11)}$$

Inserting all of the results above into $< \phi_0| : \hat{\mathcal{L}}_L : |\phi_0 >$, the complete expression is obtained as follows :

$$\begin{aligned}
< \phi_0| : \hat{\mathcal{L}}_L : |\phi_0 > = \sum_{\alpha=A} \bar{\Psi}_\alpha (i\gamma_\mu \partial^\mu - m_B) \Psi_\alpha \\
-\frac{1}{2}\alpha_s \rho_s^2 - \frac{1}{2}\alpha_{ts} \vec{\rho}_{ts}^{\,2} - \frac{1}{2}\alpha_v J^\mu_v J_{v\mu} - \frac{1}{2}\alpha_{tv} \vec{J}^\mu_v \vec{J}_{v\mu} \\
-\frac{1}{2}\delta_s \partial_\mu \rho_s \partial^\mu \rho_s - \frac{1}{2}\delta_{ts} \partial_\mu \vec{\rho}_{ts} \partial^\mu \vec{\rho}_{ts} - \frac{1}{2}\delta_v \partial_\nu J^\mu_v \partial^\nu J_{v\mu} - \delta_{tv} \partial_\nu \vec{J}^\mu_{tv} \partial^\nu \vec{J}_{tv\mu} \\
-\frac{1}{2}\theta_T J^\mu_v \partial^\nu (J_{T\nu\mu}) - \frac{1}{2}\theta_{TS} \vec{J}^\mu_{tv} \partial^\nu (\vec{J}_{tT\nu\mu}) + \mathcal{L}^{non-lin} + \mathcal{L}^{corr}_T + \mathcal{L}_A ,
\end{aligned} \qquad \text{(B.12)}$$

with

$$\frac{1}{2}\alpha_s = -[\frac{1}{2}\frac{g_s^2}{m_s^2} - (\frac{1}{16}\frac{g_s^2}{m_s^2} - \frac{4}{16}\frac{g_v^2}{m_v^2} - \frac{3}{16}\frac{g_R^2}{m_R^2}) - 2m_B^2(\frac{1}{16}\frac{g_s^2 k_s}{m_s^4} - \frac{4}{16}\frac{g_v^2 k_v}{m_v^4} - \frac{3}{16}\frac{g_R^2 k_r}{m_R^4})] \qquad \text{(B.13)}$$

$$\begin{aligned}
\frac{1}{2}\alpha_v &= -[-\frac{1}{2}\frac{g_v^2}{m_v^2} - (\frac{1}{16}\frac{g_s^2}{m_s^2} + \frac{2}{16}\frac{g_v^2}{m_v^2} + \frac{3}{32}\frac{g_R^2}{m_R^2}) - 2m_B^2(\frac{1}{16}\frac{g_s^2 k_s}{m_s^4} + \frac{2}{16}\frac{g_v^2 k_v}{m_v^4} + \frac{3}{32}\frac{g_R^2 k_r}{m_R^4}) \\
&+ 2.m_B^2(\frac{1}{16}\frac{g_s^2 k_s}{m_s^4} - \frac{4}{16}\frac{g_v^2 k_v}{m_v^4} - \frac{3}{16}\frac{g_R^2 k_r}{m_R^4})]
\end{aligned} \qquad \text{(B.14)}$$

$$\frac{1}{2}\alpha_{ts} = -[-(\frac{1}{16}\frac{g_s^2}{m_s^2} - \frac{4}{16}\frac{g_v^2}{m_v^2} + \frac{1}{16}\frac{g_R^2}{m_R^2}) - 2m_B^2(\frac{1}{16}\frac{g_s^2 k_s}{m_s^4} - \frac{4}{16}\frac{g_v^2 k_v}{m_v^4} + \frac{1}{16}\frac{g_R^2 k_r}{m_R^4})] \qquad \text{(B.15)}$$

$$\begin{aligned}
\frac{1}{2}\alpha_{tv} &= -[-\frac{1}{8}\frac{g_R^2}{m_R^2} - (\frac{1}{16}\frac{g_s^2}{m_s^2} + \frac{2}{16}\frac{g_v^2}{m_v^2} - \frac{1}{32}\frac{g_R^2}{m_R^2}) - 2m_B^2(\frac{1}{16}\frac{g_s^2 k_s}{m_s^4} + \frac{2}{16}\frac{g_v^2 k_v}{m_v^4} - \frac{1}{32}\frac{g_R^2 k_r}{m_R^4}) \\
&+ 2.m_B^2(\frac{1}{16}\frac{g_s^2 k_s}{m_s^4} - \frac{4}{16}\frac{g_v^2 k_v}{m_v^4} + \frac{1}{16}\frac{g_R^2 k_r}{m_R^4})]
\end{aligned} \qquad \text{(B.16)}$$

$$\frac{1}{2}\delta_s = -[\frac{1}{2}\frac{g_s^2k_s}{m_s^4} + \frac{1}{2}(\frac{1}{16}\frac{g_s^2k_s}{m_s^4} - \frac{4}{16}\frac{g_v^2k_v}{m_v^4} - \frac{3}{16}\frac{g_R^2k_r}{m_R^4})] \tag{B.17}$$

$$\frac{1}{2}\delta_v = -[-\frac{1}{2}\frac{g_v^2k_v}{m_v^4} + \frac{1}{2}(\frac{1}{16}\frac{g_s^2k_s}{m_s^4} + \frac{2}{16}\frac{g_v^2k_v}{m_v^4} + \frac{3}{32}\frac{g_R^2k_r}{m_R^4})] \tag{B.18}$$

$$\frac{1}{2}\delta_{ts} = -\frac{1}{2}[\frac{1}{16}\frac{g_s^2k_s}{m_s^4} - \frac{4}{16}\frac{g_v^2k_v}{m_v^4} + \frac{1}{16}\frac{g_R^2k_r}{m_R^4}] \tag{B.19}$$

$$\frac{1}{2}\delta_{tv} = -[-\frac{1}{8}\frac{g_R^2k_r}{m_R^4} + \frac{1}{2}(\frac{1}{16}\frac{g_s^2k_s}{m_s^4} + \frac{2}{16}\frac{g_v^2k_v}{m_v^4} - \frac{1}{32}\frac{g_R^2k_r}{m_R^4})] \tag{B.20}$$

$$\frac{1}{2}\theta_T = -2m_B[\frac{1}{16}\frac{g_s^2k_s}{m_s^4} - \frac{4}{16}\frac{g_v^2k_v}{m_v^4} - \frac{3}{16}\frac{g_R^2k_r}{m_R^4}] \tag{B.21}$$

$$\frac{1}{2}\theta_{TS} = -2m_B[\frac{1}{16}\frac{g_s^2k_s}{m_s^4} - \frac{4}{16}\frac{g_v^2k_v}{m_v^4} + \frac{1}{16}\frac{g_R^2k_r}{m_R^4}] \tag{B.22}$$

and

$$\mathcal{L}^{non-lin} = c_s\tilde{\mathcal{L}}_S^{non-lin} + c_v\tilde{\mathcal{L}}_V^{non-lin} + c_{ts}\tilde{\mathcal{L}}_{tS}^{non-lin} + c_{tv}\tilde{\mathcal{L}}_{tV}^{non-lin}, \tag{B.23}$$

$$\begin{aligned}
\mathcal{L}_T^{corr} &= c_T(\frac{1}{2}\partial_\mu(J_T^{\alpha\beta})\partial^\mu(J_{T\alpha\beta}) + \frac{1}{2}\partial_\mu(\vec{J}_{tT}^{\alpha\beta})\partial^\mu(\vec{J}_{tT\alpha\beta})) \\
&+ \frac{m_s^2c_T}{k_s}(J_{T\nu\mu}J_T^{\nu\mu} + \vec{J}_{tT\nu\mu}\vec{J}_{tT}^{\nu\mu}) \\
&+ \frac{1}{2}[c_s\partial^\nu(J_{T\nu\mu})\partial_\sigma(J_T^{\sigma\mu}) + c_{ts}\partial^\nu(\vec{J}_{tT\nu\mu})\partial_\sigma(\vec{J}_{tT}^{\sigma\mu})],
\end{aligned} \tag{B.24}$$

where

$$\begin{aligned}
c_s &= -(\frac{1}{16}\frac{g_s^2k_s}{m_s^4} - \frac{4}{16}\frac{g_v^2k_v}{m_v^4} - \frac{3}{16}\frac{g_R^2k_r}{m_R^4}) \\
c_v &= -(\frac{1}{16}\frac{g_s^2k_s}{m_s^4} + \frac{2}{16}\frac{g_v^2k_v}{m_v^4} + \frac{3}{32}\frac{g_R^2k_r}{m_R^4}) \\
c_{ts} &= -(\frac{1}{16}\frac{g_s^2k_s}{m_s^4} - \frac{4}{16}\frac{g_v^2k_v}{m_v^4} + \frac{1}{16}\frac{g_R^2k_r}{m_R^4}) \\
c_{tv} &= -(\frac{1}{16}\frac{g_s^2k_s}{m_s^4} + \frac{2}{16}\frac{g_v^2k_v}{m_v^4} - \frac{1}{32}\frac{g_R^2k_r}{m_R^4}) \\
c_T &= -\frac{1}{16}\frac{g_s^2k_s}{m_s^4}.
\end{aligned} \tag{B.25}$$

Finally, $\mathcal{L}_A$ is an electromagnetic Lagrangian density with an exchange correction, it just remains to approximate the exchange part by the local density (Slater) approximation [34].

–C–

ENERGY FUNCTIONAL FOR SPHERICAL SYMMETRY

To allow for the pairing correlation to come into play as in Ref [7, 2], we replace the wave operator in Eq. (2.4) by

$$|\tilde{\phi}_0 >= \prod_{\alpha=1}^{\Omega}((1-w_\alpha)^{1/2} + w_\alpha^{1/2} b_\alpha^\dagger b_{-\alpha}^\dagger)|0>, \tag{C.1}$$

where Ω is the number of shell model states included for protons or neutrons respectively. Then the same procedure is followed as before. The densities now are

$$\begin{aligned}
\rho_s(x) &= \sum_\alpha^\Omega w_\alpha \bar{\Psi}_\alpha \Psi_\alpha \\
J_v^\mu(x) &= \sum_\alpha^\Omega w_\alpha \bar{\Psi}_\alpha \gamma^\mu \Psi_\alpha \\
\vec{\rho}_{ts}(x) &= \sum_\alpha^\Omega w_\alpha \bar{\Psi}_\alpha \vec{\tau} \Psi_\alpha \\
\vec{J}_{tv}^\mu(x) &= \sum_\alpha^\Omega w_\alpha \bar{\Psi}_\alpha \gamma^\mu \vec{\tau} \Psi_\alpha \\
J_T^{\nu\mu}(x) &= \sum_\alpha^\Omega w_\alpha \bar{\Psi}_\alpha \sigma^{\nu\mu} \Psi_\alpha \\
\vec{J}_{tT}^{\nu\mu}(x) &= \sum_\alpha^\Omega w_\alpha \bar{\Psi}_\alpha \sigma^{\nu\mu} \vec{\tau} \Psi_\alpha .
\end{aligned} \tag{C.2}$$

The kinetic term and electromagnetic density also have the same form as above with w_α added in front the summation. The w_α denote occupation weights. A more detailed discussion about this function can be found in [7, 2, 6]. We follow [7] and [6] to use a constant gap pairing with Δ =11.2 MeV/ A^2 in all of our calculations. The nucleonic wave function can be expressed as [7]

$$\phi_\alpha = \begin{pmatrix} \frac{iG_\alpha(r)}{r} Y_{j_\alpha l_\alpha m_\alpha} \\ \frac{F_\alpha(r)}{r} \frac{\vec{\sigma}.\vec{p}}{r} Y_{j_\alpha l_\alpha m_\alpha} \end{pmatrix}, \tag{C.3}$$

and the radial wave functions are determined by the coupled equations

$$\begin{aligned} 0 &= [\frac{d}{dr} - \frac{k_\alpha}{r}]F_\alpha(r) + U_3(r)F_\alpha(r) + [\epsilon_\alpha - U_2(r) - U_1(r)]G_\alpha(r) \\ 0 &= [\frac{d}{dr} - \frac{k_\alpha}{r}]G_\alpha(r) - U_3(r)G_\alpha(r) - [\epsilon_\alpha + U_2(r) - U_1(r)]F_\alpha(r), \end{aligned} \tag{C.4}$$

where k_α = -(j+1/2) for j=1 +1/2 and k_α = (j+1/2) for j=1 -1/2 with

$$\begin{aligned} U_1(r) &= \alpha_v \rho_0 + \delta_v \triangle \rho_0 - \frac{1}{2}\theta_T \rho_0^T + \gamma_v \rho_0^3 \\ &+ \tau_{0,\alpha}(\alpha_{tv}\rho_{0,0} + \delta_{tv}\triangle\rho_{0,0}) \\ &+ \frac{(1+\tau_{0,\alpha})}{2}(eA_0 - e(\frac{3}{\pi})^{1/3}\rho_p^{1/3}) - \frac{1}{2}\tau_{0,\alpha}\theta_{TS}\rho_{0,0}^T \\ &+ C_3\rho_s\rho_0 + C_5\rho_s^2\rho_0 \end{aligned} \tag{C.5}$$

$$\begin{aligned} U_2(r) &= m_B + \alpha_s\rho_s + \delta_s\triangle\rho_s + \beta_s\rho_s^2 + \gamma_s\rho_s^3 \\ &+ \tau_{s,\alpha}(\alpha_{ts}\rho_{s,0} + \delta_{ts}\triangle\rho_{s,0}) \\ &+ \frac{1}{2}C_3\rho_0^2 + C_5\rho_s\rho_0^2 \end{aligned} \tag{C.6}$$

$$U_3(r) = -\frac{1}{2}(\theta_T\partial_r(\rho_0) + \theta_{TS}\tau_{0,\alpha}\partial_r(\rho_{0,0})) \tag{C.7}$$

and

$$\begin{aligned} \rho_s &= \frac{1}{4\pi r^2}\sum_\alpha w_\alpha(2j_\alpha+1)(G_\alpha^2 - F_\alpha^2) \\ \rho_{ts} &= \frac{1}{4\pi r^2}\sum_\alpha w_\alpha(2j_\alpha+1)\tau_{0,\alpha}(G_\alpha^2 - F_\alpha^2) \\ \rho_0 &= \frac{1}{4\pi r^2}\sum_\alpha w_\alpha(2j_\alpha+1)(G_\alpha^2 + F_\alpha^2) \end{aligned}$$

$$
\begin{aligned}
\rho_{0,0} &= \frac{1}{4\pi r^2}\sum_\alpha w_\alpha(2j_\alpha+1)\tau_{0,\alpha}(G_\alpha^2+F_\alpha^2) \\
\rho_0^T &= \frac{1}{4\pi r^2}\sum_\alpha w_\alpha(2j_\alpha+1)2\partial_r(G_\alpha F_\alpha) \\
\rho_p &= \frac{(\rho_0+\rho_{0,0})}{2} \\
\rho_{0,0} &= \frac{1}{4\pi r^2}\sum_\alpha w_\alpha(2j_\alpha+1)\tau_{0,\alpha}2\partial_r(G_\alpha F_\alpha).
\end{aligned}
\tag{C.8}
$$

An expression for the energy is given by the first diagonal element T_{00} of the stress-energy tensor :

$$
\begin{aligned}
E_{MF} &= \sum_\alpha w_\alpha\epsilon_\alpha - \frac{1}{2}\int d^3r[\alpha_s\rho_s^2+\delta_s\rho_s\triangle\rho_s+4/3\beta_s\rho_s^3+3/2\gamma_s\rho_s^4 \\
&+ \alpha_{ts}\rho_{s,0}^2+\delta_{ts}\rho_{s,0}\triangle\rho_{s,0}+\alpha_v\rho_0^2+\delta_v\rho_0\triangle\rho_0 \\
&+ 3/2\gamma_v\rho_0^4+\alpha_{tv}\rho_{0,0}^2+\delta_{tv}\rho_{0,0}\triangle\rho_{0,0}-\frac{1}{2}\theta_{TS}\rho_{0,0}^T\rho_{0,0} \\
&- \frac{1}{2}\theta_T\rho_0^T\rho_0+e^2A_0\rho_p-\frac{1}{2}e^2\left(\frac{3}{\pi}\right)^{1/3}\rho_p^{4/3} \\
&+ 2C_3\rho_s\rho_0^2+3C_5\rho_s^2\rho_0^2].
\end{aligned}
\tag{C.9}
$$

Bibliography

[1] R.J. Furnstahl, R.J. Perry and B.D. Serot *Phys. Rev. C*40, 321 (1989)

[2] P.G. Reinhard *Rep. Prog. Phys*52, 439 (1989)

[3] R.J. Perry *Nucl. Phys. A*467, 717 (1987)

[4] Ying Hu, **Dissertation** , Indiana University (2000)

[5] B.V. Carlson and D. Hirata *Phys. Rev. C*62, 054310 (2000)

[6] P.G. Reinhard, M. Rufa, J.A. Maruhn, W. Greiner and J.Friedrich *Z. Phys. A*323, 13 (1986)

[7] M. Rufa, P.G. Reinhard, J.A. Maruhn, W. Greiner and M.R. Strayer *Phys. Rev. C*38, 390 (1988)

[8] M.M. Sharma, G.A. Lalazissis and P.Ring *Phys. Letts. B*317, 9 (1993)

[9] Y.K. Gambhir, P. Ring and A. Thimet Ann. Phys (N.Y.)**198**, 132 (1980)

[10] H.F. Boersma *Phys. Rev. C*48, 472 (1993)

[11] G.A. Lalazissis at al *Nucl. Phys. A*608, 202 (1996)

[12] K. Rutz, **Dissertation**, in Frankfurt am Main (1999)

[13] K. Rutz at al *Phys. Rev. C*56, 238 (1997)

[14] T. Bürvenich at al Eur. Phys. J.A**3**, 139 (1998)

[15] T. Cornelius, **Diploma Thesis**, in Frankfurt am Main (2001)

[16] L. Kudling, **Diploma Thesis**, in Frankfurt am Main (2001)

[17] W. Nazarewicz at al *Phys. Rev. C***53**, 740 (1996)

[18] M. Bender at al *Phys. Rev. C***58**, 2126 (1998)

[19] T. Bürvenich, **Dissertation**, in Frankfurt am Main (2001)

[20] B.A. Nikolaus, T. Hoch and D.G. Madland *Phys. Rev. C***46**, 1757 (1992)

[21] J. J. Rusnak and R. J. Furnstahl *Nucl. Phys. A***627**, 95 (1997)

[22] S.J. Lee, **Dissertation** , Yale University (1986)

[23] L.D. Miller *Phys. Rev. C***9**, 537 (1974);*Phys. Rev. C***12**, 710 (1975)

[24] R. Fritz, H. Müther and R. Machleidt *Phys. Rev. Letts***71**, 46 (1993)

[25] T. Hoch, D. Madland, P. Manakos, T. Mannel, B.A. Nikolaus and D. Strottman *Phys. Report***242**, 253 (1994)

[26] J.K. Zhang, Y. Jin and D.S. Onley *Phys. Rev. C***48**, 2697 (1993)

[27] R.N. Schmid, E.Engel and R.M. Dreizler *Phys. Rev. C***52**, 164 (1995); *Phys. Rev. C***52**, 2804 (1995); *Foundations of Physics***27**, 1257 (1997)

[28] A. Bouyssy, J.F. Mathiot, N. V. Giai, S. Marcos *Phys. Rev. C***36**, 380 (1987)

[29] H.F. Boersma and R. Malfliet *Phys. Rev. C***49**, 233 (1994);*Phys. Rev. C***49**, 1495 (1994)

[30] R.J. Furnstahl, B.D. Serot and H.B. Tang *Nucl. Phys. A***598**, 539 (1996);*Nucl. Phys. A***615**, 441 (1997)

[31] J.J. Rusnak and R.J. Frunstahl *Nucl. Phys. A***627**, 495 (1997); *Nucl. Phys. A***627**, 495 (1997)

[32] M. Centelles and X. Vinas *Nucl. Phys. A***627**, 495 (1997)

[33] M. Centelles, M. Del Estal and X. Vinas *Nucl. Phys. A***635**, 193 (1998)

[34] M. Bender, **Dissertation** , in Frankfurt am Main (1997)

[35] P. Manakos and T. Mannel *Z. Phys. A***330**, 223 (1988);*Z. Phys. A***334**, 481 (1989)

[36] X. Campi and D.W. Srung *Nucl. Phys. A***194**, 401 (1972)

[37] P. Bernados, V.N. Fomenko, M.L. Quelle, S. Marcos, R. Niembro, L.N. Savushkin *J. Phys. G. Nucl. Part*22, 361 (1996)

[38] W.Greiner, J. Reinhard , Quantum Electrodynamics, **Springer-Verlag**, Heidelberg (1997)

[39] M. Thies *Phys. Letts. B***162**, 255 (1985); *Phys. Letts. B***166**, 23 (1986)

[40] C. J. Horowitz and B. D. Serot *Nucl. Phys. A***368**, 503 (1981)

[41] A.Bouyssy and S. Marcos *Phys. Letts. B***127**, 157 (1983)

[42] R. J. Furnstahl, J. J. Rusnak and B.D. Serot *Nucl. Phys. A***632**, 607 (1998)

[43] S.M. Kravchenko and P. Soznik *Int. J. Mod. Phys. E***8**, 137 (1999)

[44] T. S. Biró and J. Zimányi *Phys. Letts. B***391**, 1 (1997)

[45] W. Koepf and P. Ring *Z. Phys. A***339**, 81 (1991)

[46] R.Brockmann and W. Weise *Phys. Rev. C***16**, 1282 (1977)

[47] D. Vautherin and D.M. Brink *Phys. Rev. C***5**, 626 (1972)

[48] S. Hama, **Dissertation** , the Ohio State University (1984); B.C. Clark, **Los Alamos Workshop in Relativistic Dynamics and Quark-Nuclear Physics**, Eds. M.B. Johnson and A. Piclesimer, page 302-329 (1985)

[49] M. Bender, K. Rutz, P.G. Reinhard, J.A. Maruhn and W. Greiner *Phys. Rev. C***60**, 034304-1 (1999)

[50] J. A. Maruhn, T. Bürvenich, D.G. Madland Journal of Comput. Phys**238**, 169 (2001).

[51] Y. Takahashi. C. Ropchan *Prog. Theo. Phys* **76**, 1187 (1986)

[52] C.R. Hagen and W.J. Hurley *Phys. Rev. Letts***24**, 1381 (1970)

[53] J.Levy-Leblond *Comm. Math. Phys* **6**, 286 (1967)

[54] J.Caro, E. Ruiz Arriola, L.L. Salcedo *Phys. Letts. B***383**, 9 (1996)

[55] R. J. Furnstahl and B.D. Serot **e-print**, nucl-th/9912048 (1999)

[56] W.Greiner, B. M
*rmddotu*ller , Gauge Theory of Weak Interaction, **Springer-Verlag**, Heidelberg (1989)

[57] P.G. Reinhard, M. Bender and J.A. Maruhn **e-print**, nucl-th/0012095 (2000)

[58] W.D. Myers and W.J. Swiatecki Nucl. Phys**81**, 1 (1966)

[59] S.G. Nilsson et.al *Nucl. Phys. A***131**, 1 (1969)

[60] U. Mosel and W. Greiner *Z. Phys***217**, 256 (1968)

[61] U. Mosel and W. Greiner *Z. Phys***222**, 261 (1968)

[62] J. Grumann, U. Mosel, B. Fink and W. Greiner *Z. Phys***228**, 371 (1969)

[63] J. Grumann, Th. Morovic and W. Greiner Z. Naturforschung**26a**, 643 (1971)

[64] P. Holzer, U. Mosel and W. Greiner *Nucl. Phys. A***138**, 241 (1969)

[65] D. Scharnweber, U. Mosel, and W. Greiner *Z. Phys***228**, 371 (1969)

[66] E.O. Fizet and J.R. Nix *Nucl. Phys. A***193**, 647 (1972)

[67] M. Brack et.al Rev. Mod. Phys**44**, 320 (1972)

[68] S. Hofmann et. al *Z. Phys. A***350**, 277 (1995); *Z. Phys. A***350**, 281 (1995)

[69] A. Ghiorso et. al *Nucl. Phys. A***583**, 861c (1995);*Phys. Rev. C***51**, R2293 (1995)

[70] S. Hofmann et. al *Z. Phys. A***354**, 229 (1996)

[71] Yu. A. Lazarev et. al *Phys. Rev. C***54**, 620 (1996)

[72] S. Hofmann *Rep. Prog. Phys***61**, 639 (1998)

[73] Yu. A. Lazarev et. al *Phys. Rev. Letts***73**, 624 (1994)

[74] P. Reiter et. al *Phys. Rev. Letts***82**, 509 (1999)

[75] F. Tondeur *Z. Phys. A***297**, 61 (1980)

[76] S. Cwiok at al *Nucl. Phys. A***611**, 211 (1996)

[77] Pearson and Farine *Phys. Rev. C***50**, 185 (1994)

Acknowledgments

This work has not been completed without great support from many people. I would like to express my thanks to them.

I am very grateful to my advisor, Prof. Dr. Joachim.A. Maruhn. He was always willing to help and gave continuously encouragement during the course of this work. I appreciate his constructive advices and patient corrections in both physics and language of this dissertation.

I wish to extend my thanks to Prof. Dr. Dr. h.c.mult. Walter Greiner who accepted me to continue my education in the Institut für Theoretische Physik Uni-Frankfurt and support me both academically and administratively.

I also wish to thank Prof. Dr. Paul-Gerhard Reinhard for insightful suggestions and important advices.

Many thanks go to the members of the "Kernstruktur" group for the stimulating atmosphare, in particular T. Bürvenich, who read the early version of this dissertation, found numerous mistakes and made many helpful suggestions and T. Cornelius, who read carefully and give important corrections in the German part of this dissertation.

I would like to thank the Deutscher Akademischer Austauschdienst (DAAD) which provides me with financial support.

I would like also to thank my friends, who cannot all be mentioned here, for their help and friendship.

Finally, special thanks to my wive and children for their encouragement, understanding and love.

Zusammenfassung und Ausblick

Zusammenfassung

In dieser Arbeit vergleichen wir das lineare Walecka-Modell mit dem Punktkopplungsmodell in Hartree-Näherung um den Einfluss endlicher Reichweite zu untersuchen. Wir vergleichen zusätzlich zwei lineare Punktkopplungsmodelle, eines ohne und eines mit Austauschtermen, um die durch sie hervorgerufenen Effekte zu studieren. Weiterhin ist der Vergleich der verwendeten Punktkopplungsmodelle zu bekannten nichtrelativistischen Ansätzen von Interesse. Dazu wurde in dieser Arbeit der nichtrelativistische Grenzfall des Punktkopplungsmodells hergeleitet und untersucht. Weil die Modelle als effektive Theorien bezeichnet werden müssen, können sie erst nach Anpassung verschiedener Parameter an experimentelle Daten untereinander verglichen werden. Es wurden daher sowohl für das lineare Punktkopplungsmodell ohne Austauschterme (LDZ2) als auch für selbiges mit Austauschtermen (LDZ1) ein Parametersatz erstellt.

Das lineare Punktkopplungsmodell ohne die Austauschkorrektur wird in Hartree-Näherung durch folgende Lagrange-Dichte dargestellt:

$$\begin{aligned}
\mathcal{L}_H^{PC} &= \sum_{\alpha=A} \bar{\Psi}_\alpha (i\gamma_\mu \partial^\mu - m_B)\Psi_\alpha \\
&\quad + \sum_{i=S,V,R} s_i \frac{1}{2}\frac{g_i^2}{m_i^2}\Big[\sum_{\alpha\beta} (\bar{\Psi}_\alpha \Gamma_i^\nu \Psi_\alpha)(\bar{\Psi}_\beta \Gamma_{\nu i} \Psi_\beta) \\
&\qquad\qquad + \frac{k_i}{m_i^2}\sum_{\alpha\beta} \partial_\mu (\bar{\Psi}_\alpha \Gamma_i^\nu \Psi_\alpha)\partial^\mu (\bar{\Psi}_\beta \Gamma_{\nu i} \Psi_\beta)\Big] \\
&\quad + \mathcal{L}_{EM}.
\end{aligned}$$

Unter Berücksichtigung der Austauschterme erhält man folgende Lagrange-Dichte:

$$\mathcal{L}_{HF}^{PC} = \mathcal{L}_H^{PC} + \mathcal{L}_{ex\,EM}$$

$$- \sum_{j=S,V,R\ldots} C_{ji}\Big[\frac{1}{2}\frac{g_i^2}{m_i^2} J_{j\alpha} J^j_\beta + \frac{g_i^2 k_i}{m_i^4}\Big(\frac{1}{4} A_{j\alpha\mu} A^{j\mu}_\beta - B_{j\alpha\mu} B^{j\mu}_\beta + J_{j\alpha} C^j_\beta\Big)\Big],$$

wobei

$$\begin{aligned} A_{\alpha j\mu} &= \partial_\mu(\bar\Psi_\alpha \Gamma_j \Psi_\alpha) \quad , \quad B_{\alpha j\mu} = \frac{1}{2i}[\bar\Psi_\alpha \Gamma_j(\partial_\mu \Psi_\alpha) - (\partial_\mu \bar\Psi_\alpha)\Gamma_j \Psi_\alpha] \quad , \\ C_{\alpha j} &= (\partial_\mu \bar\Psi_\alpha)\Gamma_j(\partial^\mu \Psi_\alpha) \quad , \quad J_{\alpha j} = \bar\Psi_\alpha \Gamma_j \Psi_\alpha . \end{aligned}$$

Die C_{ji} werden aus der Fierz-Transformation [56] gewonnen und $\mathcal{L}_{ex\,EM}$ bezeichnet die elektromagnetischen Austauschterme. Die Dichten $B_{\alpha j\mu}$ und $C_{\alpha j}$ werden in dieser Arbeit mit Hilfe der Gordonzerlegung approximiert. Wir benutzen für die Anpassung der Parameter an experimentelle Daten das gleiche Verfahren aus [7].

Mit Hilfe der beiden erwähnten Parametersätze wurden die Bindungsenergien, die Zwei-Protonen- sowie Zwei-Neutronen-Separationsenergien, die Diffraktionsradien und die Oberflächendicken ausgewählter Isotopen- und Isotonenketten berechnet. Diese konnten mit experimentell bekannten Daten verglichen werden. Weiterhin konnten Spin-Bahn-Aufspaltungen, Einteilchenspektren und Kernmaterieeigenschaften bestimmt und diskutiert werden. Die Vorhersagen unserer beiden neuen Parametersätze wurden mit den etablierten Parametersätzen L-Z und NL-Z [2, 7] verglichen.

Der Parametersatz L-Z korrespondiert zu dem Modell:

$$\begin{aligned} \mathcal{L}^W_H &= \sum_{\alpha=A} \bar\Psi_\alpha(i\gamma_\mu \partial^\mu - m_B)\Psi_\alpha + \mathcal{L}_{EM} \\ &\quad + \sum_{i=S,V,R} s_i\Big[\frac{1}{2}(\partial_\nu \phi^\mu_i \partial^\nu \phi_{i\mu} - m_i^2 \phi^\mu_i \phi_{i\mu}) - g_i \sum_\alpha \bar\Psi_\alpha \Gamma^\mu_i \phi_{i\mu} \Psi_\alpha\Big] \end{aligned}$$

und NL-Z zu

$$\mathcal{L}^{NL-W}_H = \mathcal{L}^W_H - \frac{1}{3} b_2 \phi_s^3 - \frac{1}{4} b_3 \phi_s^4 .$$

Zusätzlich wurden in dieser Arbeit Ergebnisse des linearen Walecka-Modells mit LDA (*local density approximation*) [27] als auch unter Hartree-Fock-Näherung [26] mit unseren Resultaten verglichen.

Es zeigte sich, dass in denen von uns betrachteten Kernen und mit Hilfe der von uns verwendeten Fitstrategie keine großen systematischen Differenzen zwischen dem Punktkopplungsmodell mit kurzreichweitiger Wechselwirkung und den RMF-Modellen mit Mesonenaustausch festgestellt werden konnten. Allerdings zeigt sich ein deutlicher Einfluss der Austauschterme. Es lässt sich folgern, dass sie nicht durch Redefinition der Kopplungskonstanten im linearen RMF- sowie im Punktkopplungsmodell absorbiert werden k"onnen. Vielmehr ergibt sich, dass die nicht-linearen Terme ein wichtiger Bestandteil der Wechselwirkung sind und in den Modellen berücksichtigt und eingehender untersucht werden müssen. Weitere fundamentale Studien dieser nicht-linearen Modelle sind nötig. Dies wird zu einem tieferen Verständnis der Natur der endlichen Kerne vom Standpunkt relativistischer Modelle und der Modelle selbst führen.

Der effektive Hamilton-Operator des nicht-linearen Punktkopplungmodells im nichtrelativistischen Grenzfall wurde in dieser Arbeit hergeleitet. Er ergibt sich zu:

$$\begin{aligned} H_{\text{eff}}^{\text{class}} &= C_1\rho_0 + C_2\Delta\rho_0 + C_3\vec{\nabla}\rho_0\cdot\vec{J} + C_4\left(\frac{d\rho_0}{dr}\right)^2 + C_5\tau + C_6\vec{\nabla}\cdot\vec{J} \\ &+ \vec{p}C_7\vec{p} + C_8\left(\frac{1}{r}\frac{d\rho_0}{dr}\right)\vec{\sigma}\cdot\vec{L}. \end{aligned}$$

Die C_1, C_2,..., C_8 wurden für das lineare Punktkopplungs-Modell ohne (LDZ2) und mit den Austauschtermen (LDZ1) sowie mit einem nicht-linearen Ansatz (LDZ2a) analysiert. Diese Ergebnisse wurden mit dem linearen Walecka- und dem Skyrme-Hartree-Fock-Modell verglichen [2].

Ein wichtiges Ergebnis dieser Studien ist, dass die nicht-linearen Terme im Punktkopplungsmodell sowohl für die Beschreibung von Massen als auch für die genauen Vorhersagen der Schalenstruktur wichtig sind. Die nicht-linearen Terme in relativistischen Modellen, die sich in ihrer funktionalen Form von den nicht-relativistischen Modellen unterscheiden, erzeugen automatisch eine schwache Dichteabhängigkeit nicht nur im Zentralpotential sondern auch im Spin-Bahn-Potential. Das Zentralpotential ist wichtig für Massen- und Oberflächeneigenschaften während das Spin-Bahn-Potential für die Schalenstruktur von endlichen Kernen verantwortlich ist. Diese Ergebnisse wurden benutzt, um überschwere Kerne zu analysieren und eine Modifikation des Skyrme-Modells mit einem dichteabhängigen Spin-Bahn-Potential vorzuschlagen, das aus dem Punktkopplungsmodell hergeleitet wurde.

Diese neue Energiedichte mit einem dichteabhängigen Spin-Bahn-Potential sieht wie folgt aus:

$$\varepsilon(r) \equiv \varepsilon^0(r) + \frac{1}{2}(W_1\rho + W_2\rho^2)(\vec{J}_n.\vec{\nabla}\rho_p + \vec{J}_p.\vec{\nabla}\rho_n + \sum_q \vec{J}_q.\vec{\nabla}\rho_q).$$

Ausblick

Bevor Hartree-Fock-Bogolyubov-Rechnungen in Erwägung gezogen werden können, sollten drei Aspekte der Mean-Field-Modelle untersucht werden.

- Die Rolle der Austausch-Terme der nicht-linearen Wechselwirkung.
- Die effektive Form der nicht-linearen Terme.
- Die in dieser Arbeit verwendete Näherung bei Betrachtung der Austausch-Wechselwirkung der Ableitungsterme zeigte keine zufriedenstellenden Ergebnisse. Daher stellt ihre exakte Behandlung eine weitere Aufgabe für zukünftige Entwicklungen dar.

Die ersten beiden Aspekte sollen im folgenden kurz erläutert und untersucht werden.

Erste einfache Untersuchungen mit Hilfe der nicht-linearen Wechselwirkung:

$$\mathcal{L}_{\mathrm{NL}}^{\mathrm{a}} = -\frac{1}{3}C_2\rho_s^3 - \frac{1}{4}C_3\rho_s^4,$$

zeigten bereits gute Resultate. Zunächst wurde ein neuer Parametersatz für die neue Lagrange-Dichte erstellt (TEST-NLa). Ein Vergleich mit den oben beschriebenen Ansätzen zeigt bereits eine kleine Verbesserung in der Oberflächendicke von endlichen Kernen. Da für diese kurze Untersuchung die Austauschterme nur in Hartree-Näherung untersucht wurden, lassen sich mit Hilfe der Hartree-Fock-Näherung weitere Verbesserungen erwarten.

Wie schon angemerkt, unterscheiden sich die Vorhersagen des RMF- mit dem Punktkopplungsmodells in Bezug auf die Oberflächendicke endlicher Kerne deutlich. Es ist zu vermuten, dass die Beiträge der nicht-linearen Ableitungsterme in den nicht-linearen Termen des RMF-Modells implizit vorhanden sind. Um dies zu prüfen soll eine weitere nicht-lineare Wechselwirkung untersucht werden:

$$\mathcal{L}_{\mathrm{NL}}^{\mathrm{b}} = -\frac{1}{3}C_2\rho_s^3 - \frac{1}{4}C_3\rho_s^4 + C^b{\rho_s}^2\Delta\rho_s.$$

Zu ihr korrespondiert der Parametersatz TEST-NLb. Auch hier zeigen sich wiederum kleine Verbesserungen (siehe Tabelle 1). Eine intensive Studie der nicht-linearen Terme ist also für eine Verbesserung des Modells unumgänglich.

χ^2	E	r_{dms}	σ	Total
TEST-NLa	21.93	6.91	59.51	88.35
TEST-NLb	19.32	9.71	41.00	70.00
LDZ2a	27.65	6.57	75.79	110.01
NL-Z	23.89	18.77	29.25	71.92

Tabelle.1 : Ergebnisse der beiden getesteten nicht-linearen Ansätze im Vergleich zu den bekannten LDZ2a und NL-Z. Dargestellt ist jeweils das χ^2der Bindungsenergie E, des Diffraktionsradius r_{dms} und der Oberflächendicke σ.

Lebenslauf

Name : Anto Sulaksono
Gebursdatum : 21 April 1969
Geburtsort : Jakarta (Indonesien)
Familienstand : Verhairatet
Nationalität : Indonesisch

Ausbildung

1975-1981 : Grundschule
1981-1984 : Zwischenschule
1984-1987 : Oberschule
1987-1992 : Physik, Universitas Indonesia, Jakarta, B.S
1993-1996 : Physik, Universitas Indonesia, Jakarta, M.S
1998-2002 : Physik, Frankfurt Universität, Frankfurt am Main

Meine Akademische Lehrer waren:

Prof. Dr. J.A. Maruhn
Prof. Dr. W. Greiner
Dr. H.P. Simanjuntak
Prof. Dr. D. Kusno
Dr. L. Neise
Dr. J. Reinhardt
Prof. Dr. H. Stöcker
Prof. Dr. D. Rischke